Short Title: Role of BST4 in Chlamydomonas

Title: The role of BST4 in the pyrenoid of *Chlamydomonas reinhardtii*

Authors: Liat Adler[1,2,3], Chun Sing Lau[4], Kashif M. Shaikh[5], Kim A. van Maldegem[5], Alex L. Payne-Dwyer[4,6], Cecile Lefoulon[7], Philipp Girr[4], Nicky Atkinson[1,2], James Barrett[4], Tom Z. Emrich-Mills[4], Emilija Dukic[5], Michael R. Blatt[7], Mark C. Leake[4,6], Gilles Peltier[8], Cornelia Spetea[†5], Adrien Burlacot[†,3,9], Alistair J. McCormick[†,1,2], Luke C. M. Mackinder[†4], Charlotte E. Walker[†4]

[1]Institute of Molecular Plant Sciences, School of Biological Sciences, University of Edinburgh, EH9 3BF, United Kingdom.
[2]Centre for Engineering Biology, University of Edinburgh, EH9 3BF, United Kingdom.
[3]Department of Plant Biology, The Carnegie Institution for Science, Stanford, CA, 94305 USA
[4]Centre for Novel Agricultural Products (CNAP), Department of Biology, University of York, Heslington, York YO10 5DD, United Kingdom.
[5]Department of Biological and Environmental Sciences, University of Gothenburg, Gothenburg 40530, Sweden.
[6]School of Physics, Engineering and Technology, University of York, Heslington, York YO10 5DD, United Kingdom.
[7]Laboratory of Plant Physiology and Biophysics, Bower Building, University of Glasgow, Glasgow, United Kingdom.
[8]Aix-Marseille Université, CEA, CNRS, Institut de Biosciences et Biotechnologies Aix-Marseille, CEA Cadarache, 13108 Saint-Paul-lez-Durance, France
[9]Department of Biology, Stanford University, Stanford, CA, 94305, USA

[†]The author(s) responsible for distribution of materials integral to the findings presented in this article in accordance with the policy described in the Instructions for Authors (https://academic.oup.com/plcell/pages/General-Instructions) are:

- Cornelia Spetea, Department of Biological and Environmental Sciences University of Gothenburg, Gothenburg 40530, Sweden +46-31 786 9332, cornelia.spetea.wiklund@bioenv.gu.se

35 • Adrien Burlacot, Carnegie Institution for Science, Stanford, CA, 94305 USA,
36 aburlacot@carnegiescience.edu
37 • Alistair McCormick, School of Biological Sciences, University of Edinburgh, +44
38 1316 505316, alistair.mccormick@ed.ac.uk
39 • Luke Mackinder, Department of Biology, University of York, +44 1904 328984,
40 luke.mackinder@york.ac.uk
41 • Charlotte Walker, Department of Biology, University of York, +44 1904 328500,
42 charlotte.walker@york.ac.uk

43 *One-sentence summary*: In Chlamydomonas, the pyrenoid-localized bestrophin-like
44 protein BST4 is a putative ion channel involved in pH regulation of the thylakoid lumen,
45 possibly by mediating bicarbonate transport.

46 *Funding information*: This work was funded by the Biotechnology and Biological
47 Sciences Research Council (BBSRC) (grant number (BB/S015531/1) and Leverhulme
48 Trust (RPG-2017-402). LA acknowledges funding support by EASTBIO
49 DTP (BB/J01446X/1) and the Carnegie Institution for Science. CEW acknowledges
50 funding support from BBSRC Discovery Fellowship (BB/W009587/1). CSL was
51 supported by Bill & Melinda Gates Agricultural Innovations (Investment ID 53197). CS
52 acknowledges grants from the Swedish Research Council (VR 2016-03836 and 2021-
53 03790). KMS was recipient of a postdoctoral fellowship from the Carl Tryggers
54 Foundation (CTS 20:406). A United Kingdom Research and Innovation Future
55 Leaders Fellowship to LCMM (MR/T020679/1), Biotechnology and Biological
56 Sciences Research Council grants (BB/T017589/1, BB/S015337/1, BB/R001014/1)
57 and Engineering and Physical Research Council Grant (EP/W024063/1) with ML and
58 APD. AB acknowledges the support of the Carnegie Institution for Science. The
59 authors would like to thank the University of York Biosciences Technology Facility for
60 confocal microscopy access and support. CL was funded by BBSRC grants
61 BB/P011586/1 and BB/T013508/1 to MRB. PG was supported by the Deutsche
62 Forschungsgemeinschaft (DFG, German Research Foundation) – project number
63 456013262.

64 **ABSTRACT**

65 In many eukaryotic algae, CO_2 fixation by Rubisco is enhanced by a CO_2-
66 concentrating mechanism, which utilizes a Rubisco-rich organelle called the pyrenoid.

The pyrenoid is traversed by a network of thylakoid-membranes called pyrenoid tubules, proposed to deliver CO_2. In the model alga *Chlamydomonas reinhardtii* (**Chlamydomonas**), the pyrenoid tubules have been proposed to be tethered to the Rubisco matrix by a bestrophin-like transmembrane protein, BST4. Here, we show that BST4 forms a complex that localizes to the pyrenoid tubules. A Chlamydomonas mutant impaired in the accumulation of BST4 (***bst4***) formed normal pyrenoid tubules and heterologous expression of BST4 in *Arabidopsis thaliana* did not lead to the incorporation of thylakoids into a reconstituted Rubisco condensate. Chlamydomonas *bst4* mutant did not show impaired growth at air level CO_2. By quantifying the non-photochemical quenching (**NPQ**) of chlorophyll fluorescence, we show that *bst4* displays a transiently lower thylakoid lumenal pH during dark to light transition compared to control strains. When acclimated to high light, *bst4* had sustained higher NPQ and elevated levels of light-induced H_2O_2 production. We conclude that BST4 is not a tethering protein, but rather is an ion channel involved in lumenal pH regulation possibly by mediating bicarbonate transport across the pyrenoid tubules.

INTRODUCTION

Maintaining improvement in crop yields to keep pace with the rising demands for food is becoming increasingly challenging (Horton et al., 2021). Current models predict that an increase in food supply between 35 and 56% from 2010 to 2050 is required (van Dijk et al., 2021). A possible solution to overcome this challenge is engineering a biophysical CO_2-concentrating mechanism (**CCM**) into C3 crop plants, which has been proposed to improve crop yields by between 8 and 60%, as well as water-use and nitrogen-use efficiency (Price et al., 2013; McGrath and Long, 2014; Long et al., 2019; Fei et al., 2022; Wu et al., 2023). The biophysical CCMs in algae typically function by concentrating CO_2 into a liquid-liquid phase separated microcompartment called a pyrenoid, which is predominantly made up of a Ribulose-1,5-bisphosphate carboxylase/oxygenase (**Rubisco)**-rich matrix. This raises the $[CO_2]$:$[O_2]$ ratio around the primary CO_2-fixing enzyme Rubisco, which brings Rubisco closer to its maximal carboxylation rate and minimizes the competing oxygenation reaction. *Chlamydomonas reinhardtii* (hereafter **Chlamydomonas**) has the most well understood pyrenoid-based CCM and has become the blueprint for engineering such a CCM into C3 plants (Hennacy and Jonikas, 2020; Adler et al., 2022).

99 An important yet little understood aspect of the Chlamydomonas CCM is the function
100 and biogenesis of the thylakoid tubule network that traverses the pyrenoid, known as
101 the pyrenoid tubules. The pyrenoid tubules are continuous with the thylakoid
102 membrane (which harbors the photosynthetic electron transport chain) (Engel et al.,
103 2015) and are thought to function as a delivery system for inorganic carbon (**Ci**) to the
104 Rubisco-rich pyrenoid matrix (Mitra et al., 2005; Raven 1997). In the current model,
105 bicarbonate (**HCO_3^-**) is channelled into the thylakoid lumen by bestrophin-like proteins
106 1-3 (**BST1-3**) (Mukherjee et al., 2019) and diffuses to the pyrenoid tubules where it is
107 converted to CO_2 by carbonic anhydrase 3 (**CAH3**) (Karlsson et al., 1998; Mitra et al.,
108 2005) thanks to a low lumenal pH generated by the photosynthetic electron transport
109 chain (Burlacot et al., 2022). Traversion of the pyrenoid Rubisco-matrix by tubules is
110 predicted to be essential for an efficient CCM (Fei et al., 2022). Therefore,
111 understanding the mechanisms of pyrenoid tubule formation and function will be
112 crucial for future plant pyrenoid engineering efforts.

113 The protein **BST4** (bestrophin-like protein 4, also known as Rubisco binding
114 membrane protein 1, RBMP1; Cre06.g261750) localizes exclusively to the pyrenoid
115 tubules and has been proposed to function as a tether protein, linking the Rubisco
116 matrix to the tubules (Meyer et al., 2020). BST4 is a predicted transmembrane protein
117 and has two Rubisco binding motifs (**RBMs**) on its long, disordered C-terminus (**Fig.
118 1A**) (He et al., 2020; Meyer et al., 2020). RBMs facilitate the targeting of proteins to
119 the pyrenoid and are also hypothesized to underpin the assembly of the pyrenoid.
120 Meyer et al. (2020) proposed that BST4, together with other tether proteins, may
121 recruit Rubisco to the tubule network.

122 BST4 also has a well-conserved bestrophin domain similar to those present in the
123 thylakoid-localized BST1-3 proteins (Mukherjee et al. 2019). Bestrophins primarily act
124 as anion channels and are found in a wide diversity of organisms, including animals,
125 plants and fungi. They are best known to have permeability to chloride and HCO_3^- (Qu
126 and Hartzell, 2008), although some are reportedly permeable to cations (Yang et al.,
127 2014) and larger organic anions (Roberts et al., 2011). It is possible that BST4
128 functions as an HCO_3^- channel, like that proposed for BST1-3 (Mukherjee et al. 2019),
129 but there are currently no data to support this hypothesis.

130 In this study we aimed to elucidate the role of BST4 in the Chlamydomonas CCM. We
131 tested BST4 as a thylakoid-Rubisco tethering protein as well as its suitability in
132 promoting a thylakoid-Rubisco matrix interface in the model land plant Arabidopsis.
133 We also explored an alternative hypothesis that BST4 functions as an ion channel in
134 the pyrenoid tubules and discussed the implications this has for our current
135 understanding of CO_2 fixation by the pyrenoid.

136 **RESULTS AND DISCUSSION**

137 **BST4 is a bestrophin-like protein that is localized in the intra-pyrenoid thylakoid**
138 **tubules in Chlamydomonas**

139 The amino acid sequence of BST4 has two key unique features compared to the
140 previously characterized BST1-3 (**Fig. 1**) (Mukherjee et al. 2019). First, BST4 has an
141 extended disordered C-terminus that contains two RBMs (**Fig. 1A**) (He et al., 2020;
142 Meyer et al., 2020). Second, BST4 has a phenylalanine residue in the first position of
143 the putative selection pore, as opposed to valine which is conserved throughout BST1-
144 3 (Mukherjee et al. 2019), although the residue at this position is variable in other well
145 characterized bestrophin proteins (*Malus domestica* voltage-dependent Cl^- channel 1
146 (***Md*VCCN1**) and *Homo sapiens Bestrophin 1* (***Hs*BEST1**)) (**Fig.1B, C**). In
147 corroboration, we found the evolutionary history of BST4 diverges from BST1-3 when
148 investigated using maximum likelihood phylogenetic analysis. We analysed the full-
149 length sequence (**Fig. S1**) and a truncated version without the disordered C-terminal,
150 leaving the bestrophin domain and N-terminal (**Fig. 1D**), both of which found BST4 to
151 resolve in a distinct clade from BST1-3 but within the wider green algae group.

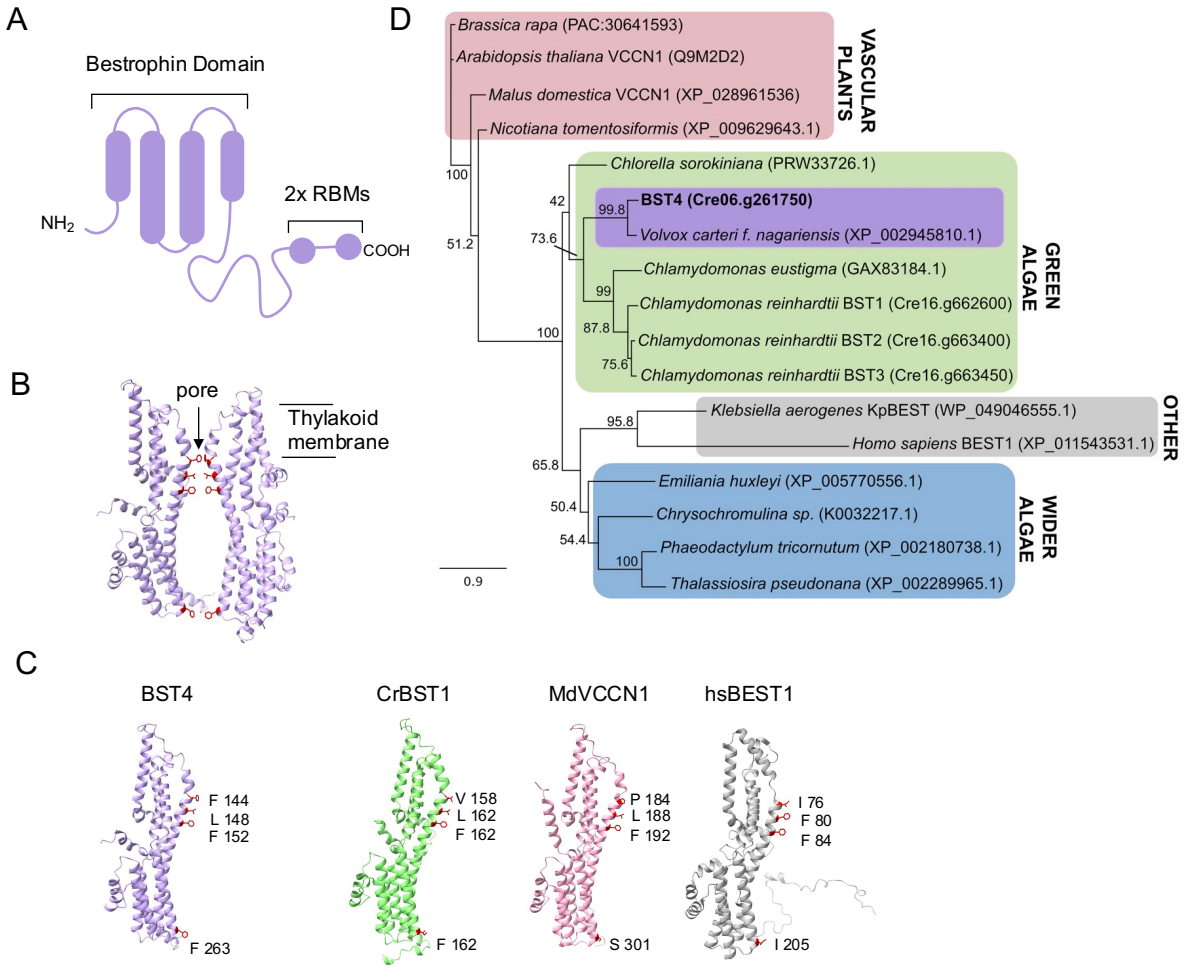

Figure 1. BST4 is a bestrophin protein that is distinct from BST1-3. A. Schematic of the topology of BST4. BST4 is predicted to have four transmembrane domains and a disordered C-terminus containing two Rubisco Binding Motifs (RBMs) **B.** AlphaFold v2 models of two BST4 bestrophin domains (amino acid residues 53-386 shown for clarity) to show a typical bestrophin channel pore. Pore lining residues are highlighted in red. **C.** AlphaFold v2 structure of the BST4 bestrophin domains alongside the predicted structure of another bestrophin-like protein from *Chlamydomonas reinhardtii* (*Cr*BST1; Alphafold amino acids 51-end shown for clarity), and experimentally determined structures of bestrophins *Malus domestica* voltage-dependent Cl^- channel 1 (*Md*VCCN1;7EK1) and *Homo sapiens* Bestrophin 1 (*Hs*BEST1; 8D1I). Residues known to line the channel pore are highlighted. **D.** Phylogenetic analysis of the BST4 bestrophin domain (bold) with the disordered C-terminal removed. The alignment used was trimmed at residue 369. The evolutionary history of BST4 was inferred by using the maximum likelihood method based on the Le and Gascuel substitution model with discrete Gamma distribution (5 categories) and 500 bootstrap replicates. The tree is drawn to scale, with branch lengths measured in the number of substitutions per site.

As well as being distinct at a sequence level, BST4 also localizes differently from BST1-3 (**Fig. 2**). While BST1-3 localize throughout the thylakoid membrane and are enriched at the pyrenoid periphery (Mukherjee et al., 2019), BST4 localizes to the centre of the pyrenoid in a pattern that resembles the pyrenoid thylakoid tubule system (**Fig. 2A, B**; Meyer et al., 2020). To confirm tubule localization, we generated a dual-tagged line that expressed BST4-mScarlet-I and the Chlamydomonas Rubisco small subunit 1 (***Cr*RBCS1**) fused to Venus. BST4-mScarlet-I was enriched where

173 *Cr*RBCS1-Venus was depleted (**Fig. 2C, D**), indicating that BST4 is located in the
174 tubules and not the Rubisco-enriched pyrenoid matrix. Previous work suggests that
175 the C-terminal RBMs of BST4 enable the protein to interact with *Cr*RBCS1 (Meyer et
176 al. 2020). We confirmed using a yeast-2-hybrid approach that the C-terminus of BST4
177 interacts with *Cr*RBCS1 (**Fig. S2A**). We also measured the efficiency of Förster
178 resonance energy transfer (**FRET**) from Venus to mScarlet-I and found that the FRET
179 efficiency was ~35%, supporting the proximity of BST4 to *Cr*RBCS1 (**Fig. S2B**).

180 Bestrophins typically form pentameric assemblies (Bharill et al., 2014; Hagino et al.,
181 2022). When five chains of BST4 were inputted to AlphaFold a typical bestrophin
182 pentameric structure was predicted (**Fig. 2E**). To test the complex assembly of BST4
183 *in vivo*, we utilized a Slimfield microscopy molecular tracking method (Plank et al.,
184 2009). For this method, it is important to have only fluorescently tagged BST4
185 molecules and no native (untagged) BST4 molecules. To find a strain that was
186 impaired in the accumulation of BST4 protein, we screened *bst4* insertional mutants
187 from the CLiP library (Zhang et al., 2014; Li et al., 2019) and confirmed a mutant strain
188 (***bst4***) (**Fig. S3** and methods). We then expressed BST4-mScarlet-I in the *bst4* mutant
189 background (**Fig. S3**). We used Slimfield microscopy to image BST4 in the pyrenoid
190 tubules and subsequent image analysis (detailed in methods) to track individual
191 fluorescent molecules of BST4-mScarlet-I and quantified the number of BST4
192 monomers per complex. The resulting probability distribution revealed that the most
193 common BST4 complex is made up of five molecules (**Fig. 2F**). Other peaks showed
194 complexes with numbers of molecules divisible by five, which may be multiple
195 pentameric channels grouping together. The interval between the probability peaks
196 was also five (**Fig. 2G**). To further support higher order complex assembly of BST4
197 we ran purified Chlamydomonas thylakoid membranes on a Blue Native-PAGE gel
198 (**BN-PAGE**) and immunodetected BST4 (**Fig. 2H**). BST4 formed a smear at ~1000
199 kDa, which is considerably larger than a pentamer (~330kDa). This could be due to
200 higher order assemblies of BST4, pentameric BST4 in a complex with other proteins
201 and/or aberrant migration during BN-PAGE due to influences by complex shape.
202 Collectively, our data support *in vivo* higher order assembly of BST4 potentially as a
203 pentamer.

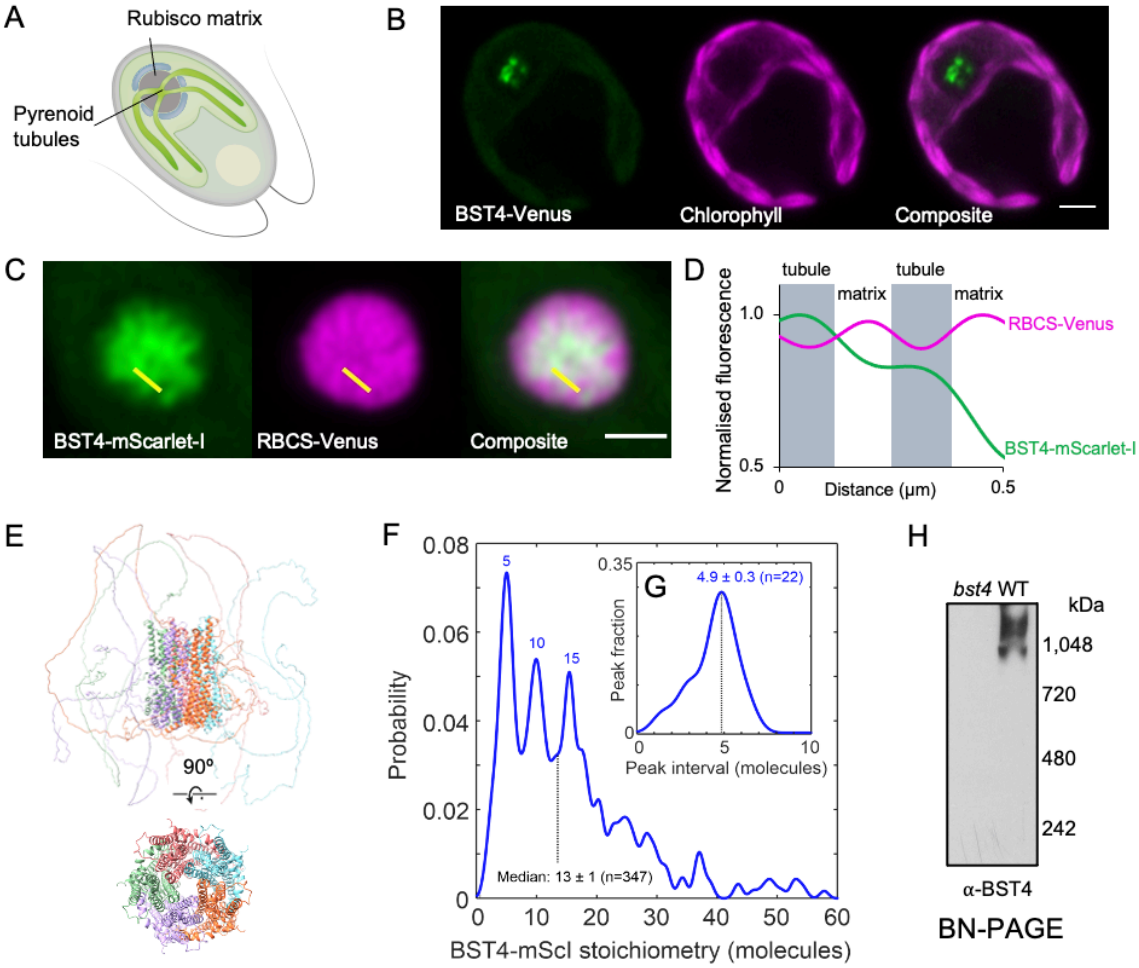

Figure 2. BST4 forms higher order assemblies in the pyrenoid tubules in Chlamydomonas. A. Diagram of a Chlamydomonas cell with the pyrenoid Rubisco matrix and pyrenoid tubules indicated. **B.** Confocal image of a Chlamydomonas cell expressing BST4-Venus. Scale bar is 2 µm. **C.** Pyrenoid in dual-tagged Chlamydomonas. BST4-mScarlet-I and RBCS-Venus are shown in green and magenta, respectively. Overlap appears white. The yellow line shows the 1D cross-section used for generating the line plot in (D). Scale bar is 1 µm. **D**. Plot of normalized fluorescence intensity values from a 1D cross-section from (C). mScarlet-I and RBCS-Venus are shown in green and magenta, respectively. **E**. AlphaFold Multimer v2 prediction of pentameric BST4 structure. Top structure includes the disordered C-terminus, bottom structure displays amino acid residues 53-386 only for clarity. **F**. BST4-mScarlet-I stoichiometry probability distribution based on single particle tracking and molecular counting in live Chlamydomonas (n=347 tracks) using Slimfield microscopy. **G**. Averaging the intervals between peaks in BST4-mScarlet-I stoichiometry (n=22 intervals) indicates a consistent pentameric unit. **H**. Immunoblot of proteins from *bst4* mutant and wild type (WT) Chlamydomonas thylakoids separated by Blue Native-PAGE.

BST4 localizes to the stroma lamellae thylakoid membrane in Arabidopsis

We used *Arabidopsis thaliana* (**Arabidopsis** hereafter) as a heterologous system to examine if BST4 was able to tether the Rubisco matrix to thylakoid membranes. In previous work, an Arabidopsis Rubisco small subunit (*At*RBCS) double mutant (*1a3b*) was complemented with *Cr*RBCS2, resulting in a line with hybrid Rubisco representing

221 ~50% of the Rubisco pool (**S2$_{Cr}$**) (Izumi et al., 2012; Atkinson et al., 2017). Subsequent
222 expression of the pyrenoid linker protein Essential PYrenoid Component 1 (**EPYC1**),
223 in S2$_{Cr}$ resulted in the formation of an EPYC1-hybrid Rubisco condensate or 'proto-
224 pyrenoid' (Atkinson et al., 2020). The S2$_{Cr}$ line was therefore used as a platform to test
225 whether BST4 acts as a tether protein.

226 We initially localized a BST4-mNeon fusion protein following stable expression in S2$_{Cr}$
227 (**Fig. 3**). BST4-mNeon was observed in chloroplasts, demonstrating that the native
228 chloroplast signal peptide was compatible with the chloroplast targeting mechanism in
229 land plants (**Fig. 3A**), as seen previously for other Chlamydomonas proteins (Atkinson
230 et al., 2016). The fluorescence signal from BST4-mNeon had a sponge-like pattern
231 that was inversely correlated with the punctate chlorophyll autofluorescence signal that
232 represents the grana stacks (**Fig. 3B, C**). The sponge-like pattern was similar to
233 previous observations of autofluorescence originating from Photosystem (**PS**) I
234 (Hasegawa et al., 2010), which is enriched in the stroma lamellae of thylakoids. We
235 subsequently generated a stable Arabidopsis transgenic line expressing untagged
236 BST4 to confirm its location by biochemical fractionation. BST4 was detected in the
237 thylakoid fraction and not in the stromal fraction (**Fig. 3D**). The thylakoids were then
238 further fractionated into grana stacks and stroma lamellae sub-fractions. BST4 was
239 found in the stroma lamellae fraction (**Fig. 3E**), which is consistent with the observed
240 sponge-like fluorescence pattern.

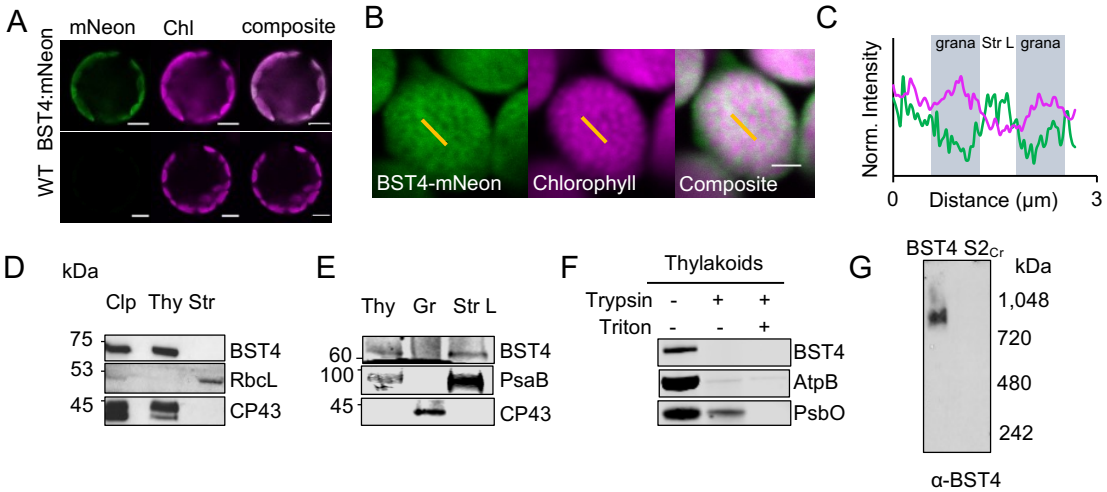

241

242 **Figure 3. BST4 assembles as a complex in the stroma lamellae of thylakoids in Arabidopsis. A.** Confocal
243 image of WT protoplasts expressing BST4-mNeon. Scale bar is 5 µm. **B.** Mesophyll chloroplast from S2$_{Cr}$
244 Arabidopsis expressing BST4-mNeon. BST4mNeon and chlorophyll autofluorescence are shown in green and
245 magenta, respectively. Overlap appears white. Scale bar is 2 µm. Yellow lines indicate selections for profile plot in

(C). **C.** Plot of normalized fluorescence intensity values from a 1D cross-section (yellow line) through two grana stacks from (B). mNeon and chlorophyll autofluorescence are shown in green and magenta, respectively. **D.** Immunoblots of sub-chloroplast fractions isolated from Arabidopsis line $S2_{Cr}$ expressing BST4. RbcL and CP43 were probed for as stromal and thylakoid controls, respectively. **E.** Immunoblots of fractionation thylakoids from Arabidopsis line $S2_{Cr}$ expressing BST4. CP43 and PsaB were used for grana stack and stroma lamellae controls, respectively **F.** Trypsin protease protection assay. Intact thylakoids containing BST4 subjected to 0 or 100 µg/ml trypsin with or without the addition of 1% (v/v) Triton. AtpB and PsbO used as controls for stromal facing (exposed) and lumen facing (protected), respectively. **G.** Immunoblot of proteins from thylakoids separated by Blue Native-PAGE from either BST4 stable line or $S2_{Cr}$ background. Abbreviations: Clp, whole chloroplast; CP43, CP43-like chlorophyll binding protein; RbcL, Rubisco large subunit; PsbO, photosystem II manganese-stabilizing polypeptide;AtpB, ATP synthase subunit beta; PsaB, photosystem I P700 chlorophyll a apoprotein A2; Str, stromal fraction; Thy, thylakoid fraction.

As BST4 has two RBMs on its C-terminus, we hypothesized that BST4 should be orientated with the C-terminus facing the stroma so that the RBMs are available to interact with *Cr*RBCS. To determine the orientation of BST4, we performed a protease protection assay on thylakoids isolated from the untagged BST4 transgenic plants. Our antibody was raised against the C-terminal end of BST4, so it could be used to assess whether the C-terminus was exposed for degradation in the stroma or if it was protected in the lumen. We found that the BST4 C-terminus was fully degraded after a 60 min treatment of trypsin, indicating that it faced the stroma (**Fig. 3F**). There was some degradation of the lumenal control, the PSII subunit PsbO, which we attribute to a portion of the thylakoid membrane preparation not being fully intact. However, PsbO was fully degraded when the membranes were solubilized, indicating that they were sufficiently intact to differentiate between lumenal- and stromal-facing peptides. Therefore, BST4 was observed in the expected location and orientation in plant thylakoid membranes.

Finally, we also tested whether BST4 forms a complex in the Arabidopsis thylakoid membrane. We subjected thylakoids from the untagged BST4 transgenic plants to BN-PAGE and detected a single band of ~850 kDa (**Fig. 3G**). Thus, BST4 forms a similar high order complex in Arabidopsis to that in Chlamydomonas but may be lacking additional interaction partners present in Chlamydomonas.

BST4 is not sufficient for integration of thylakoids into the Arabidopsis proto-pyrenoid

To test whether BST4 could facilitate incorporation of thylakoids into hybrid Rubisco condensates (i.e., proto-pyrenoids) in plants, BST4-mCherry and EPYC1-tGFP were co-expressed in the $S2_{Cr}$ background (**Fig. 4**). When we expressed EPYC1 alone, Rubisco condensates formed in chloroplasts as previously described (Atkinson et al.,

283 2020), and were visible as a ~2 μm wide puncta in the tGFP channel (**Fig. 4A**). When
284 BST4-mCherry and EPYC1-tGFP were co-expressed, approximately 60% of the
285 BST4-mCherry fluorescence signal was observed in the condensate region (**Fig. 4B,**
286 **D**), with the remaining signal exhibiting the same sponge-like pattern as seen in **Fig.**
287 **3A**.

288 To confirm that the observed co-localization was due to an interaction between BST4
289 and *Cr*RBCS2, we mutated the first two residues of each core RBM motif of BST4 to
290 glutamic acid (WR to EE, the new version noted $BST4_{WR/EE}$). Previously, these
291 substitutions have been reported to disrupt the binding interface between EPYC1 and
292 *Cr*RBCS2 (He et al., 2020). Using yeast-2-hybrid we confirmed that the interaction
293 between the C-terminus of BST4 and *Cr*RBCS2 was disrupted by these mutations
294 (**Fig. S3**). When $BST4_{WR/EE}$-mCherry was expressed with EPYC1-tGFP in $S2_{Cr}$, no
295 enrichment of the mCherry signal was observed in the Rubisco condensate (**Fig. 4C,**
296 **D**). Thus, the RBMs of BST4 were responsible for the enrichment of BST4 in the
297 vicinity of the Rubisco condensate in Arabidopsis.

298 However, when condensates were sedimented and analysed by immunoblotting,
299 BST4-mCherry was not detected in the condensate fraction (**Fig. 4E**). When leaf
300 samples were subjected to formaldehyde cross-linking prior to sedimentation of the
301 condensate, a small amount of BST4 was present in the condensate fraction. We
302 concluded that BST4 was not present in the condensate itself but preferentially
303 occupied the thylakoid membranes surrounding the *Cr*RBCS2-enriched condensate
304 (Atkinson et al., 2020), likely due to interactions with *Cr*RBCS2.

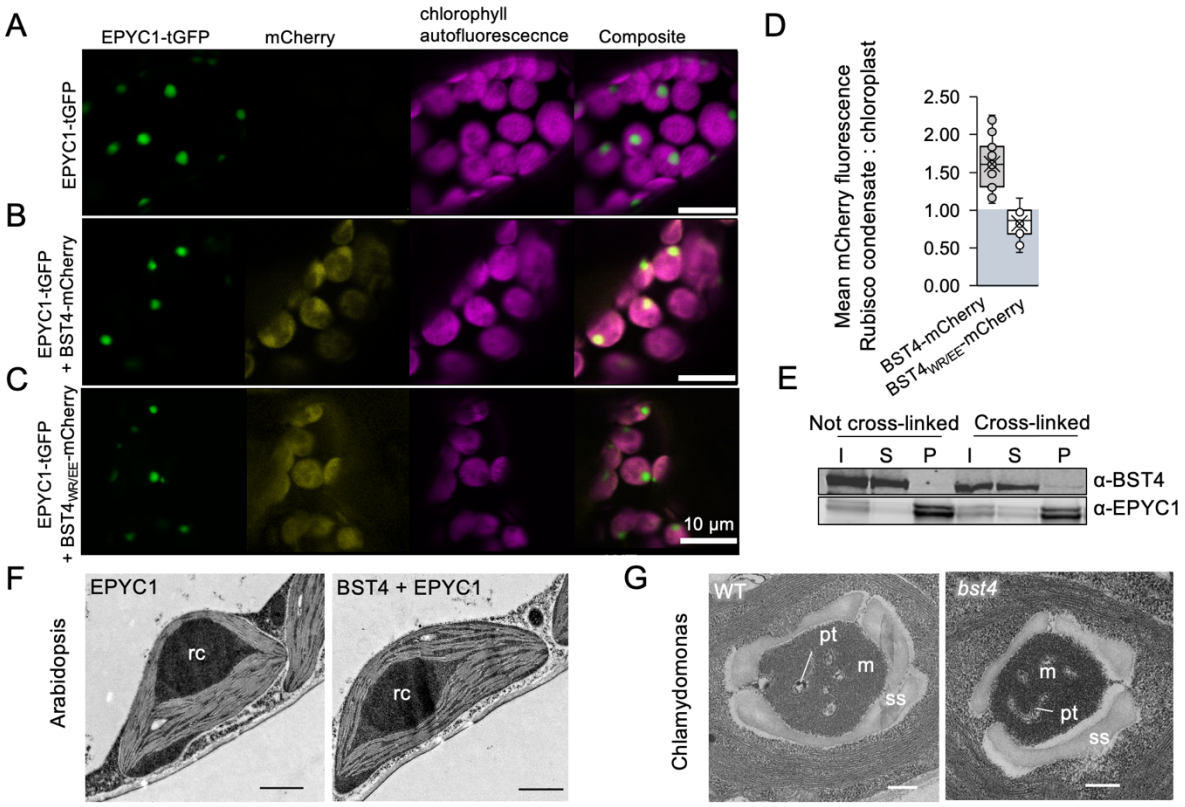

Figure 4. BST4 is not sufficient to enable the inclusion of thylakoid membranes in a Rubisco condensate in Arabidopsis and is not required for pyrenoid tubule inclusion in the Chlamydomonas pyrenoid. A. Confocal images showing EPYC1-tGFP in $S2_{Cr}$ Arabidopsis background. Scale bar is 10 µm. **B.** Confocal images showing BST4-mCherry co-expressed with EPYC1-tGFP in $S2_{Cr}$ Arabidopsis background. Scale bar is 10 µm. **C.** Confocal images showing BST4 with mutated RBMs ($BST4_{(WR/EE)}$) fused to mCherry co-expressed with EPYC1-tGFP in the $S2_{Cr}$ Arabidopsis background. **D.** Ratio of mean mCherry fluorescence associated with the Rubisco condensate compares do the rest of chloroplast when mCherry was fused to either BST4 or $BST4_{(WR/EE)}$ (n=22-23). **E.** Immunoblot of sedimented Rubisco condensates from $S2_{Cr}$ Arabidopsis expressing EPYC1-tGFP and BST4-mCherry. Abbreviations: I, input; S, supernatant; P, pellet. Rubisco condensates are enriched in the pelleted fraction. Cross-linked samples were prepared by vacuum infiltrating intact leaves with 1% (v/v) formaldehyde prior to sedimentation. **F.** Transmission electron micrograph of a chloroplast from $S2_{Cr}$ Arabidopsis expressing either EPYC1 alone or EPYC1-tGFP and BST4-mCherry. Rc is the Rubisco condensate. Scale bar is 1 µm. **G.** Transmission electron micrograph of pyrenoid from WT Chlamydomonas or *bst4* mutant. Abbreviations: pt, pyrenoid tubules; m, matrix; s, starch sheath. Scale bar is 250 nm.

Although BST4 partially co-localized with the Rubisco condensate, we found no evidence to suggest that BST4 could facilitate the inclusion of thylakoid membranes. Confocal microscopy was not sufficient to determine if chlorophyll autofluorescence was in the proto-pyrenoids of $S2_{Cr}$ lines expressing BST4-mCherry and EPYC1-tGFP. However, transmission electron microscopy (**TEM**) revealed no visible indication of thylakoid membranes in the condensates, which were structurally similar to

325 condensates in $S2_{Cr}$-EPYC1 lines lacking BST4 (**Fig. 4F**). Thus, BST4 appeared
326 insufficient to enable thylakoid inclusion in the Rubisco condensate in Arabidopsis.

327 **BST4 is not necessary for tubule formation in Chlamydomonas**

328 To investigate whether BST4 was necessary for normal formation of the thylakoid
329 tubule-structure in Chlamydomonas we compared the structure of pyrenoids of *bst4*
330 compared to the WT control strain (CMJ030) (Zhang et al., 2014; Li et al., 2019). TEM
331 images showed that pyrenoids from *bst4* were structurally comparable to the WT
332 control, including the presence of pyrenoid tubules (**Fig. 4G**). There were also no
333 differences in pyrenoid size or shape between the two lines when comparing pyrenoids
334 from 40-50 cells from each genotype (**Fig. S4**). As a result, we conclude that BST4 is
335 not necessary for the pyrenoid tubule-Rubisco matrix interface in Chlamydomonas.

336 **The C-terminus of BST4 is required for localization to the pyrenoid tubules**

337 Multiple copies of the RBM are sufficient to target proteins to the pyrenoid (Meyer et
338 al., 2020). Furthermore, we have shown that the BST4 RBMs are required for RBCS
339 interaction via yeast-2-hybrid (**Fig. S2A)** and that they are required for enrichment with
340 the proto-pyrenoid in Arabidopsis (**Fig. 4B-D**). To investigate the role of the RBMs in
341 BST4 localization in Chlamydomonas, we generated a truncated version of BST4
342 (residues 1 to 386) that lacked the C-terminus containing the two RBMs ($BST4_{\Delta C\text{-term}}$)
343 and compared localization with full-length BST4 expressed in WT and the *bst4* mutant
344 (**Fig. 5 and Fig. S5**). $BST4_{\Delta C\text{-term}}$-mScarlet expressed in the *bst4* mutant line did not
345 localize to the pyrenoid tubules but was found throughout the thylakoid membrane
346 (**Fig. 5**). This is consistent with our findings in Arabidopsis with $BST4_{WR/EE}$ (**Fig. 4C**),
347 demonstrating that localization of BST4 is driven via RBM-Rubisco interaction. Thus,
348 the C-terminus is necessary for BST4 localization to the pyrenoid tubules in the
349 presence of the matrix. Collectively these data indicate that BST4 may require a pre-
350 existing pyrenoid tubule network to be localized in the pyrenoid rather than driving the
351 inclusion of thylakoid membranes into the Rubisco matrix or is redundant as a tether
352 protein.

353 When $BST4_{\Delta C\text{-term}}$-Venus was expressed in WT Chlamydomonas (i.e., that still
354 produced non-truncated BST4), we observed fluorescence throughout the thylakoids,
355 but with the majority of the signal still localized to the pyrenoid tubules (**Fig. S5**). We

356 conclude that BST4$_{\Delta C\text{-term}}$-Venus is recruited to the pyrenoid through an interaction
357 with the native full-length BST4, which is further evidence that BST4 oligomerizes.

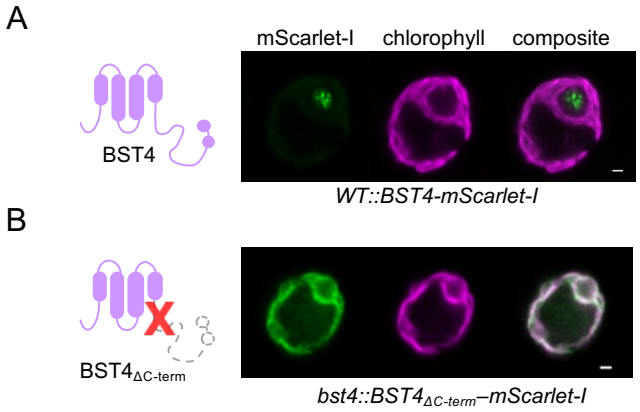

358

359 **Figure 5. C-terminus of BST4 is required for pyrenoid localization. A.** Confocal image of full length BST4-
360 mScarlet-I in WT **B**. Confocal image of BST4$_{\Delta C\text{-term}}$-mScarlet-I in *bst4*. Scale bars are 1 µm.

361 We next investigated whether BST4 localizes to the pyrenoid tubules, or whether
362 BST4 localizes to the tubules through an interaction with Rubisco. To do so, we utilized
363 a Chlamydomonas mutant generated by Genkov et al. (2010) that expresses *At*RBCS
364 but lacks both isoforms of *Cr*RBCS (*Crrbcs::AtRBCS*), and thus lacks a Rubisco matrix
365 as EPYC1 does not interact with *At*RBCS (Atkinson et al., 2019). *Crrbcs::AtRBCS*
366 retains reticulated thylakoid membranes at the canonical pyrenoid site, which are likely
367 the nascent pyrenoid tubule network (Caspari et al., 2017) (**Fig. S6A**). Caspari et al.
368 (2017) show large starch granules accumulating at the canonical pyrenoid site, which
369 we confirmed by expressing STA2-Venus as a starch marker (Mackinder et al., 2017)
370 in *Crrbcs::AtRBCS* (**Fig. S6B**). We expressed BST4-Venus in *Crrbcs::AtRBCS* and
371 found that BST4 localized to a punctum adjacent to the canonical pyrenoid site, which
372 we attribute to the nascent pyrenoid tubules (**Fig. S6C**). To confirm this, we also
373 expressed a known pyrenoid tubule marker protein, PsaF (Emrich-Mills et al., 2021)
374 in *Crrbcs::AtRBCS*, which showed a similar localization pattern to that of BST4 (Fig.
375 S6D). This suggests there may be an additional Rubisco-binding independent
376 mechanism for localization of BST4 as well as other proteins to the pyrenoid tubules.
377 Further investigation of the role of the whole C-terminal domain will be required to
378 understand the mode of BST4 pyrenoid tubule localization.

379 **Chlamydomonas *bst4* mutant is not defective in growth at air level CO_2 but**
380 **increased H_2O_2 production**
381 To test whether BST4 has a role in the operation of the CCM, we measured the growth
382 of *bst4* compared the WT control strain under various CO_2 conditions (**Figs. 6, S7**).
383 Spot assays did not reveal any reduction in growth under CO_2-limiting conditions (**Fig.**
384 **S7**). When grown in liquid medium, *bst4* even seemed to grow slightly better than WT
385 when sparged with 0.04% CO_2 (**Fig. 6A**). However, when comparing the calculated
386 specific growth rates (μ h^{-1}) for both the exponential growth phase (days 0-3, *bst4*
387 0.0402 ± 0.0003 μ h^{-1} and WT 0.0389 ± 0.0007 μ h^{-1}) or the full growth assay (days 0-
388 5, *bst4* 0.0257 ± 0.0001 μ h^{-1} and WT 0.0241 ± 0.001 μ h^{-1}), there was no statistically
389 significant increase in specific growth rates between *bst4* and WT (two-tailed t-test, p
390 = 0.17 and 0.20, respectively, n=3, full results **Table S1**). We conclude from these
391 experiments that BST4 is not essential for growth at air levels of CO_2 and might not
392 be necessary for the functioning of the CCM. We also included the complemented
393 *bst4::BST4* and *bst4::BST4*$_{\Delta C\text{-}term}$*-mScarlet-I* (hereafter *bst4::BST4*$_{\Delta C\text{-}term}$) lines in the
394 spot and liquid growth assays. While all lines grew well in the spot assay, in the liquid
395 growth *bst4::BST4*$_{\Delta C\text{-}term}$ grew comparably to WT and *bst4* whereas *bst4::BST4*
396 exhibited a slightly reduced growth than the other lines in both CO_2 conditions.

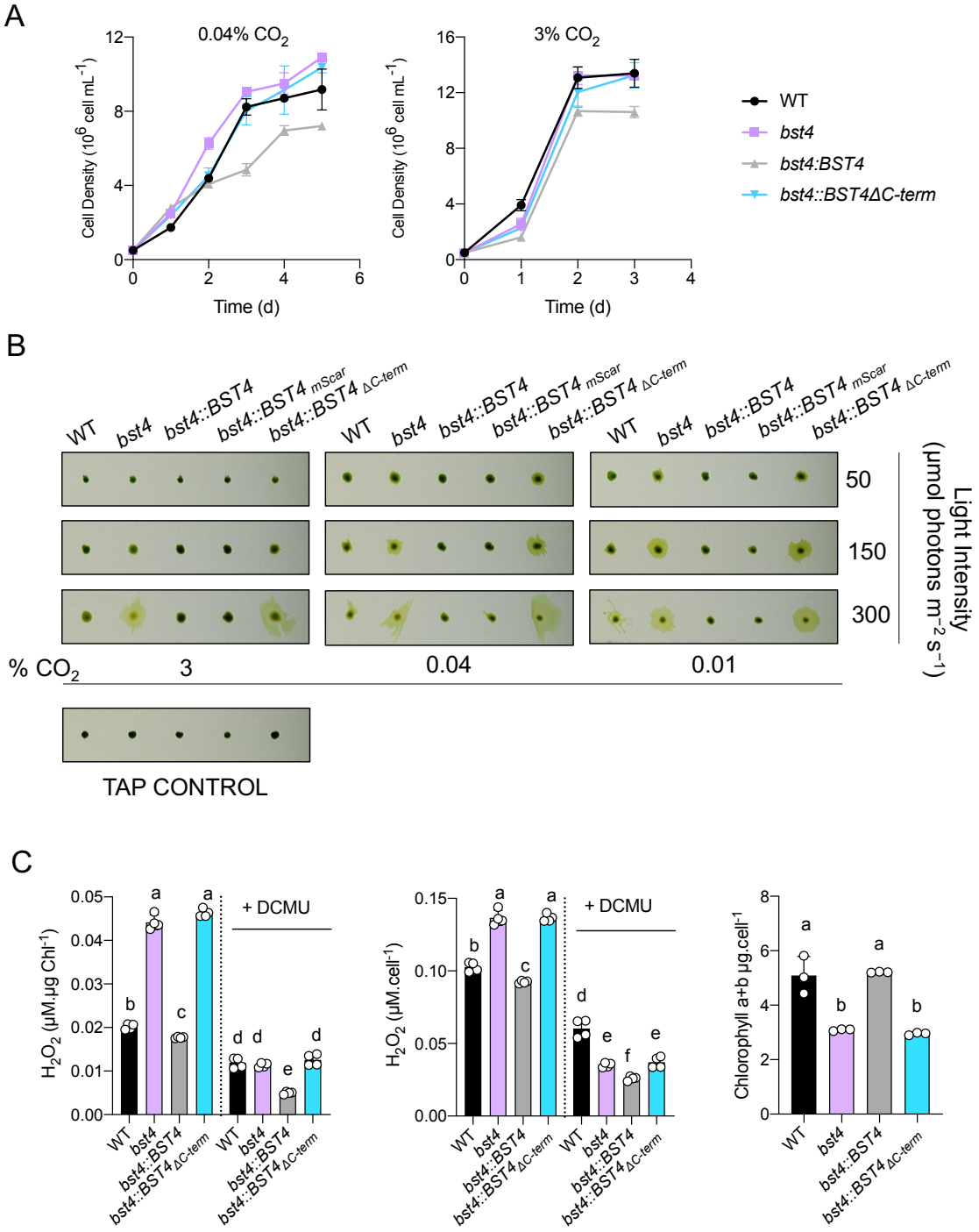

Figure 6. The *bst4* mutant does not have an impaired growth phenotype under CCM induced conditions but has increased H_2O_2 production. A. *Chlamydomonas* strains were subjected to a liquid growth assay using pH 7.4 TP media that was bubbled with 0.04% CO_2 or 3% CO_2 (+/- 2 ppm). Error bars are ± SEM (n=3). **B.** Dot assay of WT, *bst4,* complemented *bst4::BST4* and *bst4* complemented with C-terminal truncation of BST4 (*bst4::BST4*$_{\Delta C\text{-term}}$) on minimal pH 7.4 TP agar at indicated light intensities and CO_2 concentrations. **C.** H_2O_2 assay. Chlamydomonas cells were grown in pH 7.4 TP liquid media and exposed to 150 µmol photons $m^{-2}s^{-1}$ for 24 h with or without the photosynthetic inhibitor DCMU (10 µM). The concentration of H_2O_2 was subsequently quantified using Amplex Red (n=4), and is presented both proportionately to cell density and chlorophyll content. Chlorophyll content was quantified for all cell lines (n=3). Different letters indicate significance ($p<0.05$) as determined by a one-way Anova and Tukey's post-hoc test.

408 One noticeable difference between *bst4* and WT lines from the growth assays
409 conducted on solid media (**Fig. 6B and S7**) was that *bst4* cells had a distinct halo of
410 diffuse cells on the periphery of the colony. We used a range of CO_2 and light
411 conditions to investigate the diffuse colony phenotype (**Fig. 6B**) and found it was most
412 apparent under high light (300 µmol photons m^{-2} s^{-1}) and low or very low CO_2
413 conditions (0.04% CO_2, 0.01% CO_2, respectively) (**Fig. 6B**). WT, *bst4::BST4* and
414 *bst4::BST4-mScarlet-I* complemented lines had little or no diffusivity, although WT did
415 display a slightly diffuse colony phenotype at 300 µmol photons m^{-2} s^{-1}. Interestingly,
416 *bst4::*BST4$_{\Delta C\text{-term}}$ was unable to rescue the diffuse colony phenotype suggesting that
417 either the presence of the C-terminus or localization to the tubules is essential for the
418 function of BST4.

419 The diffuse colony phenotype was most apparent under high light (300 µmol photons
420 m^{-2} s^{-1}), to a slightly lesser extent at medium light (150 µmol photons m^{-2} s^{-1}), and
421 exacerbated by low CO_2 (0.01% and 0.04%). These are conditions where carbon
422 fixation can be limiting and therefore, the energy production by photosynthesis could
423 exceed the energetic demand required to fix CO_2 by the CCM and the Calvin cycle.
424 This imbalance can result in the release of Reactive Oxygen Species (**ROS**) (Erickson
425 et al., 2015). Because cells exposed to ROS have altered phototactic responses to
426 light (Wakabayashi et al., 2011), we thus thought to assess the phototactic capacity of
427 *bst4* and its control WT strain by exposing them to directional light in liquid culture
428 (**Fig. S8A**). In this assay, *bst4* cells displayed strong positive phototaxis, whereas WT
429 and complemented *bst4::BST4* lines displayed negative phototaxis. To test whether
430 the phototactic response of *bst4* was due to an increase in ROS production, we
431 recorded the direction of phototaxis in cells exposed to either ROS or a ROS quencher.
432 In the presence of the ROS quencher N,N'-dimethylthiourea (**DMTU**), *bst4* positive
433 phototaxis was disrupted, resulting in a negative response to directional light (**Fig.
434 S8A**). When the ROS H_2O_2 (75 µM) was added, WT, *bst4::BST4* and *bst4* displayed
435 positive phototaxis (**Fig. S8A**). To directly quantify the difference in ROS generation,
436 we analysed the H_2O_2 produced by cells exposed to 150 µmol photons m^{-2} s^{-1} (**Fig.
437 6C**). The *bst4* and *bst4::BST4$_{\Delta C\text{-term}}$* lines had significantly higher H_2O_2 production than
438 WT and *bst4::BST4* when normalized to both chlorophyll content and cell density. We
439 validated the assay by using the same ROS quencher DTMU from **Fig. S8A**, and saw
440 a consistent reduction in H_2O_2 detected in all lines **Fig. S8B**. To test the involvement

441 of photosynthetic activity in the increased ROS production, we also treated cells with
442 the PS II plastoquinone binding site inhibitor 3-(3,4-dichlorophenyl)-1,1-dimethylurea
443 (DCMU) whereby the concentration of H_2O_2 produced was reduced in all lines (**Fig.**
444 **6C**). The cellular chlorophyll content was also assessed, we found that *bst4* and
445 *bst4::BST4$_{\Delta C\text{-}term}$* had significantly lower cellular chlorophyll content than WT and
446 *bst4::BST4.* The reduction in cellular chlorophyll and the increase in ROS scavenging
447 pigments is a known physiological response to high light exposure and subsequent
448 elevated ROS production (Bonente et al., 2012) and is consistent with other studies
449 (Ma et al 2020; Erikson et al 2015).

450 ROS generation occurs when light energy exceeds the capacity of electron transport,
451 which can be caused by either high light conditions or limited CO_2 fixation due to an
452 impaired CCM or low CO_2 availability (Santhanagopalan et al., 2021; Choi et al., 2022).
453 As *bst4* can maintain similar growth to WT under low CO_2 conditions, we conclude that
454 the absence of BST4 might affect photosynthesis more broadly and not specifically
455 influence the sustained delivery of CO_2 to Rubisco.

456 **BST4 regulates the lumenal pH in Chlamydomonas during dark to light**
457 **transition**

458 To assess the impact of BST4 on photosynthesis, we used a pulsed amplitude
459 modulation fluorimeter (**PAM**) to measure chlorophyll fluorescence upon a dark to light
460 transition in all the strains (**Fig. 7**). We used the PAM to assess the quantum yield of
461 PSII (**Y(II)**) and the amount of non-photochemical quenching of chlorophyll
462 fluorescence (**NPQ**) (**Fig. S9**). NPQ is mediated by multiple mechanisms and harbors
463 multiple components (Erickson et al., 2015), one of them, termed energy-dependent
464 quenching, (**qE**) is quickly induced and relaxed and is mostly mediated by the activity
465 of the proton-sensing Light Harvesting Complex Stress related 3 (**LCHSR3**) protein
466 (Bonente et al., 2011; Peers et al., 2009; Steen et al., 2022; Tian et al., 2019). The
467 magnitude of qE has recently been shown to be an indicator of the lumenal pH, the
468 lower the pH, the higher the qE (Burlacot et al., 2022; Tian et al., 2019). While no
469 differences in Y(II) were observed between the strains upon a dark to light transition
470 (**Fig. S9C, D**), the NPQ of *bst4* mutant was transiently higher than WT (**Fig. 7A**), the
471 NPQ becoming undistinguishable from WT after three minutes of illumination (**Fig.**

7A). The complementing *bst4::BST4* strain was undistinguishable from the WT control during

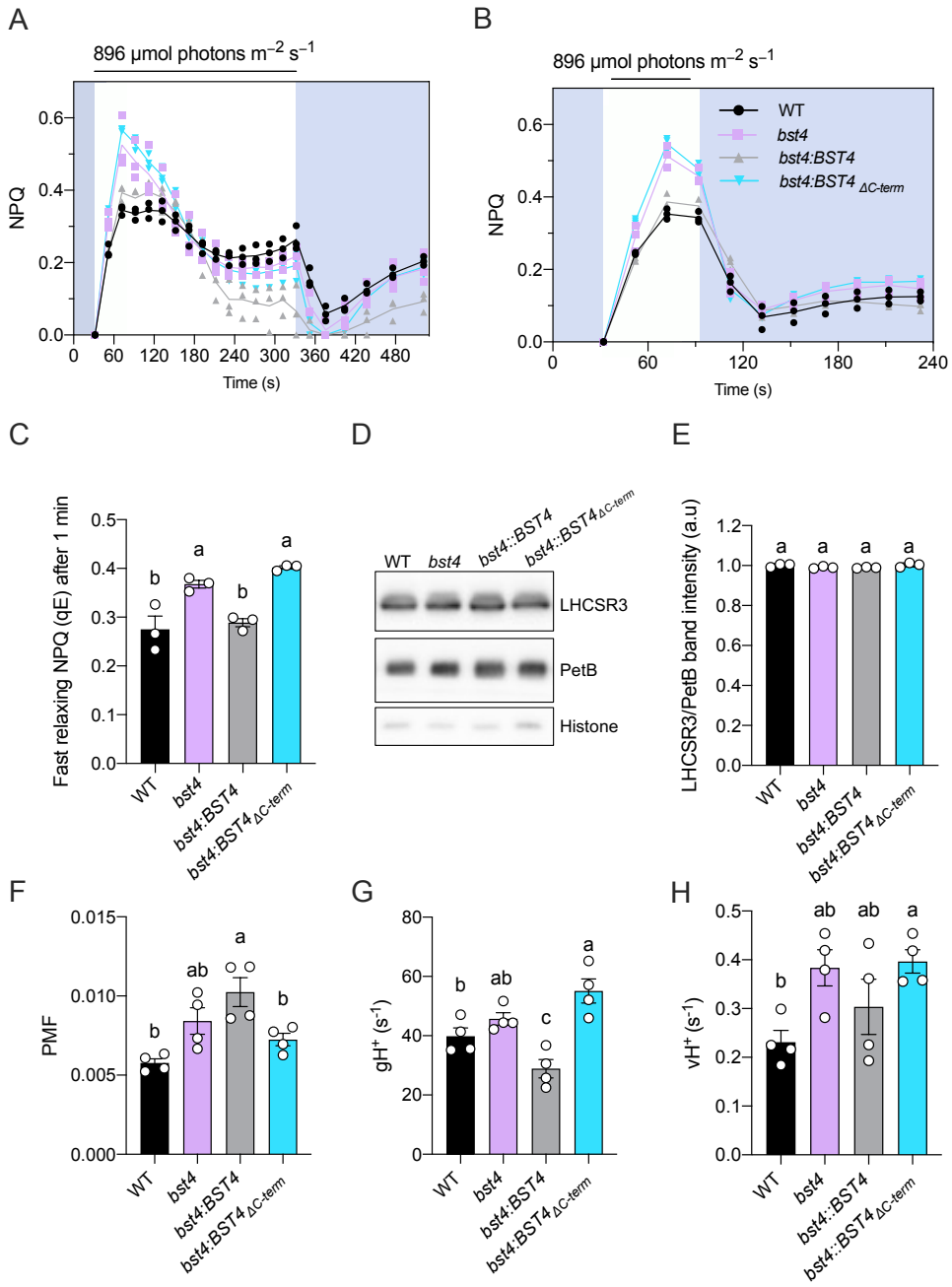

Figure 7. Chlamydomonas *bst4* mutant has an enhanced initial NPQ response under limiting Ci conditions. Wild type (WT) and mutants were grown in HS medium at 80 µmol photons m^{-2} s^{-1} and measured at 10 µg Chl ml^{-1} (prepared by dilution). The cells were dark adapted for 5 min before the measurements. **A.** Dynamics of Non-photochemical quenching (NPQ) on transition from dark to high light. Kinetics for induction of chlorophyll fluorescence were recorded during 5 min of illumination at 896 µmol photons m^{-2} s^{-1} followed by 5 min in darkness. **B.** Dynamics of NPQ during dark to light transition with one minute of light exposure. Shown are individual data points (dots) and their average (lines) **C.** Calculated fast relaxing NPQ after one minute of light exposure as determined by NPQ at the light to dark transition minus the minimum NPQ in the dark. **D.** Immunoblot of NPQ protein LHCSR3 in each strain plus PetB and Histone as loading controls.* **E.** Quantification of LHCSR3 band

483 intensity normalized to PetB. Each point is the mean of two technical replicates from one biological replicate. **F.**
484 Total proton motif force (PMF) as measured from ECS measurements. Shown are average of 3 technical replicates
485 for each biological replicates (n=4 biological replicates) **G.** Proton conductance (g_H^+) and **H.** proton flux (v_H^+) were
486 determined after 1 min illumination at 890 µmol photons m^{-2} s^{-1}. (n=4 biological replicates). Bars show the mean
487 ±SEM. Different letters indicate significance ($p<0.05$) as determined by a one-way ANOVA and Tukey's post-hoc
488 test.

489 the first three minutes of illumination and *bst4::BST4$_{\Delta C\text{-}term}$* had a NPQ similar to *bst4*
490 (**Fig. 7A**). To establish the nature of the transiently increased NPQ in *bst4*, we used a
491 shorter illumination time (**Fig. 7B**). The entirety of the 45% increase in NPQ for *bst4*
492 mutant was quickly dissipated (**Fig. 7 B, C**) suggesting that it could be attributed to
493 qE. Similar trends of NPQ kinetics were observed when cells were supplemented with
494 HCO_3^- before the measurement, although NPQ relaxation in the dark was different
495 between lines (**Fig. S10**). Since *bst4* did not accumulate more LHCSR3 as compared
496 to WT (**Fig. 7D, E**), we conclude that BST4 is involved in the lumenal pH regulation
497 upon a dark to light transition.

498 The build-up of lumenal H^+ concentration is usually accompanied with a build-up in the
499 proton motive force (**PMF**) across the thylakoid membrane, which is used by the
500 ATPase to generate ATP. We used Electrochromic Shift (**ECS**) measurements
501 (Bailleul et al., 2010) to measure the total PMF size, as well as initial PMF dissipation
502 rate (**g_H^+**) (**Fig. 7F, G & S11**). Interestingly, after one minute of illumination, which are
503 conditions where the lumenal pH was higher in *bst4* mutant, neither the PMF, g_H^+ nor
504 proton flux (**v_H^+**) differed between *bst4* and its WT strain. We conclude that the
505 changes induced by BST4 on the lumenal pH are either a small contribution to the pmf
506 formation or are compensated for in the *bst4* mutant.

507 To assess a longer timescale acclimation of the *bst4* mutant, we performed similar
508 measurements but on cells pre-treated with three hours of high light (150 µmol photons
509 m^{-2} s^{-1}) and for a longer time-period (**Fig. S12**). We found that *bst4* was able to
510 maintain a higher F_v/F_m than WT **(Fig. S12A),** had higher sustained NPQ compared to
511 WT, which was concurrent with a higher LHCSR3 expression as compared to the WT
512 strain **(Fig. S12B, G, H).** No significant differences in PMF or g_H^+ were observed
513 although v_H^+ was higher in *bst4* compared to WT (**Fig. S12D, E, I, J**). The higher v_H^+
514 together with the higher expression of LHCSR3 suggest a build-up of protons in the
515 tubule lumen. Since ROS induce photoprotective mechanisms (Roach & Na, 2017),

516 we propose that in the absence of BST4, enhanced production of ROS **(Fig. 6)** might
517 lead to enhanced NPQ and photoprotective mechanisms.

518 As a result of the NPQ difference seen between *bst4* and WT lines in response to
519 illumination, we proposed that BST4 might be an anion channel involved in regulating
520 the pH of the thylakoid lumen. Bestrophins are typically permeable to Cl^- and HCO_3^-.
521 A plant thylakoid bestrophin, *At*VCCN1, is permeable to Cl^- and is also active in the
522 first minutes of illumination to modulate the lumenal pH, although *vccn1* mutants have
523 lower NPQ (Herdean et al., 2016). Alternatively, like BST1-3, BST4 may be permeable
524 to HCO_3^- (Mukherjee et al., 2019). To determine what BST4 may be permeable to, we
525 expressed BST4 in Xenopus oocytes and measured currents in the presence of
526 different anions (**Fig. S13A**). No currents for BST4 were detected in the presence of
527 100 mM KCl or 100 mM $NaHCO_3$. As some bestrophins are autoinhibited by their C-
528 terminus (Qu et al., 2006), we also tested two C-terminal truncations of BST4 (0-386
529 and 0-591), but no currents were detected. Another possibility is that BST4 is
530 permeable to organic ions, similarly to *Hs*Best1, which has been shown to be
531 permeable to **γ**-aminobutyric acid (GABA) (Lee et al., 2010) and glutamate (Woo et
532 al., 2012), as well as Cl^- and HCO_3^- anions. Fei et al. (2022) proposed a model
533 whereby RuBP acts as proton carrier to increase H^+ concentration in the pyrenoid
534 tubules. It is possible that BST4 is the channel that facilitates RuBP translocation in
535 the tubules in this model. To test this hypothesis, we used small molecule analogues
536 K-PEP and K-Gluconate but no currents were detected for these either (**Fig. S13A**).
537 Therefore, we were unable to draw conclusions as to what BST4 is permeable to.
538 BST4 may require certain conditions to be open that are not met in the oocyte system,
539 such as post-translational modifications, a specific pH, a specific voltage, or an
540 interaction partner. BST4 was found to be phosphorylated and had an oxidized
541 methionine residue in its C-terminus (Bergner et al., 2015). Methionine oxidation can
542 serve as channel-regulating post translational modification (Ciorba et al., 1999), which
543 would fit with the role that BST4 appears to have in preventing oxidative stress.

544 **BST4 has no impact on growth and photosynthesis in Arabidopsis $S2_{Cr}$ line**

545 Although the permeability is undefined, if BST4 is a functional ion channel, it is possible
546 that its presence in plant thylakoid membranes might have an effect. We generated
547 three independent BST4 no tag lines in the $S2_{Cr}$ background and used them to assess

548 the impact of BST4 on Arabidopsis physiology (**Fig. S14A**). We found there was no
549 difference in growth between plant expressing BST4 and their azygous segregants,
550 as determined by the rosette area (**Fig. S14B**). We also found that BST4 expressing
551 plants tended to have slightly lower F_v/F_m as compared to azygous segregants and
552 the parent line, although this was not significant (**Fig. S15A**). Further measurements
553 were made for lines 2 and 3 on the kinetics of NPQ, Y(II) and for PMF size and
554 partitioning but no consistent differences were observed (**Fig. S15**).

555 **Proposed model for the role of BST4 in the Chlamydomonas pyrenoid**

556 Based on these findings, we propose that BST4 moderates the thylakoid lumen
557 through its function as a bestrophin channel and is influential in this role during the
558 transition from dark to light. Specifically, we propose that BST4 is a pentameric HCO_3^-
559 transmembrane channel found within the pyrenoid tubules but is not crucial for
560 Rubisco matrix tethering. Rather, BST4 is targeted to the tubules by the C-terminal
561 RBMs to facilitate its role in the pyrenoid. In its proposed primary role as a HCO_3^-
562 channel, BST4 may form part of a recovery system to take up HCO_3^- from within the
563 pyrenoid, allowing HCO_3^- to be transported back into the tubules where it could be
564 dehydrated to CO_2 and thus available to be fixed by Rubisco **(Fig. 8).** The close
565 proximity of BST4 to the luminal carbonic anhydrase CAH3 further supports this
566 hypothesis. As indicated by our NPQ data, this role might be helpful during the dark to
567 light transition where HCO_3^- is needed immediately to both moderate lumenal H^+
568 concentration and begin Ci uptake when Ci has not yet been transported into the
569 thylakoid tubules. In this scenario, the absence of BST4 would lead to an initial build-
570 up of protons as they are not being consumed by HCO_3^- dehydration, thus the initial
571 high NPQ. After a minute, the standard BST1-3 HCO_3^- uptake system would take over,
572 protons being used for HCO_3^- dehydration and resulting in pH stabilization and NPQ
573 relaxation. Over the longer term, a lack of BST4 may lead to a slight reduction in CCM
574 operation efficiency, perhaps not sufficient to cause a growth penalty but enough to
575 alter the homeostasis of photosynthesis and thus increase ROS production. Future
576 work is needed to determine what species BST4 is permeable to and how it is
577 regulated. In summary, BST4 might play a role in modulating the intricate dynamics
578 between the CCM and photosynthetic ion management, two physiological processes
579 that are key to algal primary productivity.

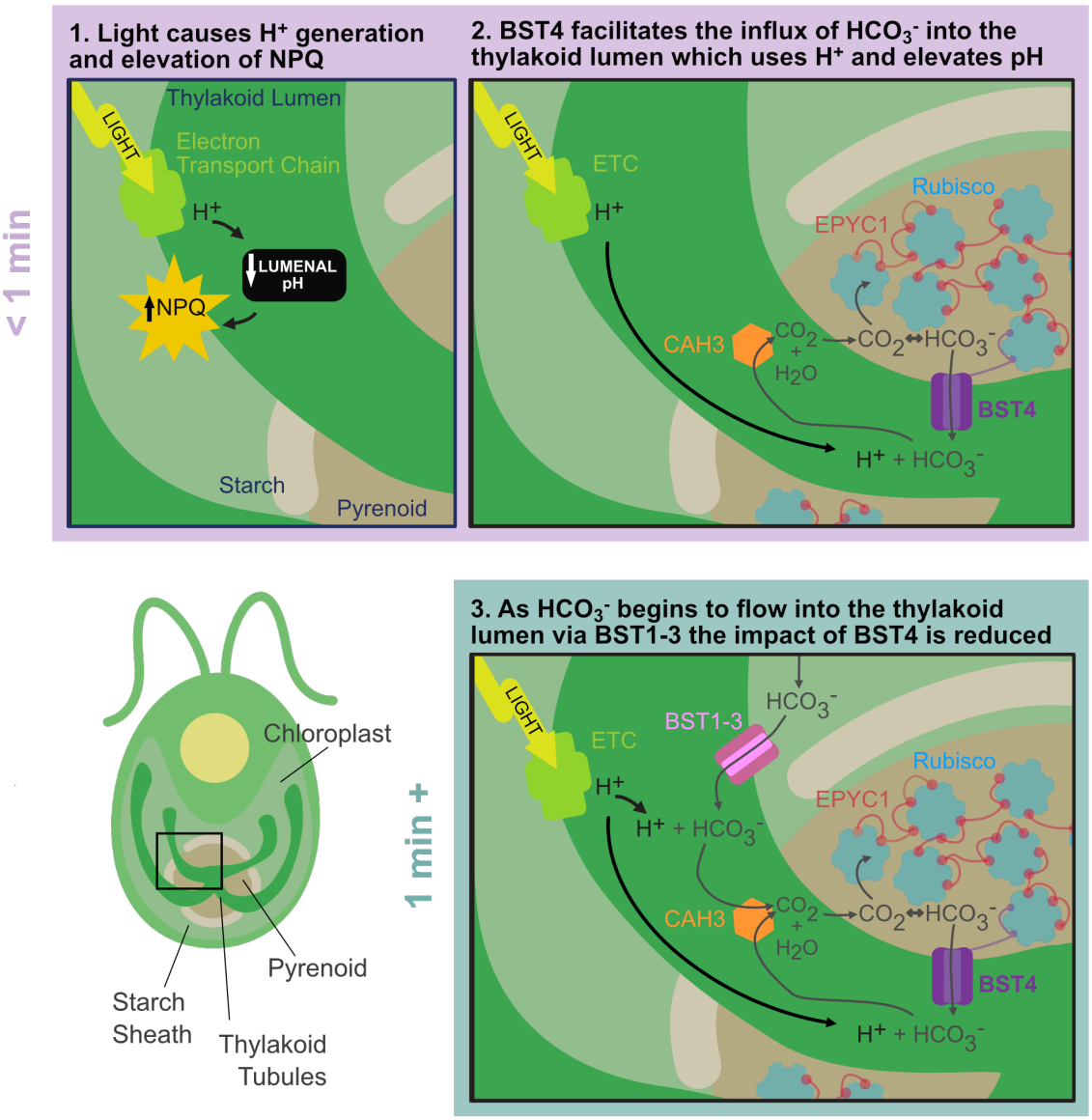

Figure 8. The role of BST4 in light and CO_2 limiting conditions. The data presented here indicate that BST4 moderates the thylakoid lumen through its function as a bestrophin channel and is influential in this role during the transition from dark to light**.** 1) When the light is turned on, protons are generated by the electron transport chain (ETC) resulting in a luminal pH decrease and NPQ is initiation. 2) BST4 allows the passage of HCO_3^- from the pyrenoid Rubisco-matrix into the lumen. The HCO_3^- is then dehydrated by the carbonic anhydrase CAH3 to generate CO_2, which can subsequently diffuse out of the lumen into the pyrenoid Rubisco-matrix for fixation. The conversion of HCO_3^- to CO_2 also acts as a sink for the protons generated by the ETC, increasing the luminal pH and reducing NPQ. This mechanism (shown in 1, 2) is most impactful in the first minute of illumination, after which **(3)** HCO_3^- also begins to enter the thylakoid lumen through BST1-3 and the impact of BST4 uptake is reduced.

593 **MATERIALS AND METHODS**

594 **Phylogenetic Analysis**

595 Amino acid sequences for phylogenetic analysis were compiled by blasting BST4
596 (Cre06.g261750) in the NCBI database (Sayer et al 2022) and the manual addition of
597 other well characterized bestrophin proteins including BEST1 *Homo sapiens*
598 (XP_011543531.1), KpBEST *Klebsiella aerogenes* (WP_049046555.1), VCCN1 from
599 *Arabidopsis thaliana* (Q9M2D2) and BST1-3 *Chlamydomonas reinhardtii*
600 (Cre16.g662600, Cre16.g663400 and Cre16.g663450). Sequences were aligned
601 using MAFFT (Katoh and Standley, 2013) visually inspected and manually trimmed
602 (specified). Finalized alignments were run through IQTREE webserver (Minh et al.,
603 2020) to identify the most appropriate substitution model. Maximum likelihood trees
604 were then generated in Geneious v11 using the PhyML 3.0 (Guindon et al., 2010)
605 plugin with a LG substitution model (Le and Gascuel, 2008) with Gamma distribution
606 (4 categories) and 500 bootstrap iterations. Full alignments are found in **Fig. S16**.

607 **Alphafold structure prediction**

608 Five chains of BST4 were submitted to Alphafold Multimer v2 with default settings.
609 using the ColabFold server (Mirdita et al., 2022). All protein structure figures were
610 generated using UCSF ChimeraX, developed by the Resource for Biocomputing,
611 Visualization, and Informatics at the University of California, San Francisco, with
612 support from National Institutes of Health R01-GM129325 and the Office of Cyber
613 Infrastructure and Computational Biology, National Institute of Allergy and Infectious
614 Diseases (Pettersen et al., 2021). The top ranked model of five was used for figure
615 generation.

616 **Generation of plasmids**

617 The plasmids for BST4 mutant complementation in *Chlamydomonas* were prepared
618 using a recombineering method described previously (Emrich-Mills et al., 2021). BST4
619 is expressed under native promotor with either without a tag or with an mScarlet-I C-
620 terminal tag, and a hygromycin AphVII selection marker. The same approach was
621 used to generate STA2-Venus lines in the *Crrbcs::AtRBCS* background (Genkov et
622 al., 2010).

623 Plasmids for plant expression were generated using the MoClo system (Engler et al.,
624 2014). For visualisation, BST4 was combined with 35S promoter (pICH51277),

625 mNeonGreen C-terminal tag (pICSL50015), HSP terminator and acceptor plasmid
626 (pICH47732) and a pFAST-R section cassette used for selection. For all other
627 experiments a no-tag BST4 construct was generated with the 35S protomer and HSP
628 terminator parts and a Kanamycin resistance cassette was used for selection.

629 Plasmids for Xenopus expression were generated by using the Gateway system by
630 cloning the coding sequence for BST4 into pGT vector (Grefen et al., 2010). *BST4*
631 was amplified with Gateway adaptor sequences from a synthesized as g-block (IDT)
632 with the PredAlgo (Tardif et al., 2012) predicted transit peptide removed from the N-
633 terminal (sequence begins R35), any subsequent mutations were made via PCR.

634 **Arabidopsis transformation**

635 Arabidopsis was transformed by floral dip as previously described in (Atkinson et al.,
636 2016). BST4-mNeon primary transformants were screened for transgene insertion by
637 seed fluorescence from pFAST-R and BST4 expression was confirmed by checking
638 for mNeon fluorescence and by immunoblot. BST4 no tag primary transformants were
639 screened using kanamycin resistance and immunoblot. Zygosity was checked via
640 seed fluorescence from pFAST-R or kanamycin resistance.

641 **Chlamydomonas cell culture conditions and strain details**

642 *Chlamydomonas reinhardtii* cultures were maintained as previously described (Ma et
643 al., 2011). Tris-Acetate-Phosphate (TAP) and minimal (TP) media (acetate free) were
644 prepared according to Sueoka (1960). TAP and TP agar plates for growth were made
645 by adding 1.5% (w/v) agar. CMJ030 (CC-4533; *cw15, mt$^-$)* and *bst4* (BST4 knock-out
646 LMJ.RY0402.159478) were obtained from the CLiP collection at the *Chlamydomonas*
647 culture collection (Zhang et al., 2014; Li et al., 2019). This CLiP mutant has two other
648 mapped CIB1 cassette insertions at loci Cre04.g230046 and Cre08.g367750. The
649 insertion of the CIB1 cassette in *BST4* locus was confirmed by PCR amplifying the
650 insertion locus from genomic DNA (Fig. S3A) using loci specific primers (forward
651 GAGCTTCGTGGATGGATGTT and reverse GTATGAAGGTCACCGCCTGT) in
652 parallel with a control locus (forward ATGCTTCTCTGCATCCGTCT and reverse
653 ATGTTTTACGTCCAGTCCGC). The additional two insertions were also confirmed
654 using loci specific primers for Cre04.g230046 (forward TGTGCCTCTGTCAGTCTTGG
655 and reverse TGCGTGGATGGGTAACAGTA), Cre08.g367750 (forward
656 AATCAAGAAGCTTCCCAGCA and reverse CCTACCGCTATCTCAGCCAG) and

657 STT7 locus as a control (forward GCACGAACCAAGACACACATAG and reverse
658 GTAGACGATGTCACCGCACTT). Therefore, the *bst4* knock-out was complemented
659 with *BST4* constructs described herein. All complemented lines were validated by
660 western blotting of BST4 and specified epitope tags, described below (Fig. S3B-E).

661 **Chlamydomonas transformation**

662 For each Chlamydomonas transformation, 28 ng kbp^{-1} of plasmid was linearized by
663 restriction digest. Cells were grown to 2 - 4 x 10^6 cell mL^{-1}, harvested by centrifugation
664 at 1000 xg for 10 min and resuspended in TAP with 40 mM sucrose at a concentration
665 of 2 × 10^8 cells mL^{-1}. Linearized plasmid was mixed with 250 µL of cells at 15°C in a
666 0.4 cm gap electroporation cuvette and transformed immediately by electroporation
667 using a Gene Pulser II (Bio-Rad) set to 800V and 25 µF. Cells were recovered
668 overnight in TAP sucrose while shaking gently (140 rpm) in the dark. Transformed cell
669 were subsequently subjected to selection by growth on TAP agar plates with
670 paromomycin (20 µg mL^{-1}) or hygromycin (25 µg mL^{-1}) which were kept in low light
671 (5–10 µmol photons m^{-2} s^{-1}) until screening positive transformants.

672 **Chlamydomonas Growth Assays**

673 Spot Tests: Cells were grown heterotrophically in TAP media. Once cultures reached
674 2 - 4 x 10^6 cell mL^{-1}, 1 x 10^6 cells were harvested by centrifugation at 1000 xg for 10
675 min. Cell were washed and resuspended at a concentration of 1 x 10^6 cell ml^{-1} in TP
676 media. Liquid cultures were spotted onto TP agar (1.5%) in 1000, 100 and 10 cell
677 spots at a range of pHs (specified). The plates were incubated in 3, 0.04 and 0.01%
678 CO_2 and illuminated under constant light at 400 µmol photons m^{-2} s^{-1}. Growth was
679 monitored for up to 10 days.

680 Liquid Growth: Cells were grown heterotrophically in TAP media. Once cultures
681 reached 2-4 x 10^6 cell mL^{-1}, cells were harvested by centrifugation at 1000 xg and
682 resuspended at a starting concentration of 1 x 10^5 cell ml^{-1} in TP media pH 7.4.
683 Cultures were incubated in a CellDEG HDC 22.10 culture platform (CellDeg GMBH,
684 Berlin) bubbled with 0.04 and 3% CO_2, illuminated at 150 µmol photons m^{-2} s^{-1} and
685 consistently stirred at 180 rpm. Cell density and optical destiny (750 nm)
686 measurements were taken daily for up to 10 days. Specific growth rates (SGR) per h
687 were calculated using the following formula: $\mu = ln(N_2/N_1)/t$ whereby N = cell density

688 Dot tests: Cultures were grown in a 96 format on agar plates and replicated by a Rotor+
689 (Singer Instruments) high throughput replication robot. The cultures were stamped
690 onto pH 7.8 TP agar plates, incubated in 3, 0.04 and 0.01% CO_2 and illuminated under
691 constant light at a range of intensities (specified). Growth was monitored for up to 10
692 days.

693 **Phototaxis Assays**

694 Chlamydomonas cells were grown heterotrophically in TAP media until they reached
695 2 - 4 x 10^6 cell mL^{-1} and harvested by centrifugation at 1000 xg for 10 min. Pelleted
696 cells were either re-suspended in TP media or, for ROS manipulation assays, a
697 phototaxis buffer described previously by Ueki et al. (2016) (5 mM Hepes pH 7.4, 0.2
698 mM EGTA, 1 mM KCl, and 0.3 mM $CaCl_2$). The assays took place in 12-well dishes
699 with a thin layer of TP agar (0.8%) on the well bottom and approximately 1.5 x 10^7
700 cells in 400 µL of homogenous suspension laid on top. The dishes were illuminated
701 from one direction with 150 µmol photons m^{-2} s^{-1} illumination for up to 3 h. Plates were
702 imaged using a Flatbed Scanner at specified intervals.

703 **Quantification of H_2O_2**

704 Cells were grown heterotrophically in TAP media. Once cultures reached 2 - 4 x 10^6
705 cell mL^{-1}, cells were harvested by centrifugation at 1000 xg and resuspended at a
706 concentration of 2 x 10^6 cell ml-1 in TP media pH 7.4, illuminated at 150 µmol photons
707 m^{-2} s^{-1} for 24 h and shaken at 140 rpm. For H_2O_2 quantification, 1 mL of culture was
708 diluted at a 1:1 ratio with fresh TP media, containing 1U of horseradish peroxidase
709 and 5 µM of Amplex Red (ThermoFisher) and incubated for 1 h (illuminated at 150
710 µmol photons m^{-2} s^{-1}, shaking 140 rpm). Cells were removed by centrifugation. The
711 H_2O_2 of the media was immediately quantified using a ClarioStar Plate Reader
712 Excitation/Emission 520/570-600 and compared against a linear H_2O_2 standard curve
713 up to 5 µM. Additional controls were included; some cells were treated with the ROS
714 quencher N,N' dimethylthiourea (DMTU) at a final concentration of 150 µM; and some
715 with the PSII plastoquinone binding site blocker 3-(3,4-dichlorophenyl)-1,1-
716 dimethylurea (DCMU) was dissolved in methanol at a final concertation of 10 µM prior
717 to H_2O_2 quantification (specified). All measurements were conducted with a minimum
718 of four technical replicates. The data shown represents one of a multiple of
719 experimental repeats conducted on different days with fresh cultures. All H_2O_2

720 concentrations were normalized to cell density, calculated as described previously,
721 and chlorophyll content, described below.

722 Total chlorophyll was calculated by resuspending 1 mL of harvested cells in 1 mL of
723 methanol. All samples were protected from the light after menthol addition. After
724 vortexing for 1 min to resuspend the pellet and incubating for 10 min, the cells were
725 removed by centrifugation. The absorbance of the supernatant was analysed by
726 spectrophotometer at 652 and 665 nm. Total chlorophyll was calculated using the
727 formula below. All measurements are averaged from three technical replicates. Total
728 chlorophyll (µg/mL) = 22.12 x Abs652 + 2.71 x Abs665.

729 **Growth of Arabidopsis**

730 Arabidopsis seeds were sown on moist F2+S soil and stratified in the dark at 4℃ for 2
731 days. For growth experiments seeds were grown in a Percival SE-41AR3cLED
732 chamber (CLF PlantClimatics GmbH, Wertingen, Germany) equipped with cool white
733 LED lights under 12 h light (175-180 µmol photons m^{-2} s^{-1})/12 h dark cycles at 21°C,
734 respectively and 70% relative humidity.

735 **Chlamydomonas Confocal Microscopy**

736 Transgenic fluorescent strains were initially grown heterotrophically in TAP media until
737 reaching 2 – 4 $\times 10^6$ cells mL^{-1} and resuspended in TP media overnight prior to
738 imaging. Cells were mounted on 8-well chamber slides and overlayed with 1.5% low
739 melting point agarose made with TP-medium. Images were collected on a LSM880
740 (Zeiss) equipped with an Airyscan module using a 63× objective. Laser excitation and
741 Emission setting for each channel used are set as below: Venus (Excitation: 514 nm;
742 Emission 525 – 500 nm); mScarlet-I (Excitation: 561 nm; Emission 570 – 620 nm);
743 Chlorophyll (Excitation: 633 nm; Emission 670 – 700 nm).

744 **Yeast-2-Hybrid**

745 Yeast two-hybrid to detect interactions between BST4 C-terminus and RbcS1 was
746 carried out as described in He et al., (2020). BST4 C-terminus (amino acids 387-end)
747 was cloned into the two-hybrid vector pGBKT7 to create a fusion with the GAL4 DNA-
748 binding domain. Point mutations were introduced by PCR into BST4 RBMs, which was
749 then cloned into the same vector. Mature CrRBCS1 was cloned into the vector
750 pGADT7 to create a fusion with the GAL4 activation domain. Yeast cells were then co-

751 transformed with binding and activation domain vectors. Successful transformants
752 were cultured, diluted to an optical density at 600 nm (OD_{600}) of 0.5 or 0.1 and plated
753 onto SD-L-W (double drop out, DDO) and SD-L-W-H (triple drop out, TDO) media. The
754 plates were imaged after three days and **Fig. S2** shows yeast spots from cultures
755 diluted to an OD_{600} of 0.5.

756 **Slimfield microscopy**

757 Chlamydomonas lines *bst4::BST4-mScarlet-I* and the unlabelled control line *bst4* were
758 prepared overnight in TP media. Each was harvested and spotted onto a slide-
759 mounted agar pad (GeneFrames, ThermoFisher), consisting of TP media with 1.5%
760 low melting point agarose. Fluorescence imaging with single-molecule sensitivity was
761 performed using a custom Slimfield microscope (Syeda et al., 2019). The setup used
762 a high-magnification objective (NA 1.49 Apo TIRF 100× oil immersion, Nikon) and the
763 detector was a Prime95B sCMOS camera (Teledyne Photometrics) operating in 12-
764 bit 'sensitivity' gain at a high total magnification of 53 nm/pixel. The samples were
765 illuminated either in brightfield, or for Slimfield fluorescence in camera-triggered
766 frames by a collimated 561 nm wavelength, Gaussian mode OPSL laser (Coherent,
767 Obis LS) at a peak intensity of 5 kW/cm^2 at the sample plane. This beam was tilted
768 into a HILO configuration (Payne-Dwyer and Leake, 2022) to reduce out-of-focus
769 excitation while retaining quantitative molecular sensitivity. The fluorescence image
770 was split into two parallel channels comprising emission bandpass filters (Semrock
771 BrightLine®): one with a 585/15 emission filter (central wavelength/spectral bandwidth
772 in nm) optimized to isolate the mScarlet-I signal, and a second with a 525/25 emission
773 filter, used only to indicate autofluorescence background. The total length of each
774 acquisition sequence was ~5 s; sufficient to observe the full course of mScarlet-I
775 photobleaching, from the initial unbleached state to single-molecule blinking, while
776 also rapid enough (10 ms exposure/frame at 180 frames/s) to capture the motion of
777 individual molecular assemblies.

778 **Single particle tracking and molecular counting**

779 Slimfield image sequences were segmented manually in ImageJ to include only the
780 pyrenoids in downstream analysis. The centroid positions of fluorescent tracks were
781 identified from local intensity maxima in each frame using ADEMScode software in
782 MATLAB (Wollman et al., 2022). The summed intensity of each candidate track was

783 calculated in each frame by adding all pixel values within 5 pixels of the centroid, then
784 subtracting the local background averaged between 5 - 8 pixels from the centroid.
785 Candidates with a summed intensity <0.4× the standard deviation in the background
786 region were discarded.

787 Fluorescent proteins are known to exhibit a characteristic integrated intensity per
788 molecule under stable Slimfield imaging conditions and within the quasi-uniformly
789 illuminated area within half the beam waist (Shepherd et al., 2021). After sufficient
790 photobleaching of mScarlet-I in the Slimfield image sequences, only step-like blinking
791 was observed at the end of each track. The modal integrated intensity of these steps
792 was used to estimate this characteristic single molecule brightness, equivalent to 56
793 ± 9 photoelectrons per frame per molecule.

794 At the start of each track, we obtained an initial integrated intensity (independent of
795 photobleaching) by linearly extrapolating the summed intensity backwards over the
796 first 4 frames of the exposure. This initial intensity was then divided by the
797 characteristic brightness of a single mScarlet-I to estimate the number of molecules,
798 or stoichiometry, in that track. This estimate was precise enough to detect
799 stoichiometry steps of up to 12 tagged molecules without ambiguity.

800 Stoichiometry distributions may exhibit peaks which are separated by a characteristic
801 interval. The smallest consistent interval between peaks can be used to infer the size
802 of a physical repeat unit or 'periodicity' within assemblies (Hunter et al., 2022; Payne-
803 Dwyer et al., 2022). A kernel width of 0.7 molecules was chosen to generate the
804 stoichiometry distribution (Fig. 2F), reflecting the background standard deviation.
805 Peaks were pinpointed using MATLAB's *findpeaks*.

806 The intervals between all peaks for each acquisition were aggregated across the
807 pyrenoid population, weighted by inverse square-root distance (thereby accounting for
808 shot-noise in broader intervals). A second distribution **(Fig. 2G)** was then generated
809 from this weighted population of intervals. The kernel width in this estimate was 0.7
810 molecules multiplied by the square root of the mean stoichiometry divided by the root
811 number of intervals (thereby accounting for shot-noise in intervals between peaks of
812 higher stoichiometry). The periodicity was then reported as the mode of this
813 distribution and its 95% confidence interval.

814 **Arabidopsis Confocal microscopy**

815 Small sections of 3 – 4 week-old leaf tissue (~5 - 10 mm^2) were adhered to slides using
816 double-sided tape with basal side up. A x40 water immersion objective lens was used.
817 Samples were excited by 488 nm at 1% laser power, chlorophyll autofluorescence was
818 collected at 680 – 750 nm and mNeonGreen fluorescence at 503–532 nm. For dual
819 tagged lines, we used sequential acquisition to minimize bleed-through. mCherry was
820 excited using the 542 nm laser and emission collected at 601-620 nm and mNeon as
821 before. Images were acquired using the SP8 Confocal system and Leica LAS AF
822 software (http://www.leica-microsystems.com/). Figures were prepared using ImageJ
823 (http://fiji.sc/Fiji).

824 **Immunoblot detection**

825 Two leaf disks (6 mm diameter) were harvested and immediately frozen in liquid
826 nitrogen. Two steel balls (3 mm) were added and tissue was homogenized using a
827 tissue-lyser twice for 30 Hz for 30 s. A four times volume of cold extraction buffer (20
828 mM Tris-HCl pH = 7.5, 5 mM $MgCl_2$, 300 mM NaCl, 5 mM DTT, 1% (v/v) Triton X-100,
829 1 x Protease inhibitor (Roche)) was added and samples vortexed for 30 s. Samples
830 were solubilized on ice for 5 mins and then centrifuged at 5000 xg for 5 min at 4℃.
831 17.5 µL of supernatant was used to make up 1x LDS and 100 uM DTT. 20 µL was
832 loaded on a Novex™ 4 - 12% Bis-Tris Mini Gel, (Thermo Fisher, Catalogue number:
833 NP0322BOX). The gel was run at 150 V for 60 minutes. Proteins were transferred to
834 a nitrocellulose membrane using an iBlot 2, programme 0. The membrane was probed
835 with primary antibody in 5% milk in 1 x TBST at the following dilutions: BST4 (1:1000;
836 generated for this study, peptide from C-terminus: SDTELSEANRPRTRPDWRN)
837 (YenZym, Antibodies LLC, USA), AtpB (1:2000; Agrisera:AS05085), RbcL (1:1000;
838 kind gift from Griffiths lab), CP43 (1:3000; Agrisera: AS111787), PsaB (1:1000;
839 Agrisera: AS10695), PsbO (1:2000; Agrisera:AS06142-33). Secondary antibody (goat
840 α-rabbit IR-800; Li-COR: 925-32211). Membrane was imaged using the Li-COR
841 Odyssey CLx scanner.

842 In order to quantify BST4 protein in Chlamydomonas lines, cells were grown in TP
843 media at ambient CO_2 until reaching 2 - 4 x 10^6 cells mL^{-1}. Cells were harvested by
844 centrifugation at 1000 x g for 10 mins, normalized to Chl content and resuspended in
845 the extraction buffer described above. Samples were freeze-thawed three times and

846 spun at 20, 000 x g for 20 min at 4℃. Protein extractions containing 5 µg of Chl with 1
847 x SDS loading buffer were boiled at 100℃ for 5 min and loaded onto a 4 - 20%
848 polyacrylamide gel (Mini Protean TGX, Biorad Laboratories). Proteins were
849 transferred to a PVDF-FL membrane on a Biorad semidry blotting system. BST4
850 primary antibody was used as described above alongside alpha-tubulin primary
851 antibody raised in mouse (Agrisera), as a loading control. Anti-rabbit and anti-mouse
852 fluorescent secondary antibodies, Invitrogen AlexaFluor 488 and 555 respectively,
853 were used at a 1:20 000 dilution. Immunoblots were imaged using an Amersham
854 typhoon 5 scanner with 488 and 535 excitation lasers and Cy2 and Cy3 emission
855 filters. BST4 band fluorescent intensity was quantified using FIJI (Image J) (Schindelin
856 et al., 2012) and normalized to alpha-tubulin loading control. All Chlamydomonas lines
857 for quantification were extracted and analysed in triplicate. For LHCSR3 protein
858 quantification, cells were seeded at 0.1 OD_{750} in TAP media for 4 days and then
859 switched to TP media at a concentration of 30 µg Chl ml^{-1} and exposed to 150 µmol
860 photons m^{-2} s^{-1} for 3 h. Protein was extracted according to Burlacot et al. 2022 and
861 separated by SDS-PAGE as described for BST4 immunoblots.

862 Oocytes for expression of BST4 were collected after recording and prepared for
863 western blot as described in Lefoulon et al., 2018. The BST4 primary antibody was
864 used as described above and the secondary antibody used was horseradish
865 peroxidase-coupled goat, anti-rabbit (dilution 1:10000 Abcam). Proteins were detected
866 with ECL Advance kit (GE Healthcare,Poole UK).

867 **Blue-Native PAGE**

868 A crude thylakoid enrichment was performed according to (Aro et al., 2004). Thylakoid
869 membranes were solubilized in 0.5% DDM, 1x NativePAGE buffer (Thermo: BN2003),
870 1x cOmplete protease inhibitor tab (Roche;10x stock made by dissolving 1 tablet in 1
871 mL dH_2O) for at a concentration of 0.8 µg Chl/µl for 15 min on ice. Unsolubilized
872 material was removed by two rounds of centrifugation at 17,000 xg at 4°C for 15 min.
873 19.5 µL of supernatant was combined with 0.5 µL of Coomassie additive and loaded
874 immediately onto a 4-16% Bis-tris gel (Thermo: BN1002BOX). Electrophoresis was
875 performed at room temperature at 150 V for 90 min. Cathode buffer was swapped
876 from dark to light when the dye front was a third way through the gel. Separated

877 proteins were transferred to a nitrocellulose membrane by electrophoresis at 100 V for
878 90 min at 4 ℃.

879 Proteins were visualized using chemiluminescence. Secondary antibody (goat α-
880 rabbit, HRP;1:10,000; Abcam: ab6721). Chemiluminescence substrate SuperSignal
881 West Pico PLUS (ThermoScientific, ref number: 34579) according to manufacturer's
882 instructions. Chemiluminescence was detected using clear blue X-Ray Film CL-
883 Xposure™ Film (ThermoScientific, ref number: 34090).

884 **Chlorophyll fluorescence measurements in Chlamydomonas for Fig. 7**

885 To measure PSII activity in Chlamydomonas, cells were grown in HS media under 80
886 μmol photons m^{-2} s^{-1} for 3 days at 120 rpm (in a Multitron, Infors-ht) to reach
887 logarithmic phase and then maintained at ~10 μg Chl mL^{-1}. Two millilitres of cells were
888 added to a cuvette and bubbled with air (10 cc/min) and continuous stirring. Cells were
889 incubated in the dark for five minutes before recording Chl fluorescence using DUAL-
890 PAM-100 (Walz, Effeltrich, Germany). A saturating pulse of 8,000 μmol photons m^{-2}
891 s^{-1} of 300 ms was applied to the samples for determination of the maximal
892 fluorescence yield in the dark state (F_m) and maximal fluorescence yield during the
893 period with actinic light (F_m'). The maximal quantum efficiency of PSII was calculated
894 as $(F_m'-F)/F_m$ where F is the stationary fluorescence. NPQ was calculated as (F_m–
895 F_m')/F_m' . Far-red light (4 μmol photons m^{-2} s^{-1}) was used throughout the entire
896 experiment to limit state transition from contributing to the NPQ. NPQ and Y(II) were
897 calculated based on changes in Chl fluorescence as (F_m–F_m')/F_m' and (F_m'–F)/ F_m',
898 respectively, according to Genty et al., (1989). When indicated, cells were
899 supplemented with a final concentration of 500 μM HCO_3^- at the beginning of the dark
900 adaptation.

901 **Electrochromic shift (ECS) in Chlamydomonas for Fig. 7**

902 Electrochromic shift (ECS) in Chlamydomonas was assessed by measuring the
903 absorbance changes of cells at 520 and 545 nm using a JTS-100 spectrophotometer
904 (BioLogic). Cells were grown and prepared as for Chl fluorescence experiments
905 described previously except cells were resuspended to 150 μg Chl mL^{-1} before being
906 loaded into a custom vertical light path cuvette. Cells were dark adapted for 1 min and
907 then exposed to 890 μmol photons m^{-2} s^{-1} red light (630 nm) for 1 min. The light was
908 switched off and decay kinetics were measured. ECS signal was calculated as the

909 difference between absorbance changes measured at 520 and 545 nm. For each
910 biological replicate, 3 technical replicates were taken and averaged. PMF size was
911 calculated as the difference between the ECS signal in light and the minimum value
912 of the ECS signal immediately after the light was turned off. The g_{H^+} parameter was
913 calculated as 1/τ (time constant for decay during the first 100 ms (Cruz et al., 2005).

914 **Chlorophyll fluorescence measurements in Chlamydomonas for Fig. S12**

915 To measure PSII activity in Chlamydomonas, cells were grown in TAP in low light (20
916 μmol photons m^{-2} s^{-1}) for 4 days at 50 rpm to reach logarithmic phase. Cells were
917 then washed, resuspended to 30 μg Chl mL^{-1} in TP media and exposed to 150 μmol
918 photons m^{-2} s^{-1} light for 3 h, followed by 1 h incubation in darkness at 50 rpm before
919 recording Chl fluorescence using DUAL-PAM-100 (Walz, Effeltrich, Germany). A
920 saturating pulse of 3,000 μmol photons m^{-2} s^{-1} of 800 ms was applied to the samples
921 in a cuvette under continuous stirring for determination of the maximal fluorescence
922 yield in the dark state (F_m) and maximal fluorescence yield during the period with
923 actinic light (F_m'). The maximal photochemical efficiency of PSII (F_v/F_m) was
924 calculated. NPQ was determined from slow kinetics during actinic illumination at 1,500
925 μmol m^{-2} s^{-1} for 17 min followed by 5 min of dark relaxation. NPQ and Y(II) were
926 calculated based on changes in Chl fluorescence as $(F_m–F_m')/F_m'$ and $(F_m'–F)/ F_m'$,
927 respectively, according to Genty et al., (1989).

928 **Electrochromic shift (ECS) in Chlamydomonas for Fig. S12**

929 ECS measurements in Chlamydomonas were carried out using a the Dual-PAM-100
930 equipped with a P515/535 module (Walz). Cells grown and prepared as for Chl
931 fluorescence experiments described previously were layered on a glass slide and
932 exposed to actinic red light for the given period. The light was switched off and decay
933 kinetics were measured. PMF size was calculated as the difference between the ECS
934 signal in light and the minimum value of the ECS signal immediately after the light was
935 turned off. Calculation of ΔpH and ΔΨ was performed using the steady-state time point
936 of the ECS signal in darkness (Cruz et al., 2001). Before each ECS measurement, a
937 3 saturating 50-μs actinic red flashes of 200,000 μmol photons m^{-2} s^{-1} was applied to
938 determine the ECS_{ST}; subsequently, the ECS_{ST} amplitude was used to normalize the
939 ECS signal before the calculation of PMF size and partitioning values. To determine
940 H^+ conductivity (g_{H^+}), the light was switched off at specific time points to record the

941 ECS signal decay during 620 ms dark intervals. The g_{H^+} parameter was calculated as
942 1/τ (time constant for decay during the first 100 ms (Cruz et al., 2005). The total proton
943 flux across the membrane was calculated as v_{H^+} = PMF × g_{H^+} (Cruz et al, 2001).

944 **Chlorophyll fluorescence measurements for Arabidopsis**

945 Plants were grown for 8 weeks on S-Hasselfors soil in a Percival AR-82L chamber
946 (CLF Plant Climatics, Wertingen, Germany) using 12 h light (180 µmol photons m^{-2}
947 s^{-1})/ 12 h dark cycles at 21°C/19°C, respectively, and 70% relative humidity. Slow
948 kinetics of Chl *a* fluorescence induction were recorded with a pulse-amplitude
949 modulated fluorometer DUAL-PAM 100 equipped with DUAL-DB and DUAL-E emitter-
950 detector module (Walz) on attached leaves of 30 min dark-adapted plants using actinic
951 red light of 830 µmol photons m^{-2} s^{-1} for 10 min, followed by a 5 min dark period. The
952 saturating pulse applied was 5,000 µmol photons m^{-2} s^{-1} and of 800 ms duration. NPQ
953 and (Y(II)) were calculated based on changes in Chl fluorescence as $(F_m–F_m')/F_m'$ and
954 $(F_m'–F)/ F_m'$, respectively (Genty et al., 1989).

955 **Electrochromic shift (ECS) for Arabidopsis**

956 ECS was recorded with a DUAL-PAM 100 system equipped with a P515/535
957 emitter/detector module (Walz). First, plants were dark adapted for 30 min, then
958 illuminated with actinic red light at 830 µmol photons m^{-2} s^{-1} for 3 min followed by a
959 60 s dark period in which the ECS decay kinetics were recorded. Before each
960 measurement, three pulses of 5 µs and 200,000 µmol photons m^{-2} s^{-1} were applied to
961 determine ECS_{ST}, which was used to normalize the ECS_T values of each
962 measurement.

963 **Sedimentation of proto-pyrenoid**

964 Cross-linked samples were prepared by vacuum infiltrating intact leaves 1%
965 formaldehyde prior to sedimentation 200 mg of leaf tissue was flash frozen in liquid
966 nitrogen and ground by bead beating twice at 30 Hz for 30 s. Four times volume of
967 extraction buffer (50 mM HEPES-KOH pH 7.5, 17.4% (v/v) glycerol, 2% (v/v) Triton X-
968 100, cOmplete protease inhibitor tab) was added and sample mixed by bead beating
969 again. Extract was filtered through one layer of miracloth. A small aliquot of filtered
970 extract was saved as the input. Extract was then centrifuged at 500 x g for 3 min at 4
971 ℃ and the pellet discarded. The supernatant was centrifuged at 500 x g for 12min, 4
972 ℃. The pellet was washed once with extraction buffer and then centrifuged again. The

973 pellet was resuspended in 100 µl extraction buffer then centrifuged for a further 5 min.
974 Pellet was finally resuspended in 25 µl extraction buffer. Fractions were made up in
975 1x LDS loading buffer and 200 mM DTT. Ten microlitres was subjected to SDS-PAGE
976 (NuPAGE™ 4-12% Bis-Tris Mini Gel, Thermo Fisher, Catalogue number:
977 NP0322BOX) at 150 V for 60 min.

978 **Chloroplast fractionation**

979 In order to biochemically localize transgenically expressed BST4, chloroplasts were
980 fractionated as described in Herdean et al. (2016) using 100 g of leaf tissue from four-
981 five week-old BST4 transgenic plants. The stromal fraction was concentrated using a
982 10,000 MWCO centrifugal concentrator (Sartorius Stedim Biotech GmbH, product
983 number: VS1502).

984 **Electron microscopy of Chlamydomonas**

985 High (3%) and low (0.04%) CO_2 acclimated cells were harvested by centrifugation
986 (×1000g, 4 minutes, 20°C). Primary fixation was performed in 1.25% glutaraldehyde
987 in 50 mM sodium cacodylate (pH 7.15) in TP medium for 15 minutes followed by 2.5%
988 Glutaraldehyde in 50 mM cacodylate for 2 hours. Fixed samples were washed three
989 times with 50 mM sodium cacodylate by centrifugation. Samples were then osmicated
990 with 1% OsO4 in 50 mM sodium 25 cacodylate for 1 hour on ice and washed with de-
991 ionised water. Samples were block stained in 1% uranyl acetate in the dark for 1 hour.
992 Samples were washed twice with dH_2O and twice with 50 mM sodium cacodylate.
993 Fixed samples were dehydrated in an acetone series (25%, 50%, 75%, 90% and
994 100%) ~20 minutes each step. Dehydrated samples were infiltrated with Spurr's resin
995 by incubating in 25% then 50% Spurr resin in acetone for 30 minutes and transferred
996 to 75% for 45 minutes at room temperature. They were then incubated in 100% Spurr
997 resin overnight before polymerising at 70 °C for 24 hours. Sections ~70 nm thick were
998 collected on Copper grids and stained with saturated uranyl acetate and lead citrate.
999 Images were collected with a FEI Tecnai 12 BT at 120kV using a Ceta camera.

1000 **Electron microscopy of Arabidopsis**

1001 Leaves were cut into small 5 mm strips and fixed in 4% (v/v) Paraformaldehyde/0.5%
1002 glutaraldehyde in 0.05M sodium cacodylate (pH = 7.2) by vacuum infiltration three
1003 times for 15 min and incubation at 4 °C overnight with gentle agitation followed by
1004 dehydration in increasing amounts of ethanol 50/70/80/90/100% 1 hr each then

1005 overnight rotation. 100% ethanol was repeated 3 times, 1 hr each and a final over
1006 night at 4 °C. Samples were then fixed in LR resin by infiltrating with increasing
1007 concentration (50/70/100%) with a repeat of 100% and then polymerized overnight at
1008 50 °C. Ultrathin sections were cut and mounted onto plastic-coated copper grids. Grids
1009 were stained with 2% uranyl acetate and visualized by transmission electron
1010 microscopy (TEM).

1011 **Protease protection assay**

1012 Investigation of the orientation of BST4 in isolated thylakoid membranes was
1013 conducted as described in Stepien and Johnson (2018). Briefly, trypsin made up in 50
1014 mM acetic acid according to the manufacturer's instructions (Thermo Scientific, ref
1015 number: 90057). To disrupt the thylakoid membrane and allow degradation to lumen-
1016 facing peptides, 1% (v/v) Triton X-100 was added, and tubes gently agitated prior to
1017 addition of trypsin.

1018 **Xenopus oocyte electrophysiology**

1019 Destination clones containing BST4 for Xenopus expression were linearized with
1020 EcoRI, before proceeding to the *in vitro* transcription (mMessage mMachine T7
1021 transcription kit, Thermofisher Scientific, ref number AM1344). Stage IV oocytes were
1022 injected with 20 ng of RNA per oocyte. Measurements of ion transport was done by
1023 voltage clamp using an Axoclamp 2B amplifier (Axon instruments, Foster City, CA)
1024 (Lefoulon et al., 2014; Leyman et al., 1999). They were performed under perfusion of
1025 either 100 mM KCl, K-HCO_3, Na-HCO_3, K-PEP, or K-Gluconate, with 1 mM $CaCl_2$, 1.5
1026 mM $MgCl_2$, and 10 mM HEPES-NaOH, pH 7.3. Recordings were obtained and
1027 analysed using Henry IV software (Y-Science, Glasgow, UK). BST4 expression in
1028 oocytes was validated by western blotting (Fig S10B), as described above.

1029 **ACKNOWLEDGEMENTS**

1030 The authors thank the University of York Horticulture team who helped with setting up
1031 the Chlamydomonas phototaxis assays. TEM for Arabidopsis was carried out with the
1032 support of Stephen Mitchell and the Wellcome Trust Multi User Equipment Grant
1033 (WT104915MA)

1034 For the purpose of open access, a Creative Commons Attribution (CC BY) licence is
1035 applied to any Author Accepted Manuscript version arising from this submission.

1036 **AUTHOR CONTRIBUTIONS**

1037 LA, CW, CSL, AB, CS, AM and LM conceived and designed the study with input from
1038 all authors. LA performed all Arabidopsis experiments, BN-PAGE and immunoblots.
1039 CW performed Chlamydomonas physiology experiments and immunoblots. CSL
1040 performed Chlamydomonas microscopy imaging and immunoblots. LA, AB, KMS,
1041 KAvM, and ED performed Chlamydomonas and Arabidopsis Chl fluorescence and
1042 ECS experiments and generated figures. APD and CW performed molecular tracking
1043 experiments with input from ML. CL and MB performed xenopus oocyte work. PG and
1044 JB did *in silico* structure predictions. TEM contributed to the complementation of
1045 Chlamydomonas *bst4* mutant. NA contributed to Arabidopsis transgenic line
1046 generation. GP assisted with experimental design and data interpretation. LA and CW
1047 generated figures. LA led the writing of the manuscript with input from CW. All other
1048 authors provided manuscript feedback.

1049 **REFERENCES**

1050 Adler L, Díaz-Ramos A, Mao Y, Pukacz KR, Fei C, Mccormick AJ (2022) New
1051 horizons for building pyrenoid-based CO_2-concentrating mechanisms in plants
1052 to improve yields. Plant Physiol 190: 1609-1627
1053 Aro E-M, Rokka A, Vener A V (2004) Determination of Phosphoproteins in Higher
1054 Plant Thylakoids BT - Photosynthesis Research Protocols. *In* R Carpentier,
1055 ed,Humana Press, Totowa, NJ, pp 271–285
1056 Atkinson N, Feike D, Mackinder LCM, Meyer MT, Griffiths H, Jonikas MC, Smith AM,
1057 Mccormick AJ (2016) Introducing an algal carbon-concentrating mechanism into
1058 higher plants: Location and incorporation of key components. Plant Biotechnol J
1059 14: 1302–1315
1060 Atkinson N, Leitão N, Orr DJ, Meyer MT, Carmo-Silva E, Griffiths H, Smith AM,
1061 McCormick AJ (2017) Rubisco small subunits from the unicellular green alga
1062 Chlamydomonas complement Rubisco-deficient mutants of Arabidopsis. New
1063 Phytol 214: 655–667
1064 Atkinson N, Mao Y, Chan KX, McCormick AJ (2020) Condensation of Rubisco into a
1065 proto-pyrenoid in higher plant chloroplasts. Nat Commun 11: 6303
1066 Bailleul B, Cardol P, Breyton C, Finazzi G. (2010) Electrochromism: a useful probe to
1067 study algal photosynthesis. Photosynthesis research 106:179-89
1068 Bergner SV, Scholz M, Trompelt K, Barth J, Gäbelein P, Steinbeck J, Xue H, Clowez
1069 S, Fucile G, Fufezan C, et al (2015) STATE TRANSITION7-Dependent
1070 Phosphorylation Is Modulated by Changing Environmental Conditions , and Its
1071 Absence Triggers Remodeling of Photosynthetic Protein Complexes 1. Plant
1072 Physiol *168*: 615-634
1073 Bharill S, Fu Z, Palty R, Isacoff EY (2014) Stoichiometry and specific assembly of
1074 Best ion channels. Proc Natl Acad Sci U S A 111: 6491–6496
1075 Bonente G, Ballottari M,Truong TB, Morosinotto T, Ahn TK, Fleming GR, Niyogi KK,
1076 Bassi R (2011) Analysis of LhcSR3, a Protein Essential for Feedback De-

1077 Excitation in the Green Alga *Chlamydomonas reinhardtii* PLoS biology. 2011
1078 Jan 18;9(1):e1000577
1079 Bonente G, Pippa S, Castellano S, Bassi R, Ballottari M. (2012) Acclimation of
1080 Chlamydomonas reinhardtii to different growth irradiances. J Biol Chem
1081 287:5833-47
1082 Burlacot A, Dao O, Auroy P, Cuiné S, Li-Beisson Y, Peltier G (2022) Alternative
1083 photosynthesis pathways drive the algal CO_2-concentrating mechanism. Nature
1084 605: 366–371
1085 Caspari OD, Meyer MT, Tolleter D, Wittkopp TM, Cunniffe NJ, Lawson T, Grossman
1086 AR, Griffiths H (2017) Pyrenoid loss in *Chlamydomonas reinhardtii* causes
1087 limitations in CO_2 supply, but not thylakoid operating efficiency. J Exp Bot 68:
1088 3903–3913
1089 Choi BY, Kim H, Shim D, Jang S, Yamaoka Y, Shin S, Yamano T, Kajikawa M, Jin
1090 ES, Fukuzawa H, et al (2022) The Chlamydomonas bZIP transcription factor
1091 BLZ8 confers oxidative stress tolerance by inducing the carbon-concentrating
1092 mechanism. Plant Cell 34: 910–926
1093 Ciorba MA, Heinemann SH, Weissbach H, Brot N, Hoshi T (1999) Regulation of
1094 voltage-dependent K^+ channels by methionine oxidation: effect of nitric oxide
1095 and vitamin C. FEBS Lett 442: 48–52
1096 Cruz JA, Avenson TJ, Kanazawa A, Takizawa K, Edwards GE, Kramer DM (2005)
1097 Plasticity in light reactions of photosynthesis for energy production and
1098 photoprotection. J Exp Bot 56: 395–406
1099 Cruz JA, Sacksteder CA, Kanazawa A, Kramer DM (2001) Contribution of electric
1100 field (Δψ) to steady-state transthylakoid proton motive force (pmf) in vitro and in
1101 vivo. Control of pmf parsing into Δψ and ΔpH by ionic strength. Biochemistry 40:
1102 1226–1237
1103 Emrich-Mills TZ, Yates G, Barrett J, Girr P, Grouneva I, Lau CS, Walker CE, Kwok
1104 TK, Davey JW, Johnson MP, et al (2021) A recombineering pipeline to clone
1105 large and complex genes in Chlamydomonas. Plant Cell 33: 1161–1181
1106 Engel BD, Schaffer M, Kuhn Cuellar L, Villa E, Plitzko JM, Baumeister W (2015)
1107 Native architecture of the Chlamydomonas chloroplast revealed by in situ cryo-
1108 electron tomography. Elife 4: e11383
1109 Engler C, Youles M, Gruetzner R, Ehnert T-M, Werner S, Jones JDG, Patron NJ,
1110 Marillonnet S (2014) A Golden Gate Modular Cloning Toolbox for Plants. ACS
1111 Synth Biol 3: 839–843
1112 Erickson E, Wakao S, Niyogi KK (2015) Light stress and photoprotection in
1113 *Chlamydomonas reinhardtii*. Plant J 82: 449–465
1114 Fei C, Wilson AT, Mangan NM, Wingreen NS, Jonikas MC (2022) Modelling the
1115 pyrenoid-based CO_2-concentrating mechanism provides insights into its
1116 operating principles and a roadmap for its engineering into crops. Nat Plants 8:
1117 583–595
1118 Genkov T, Meyer M, Griffiths H, Spreitzer RJ (2010) Functional hybrid rubisco
1119 enzymes with plant small subunits and algal large subunits: Engineered rbcS
1120 cDNA for expression in chlamydomonas. J Biol Chem 285: 19833–19841
1121 Genty B, Briantais JM, Baker NR (1989) The relationship between the quantum yield
1122 of photosynthetic electron transport and quenching of chlorophyll fluorescence.
1123 Biochim Biophys Acta - Gen Subj 990: 87–92
1124 Grefen C, Chen Z, Honsbein A, Donald N, Hills A, Blatt MR (2010) A Novel Motif
1125 Essential for SNARE Interaction with the K^+ Channel KC1 and Channel Gating
1126 in Arabidopsis . Plant Cell 22: 3076–3092

1127 Guindon S, Dufayard J-F, Lefort V, Anisimova M, Hordijk W, Gascuel O (2010) New
1128 Algorithms and Methods to Estimate Maximum-Likelihood Phylogenies:
1129 Assessing the Performance of PhyML 3.0. Syst Biol 59: 307–321
1130 Hagino T, Kato T, Kasuya G, Kobayashi K, Kusakizako T, Hamamoto S, Sobajima T,
1131 Fujiwara Y, Yamashita K, Kawasaki H, et al (2022) Cryo-EM structures of
1132 thylakoid-located voltage-dependent chloride channel VCCN1. Nat Commun 13:
1133 2505
1134 Hasegawa M, Shiina T, Terazima M, Kumazaki S (2010) Selective excitation of
1135 photosystems in chloroplasts inside plant leaves observed by near-infrared
1136 laser-based fluorescence spectral microscopy. Plant Cell Physiol 51: 225–238
1137 He S, Chou H, Matthies D, Wunder T, Meyer MT, Martinez-sanchez A, Jeffrey PD,
1138 Port SA, He G, Chen VK, et al (2020) The Structural Basis of Rubisco Phase
1139 Separation in the Pyrenoid. 6: 1480–1490
1140 Hennacy JH, Jonikas MC (2020) Prospects for Engineering Biophysical CO_2
1141 Concentrating Mechanisms into Land Plants to Enhance Yields. Annu Rev Plant
1142 Biol 71: 461-485
1143 Herdean A, Teardo E, Nilsson AK, Pfeil BE, Johansson ON, Ünnep R, Nagy G,
1144 Zsiros O, Dana S, Solymosi K, et al (2016) A voltage-dependent chloride
1145 channel fine-tunes photosynthesis in plants. Nat Commun 7: 11654
1146 Horton P, Long SP, Smith P, Banwart SA, Beerling DJ (2021) Technologies to
1147 deliver food and climate security through agriculture. Nat Plants 7: 250–255
1148 Hunter P, Payne-Dwyer AL, Shaw M, Signoret N, Leake MC (2022) Single-molecule
1149 and super-resolved imaging deciphers membrane behavior of onco-
1150 immunogenic CCR5. iScience 25: 105675
1151 Izumi M, Tsunoda H, Suzuki Y, Makino A, Ishida H (2012) RBCS1A and RBCS3B,
1152 two major members within the Arabidopsis RBCS multigene family, function to
1153 yield sufficient Rubisco content for leaf photosynthetic capacity. J Exp Bot 63:
1154 2159–2170
1155 Karlsson J, Ciarke AK, Chen ZY, Hugghins SY, Park Y II, Husic HD, Moroney J V.,
1156 Samuelsson G (1998) A novel α-type carbonic anhydrase associated with the
1157 thylakoid membrane in *Chlamydomonas reinhardtii* is required for growth at
1158 ambient CO_2. EMBO J 17: 1208–1216
1159 Katoh K, Standley DM (2013) MAFFT Multiple Sequence Alignment Software
1160 Version 7: Improvements in Performance and Usability. Mol Biol Evol 30: 772–
1161 780
1162 Le SQ, Gascuel O (2008) An Improved General Amino Acid Replacement Matrix.
1163 Mol Biol Evol 25: 1307–1320
1164 Lee S, Yoon B-E, Berglund K, Oh S-J, Park H, Shin H-S, Augustine GJ, Lee CJ
1165 (2010) Channel-mediated tonic GABA release from glia. Science 330: 790–796
1166 Lefoulon C, Waghmare S, Karnik R, Blatt MR (2018) Gating control and K^+ uptake by
1167 the KAT1 K^+ channel leaveraged through membrane anchoring of the trafficking
1168 protein SYP121. Plant Cell Environ 41: 2668–2677
1169 Li X, Patena W, Fauser F, Jinkerson RE, Saroussi S, Meyer MT, Ivanova N,
1170 Robertson JM, Yue R, Zhang R, Vilarrasa-Blasi J, Wittkopp TM, Ramundo S,
1171 Blum SR, Goh A, Laudon M, Srikumar T, Lefebvre PA, Grossman AR, Jonikas
1172 MC (2019)*Nature Genetics* 51: 627-35
1173 Long S, Burgess S, Causton I (2019) Redesigning Crop Photosynthesis. Sustain.
1174 Glob. Food Secur. Nexus Sci. Policy. pp 131–141
1175 Ma X, Zhang B, Miao R, Deng X, Duan Y, Cheng Y, Zhang W, Shi M, Huang K, Xia
1176 XQ. (2020) Transcriptomic and Physiological Responses to Oxidative Stress in

a *Chlamydomonas reinhardtii* Glutathione Peroxidase Mutant. Genes (Basel) 11: 463.

Ma Y, Pollock S V., Xiao Y, Cunnusamy K, Moroney J V. (2011) Identification of a novel gene, *CIA6*, required for normal pyrenoid formation in *Chlamydomonas reinhardtii*. Plant Physiol 156: 884–896

Mackinder LCM, Chen C, Leib RD, Patena W, Blum SR, Rodman M, Ramundo S, Adams CM, Jonikas MC (2017) A Spatial Interactome Reveals the Protein Organization of the Algal CO_2-Concentrating Mechanism. Cell 171: 133–147

McGrath JM, Long SP (2014) Can the cyanobacterial carbon-concentrating mechanism increase photosynthesis in crop species? A theoretical analysis. Plant Physiol 164: 2247–2261

Meyer MT, Itakura AK, Patena W, Wang L, He S, Emrich-Mills T, Lau CS, Yates G, MacKinder LCM, Jonikas MC (2020) Assembly of the algal CO_2-fixing organelle, the pyrenoid, is guided by a Rubisco-binding motif. Sci Adv 6: eabd2408

Minh BQ, Schmidt HA, Chernomor O, Schrempf D, Woodhams MD, von Haeseler A, Lanfear R (2020) IQ-TREE 2: New Models and Efficient Methods for Phylogenetic Inference in the Genomic Era. Mol Biol Evol 37: 1530–1534

Mirdita M, Schütze K, Moriwaki Y, Heo L, Ovchinnikov S, Steinegger M (2022) ColabFold: making protein folding accessible to all. Nat Methods 19: 679–682

Mitra M, Mason CB, Xiao Y, Ynalvez RA, Lato SM, and Moroney JV. 2005. The carbonic anhydrase gene families of *Chlamydomonas reinhardtii*. *Canadian Journal of Botany*. 83: 780-795

Mukherjee A, Lau CS, Walker CE, Rai AK, Prejean CI, Yates G, Emrich-Mills T, Lemoine SG, Vinyard DJ, Mackinder LCM, et al (2019) Thylakoid localized bestrophin-like proteins are essential for the CO_2 concentrating mechanism of Chlamydomonas reinhardtii. Proc Natl Acad Sci U S A 116: 16915–16920

Payne-Dwyer AL, Leake MC (2022) Single-Molecular Quantification of Flowering Control Proteins Within Nuclear Condensates in Live Whole Arabidopsis Root BT - Chromosome Architecture: Methods and Protocols. *In* MC Leake, ed,Springer US, New York, NY, pp 311–328

Payne-Dwyer AL, Syeda AH, Shepherd JW, Frame L, Leake MC (2022) RecA and RecB: probing complexes of DNA repair proteins with mitomycin C in live Escherichia coli with single-molecule sensitivity. J R Soc Interface 19: 20220437

Peers G, Truong TB, Ostendorf E, Busch A, Elrad D, Grossman AR, Hippler M, Niyogi KK (2009) An ancient light-harvesting protein is critical for the regulation of algal photosynthesis. Nature 462: 518–521

Pettersen EF, Goddard TD, Huang CC, Meng EC, Couch GS, Croll TI, Morris JH, Ferrin TE (2021) UCSF ChimeraX: Structure visualization for researchers, educators, and developers. Protein Sci 30: 70–82

Plank M, Wadhams GH, Leake MC (2009) Millisecond timescale slimfield imaging and automated quantification of single fluorescent protein molecules for use in probing complex biological processes. Integr Biol (Camb) 1: 602–612

Price GD, Pengelly JJL, Forster B, Du J, Whitney SM, von Caemmerer S, Badger MR, Howitt SM, Evans JR (2013) The cyanobacterial CCM as a source of genes for improving methylation and chromatin patterning photosynthetic CO_2 fixation in crop species. J Exp Bot 64: 753–768

Qu Z, Cui Y, Hartzell C (2006) A short motif in the C-terminus of mouse bestrophin 4 inhibits its activation as a Cl^- channel. FEBS Lett 580: 2141–2146

Qu Z, Hartzell HC (2008) Bestrophin Cl^- channels are highly permeable to HCO_3^- . Am J Physiol Physiol 294: C1371–C1377

RAVEN J A (1997), CO_2-concentrating mechanisms: a direct role for thylakoid lumen acidification?. Plant, Cell & Environment, 20: 147-154

Roach T, Na CS (2017) LHCSR3 affects de-coupling and re-coupling of LHCII to PSII during state transitions in Chlamydomonas reinhardtii. Scientific Reports 7:43145

Roberts SK, Milnes J, Caddick M (2011) Characterisation of *An*BEST1 , a functional anion channel in the plasma membrane of the filamentous fungus , *Aspergillus nidulans*. Fungal Genet Biol 48: 928–938

Santhanagopalan I, Wong R, Mathur T, Griffiths H (2021) Orchestral manoeuvres in the light: Crosstalk needed for regulation of the Chlamydomonas carbon concentration mechanism. J Exp Bot 72: 4604–4624

Schindelin J, Arganda-Carreras I, Frise E, Kaynig V, Longair M, Pietzsch T, Preibisch S, Rueden C, Saalfeld S, Schmid B, et al (2012) Fiji: an open-source platform for biological-image analysis. Nat Methods 9: 676–682

Shepherd JW, Payne-Dwyer AL, Lee JE, Syeda A, Leake MC (2021) Combining single-molecule super-resolved localization microscopy with fluorescence polarization imaging to study cellular processes. JPhys Photonics. 3: 034010

Steen C J, Burlacot A, Short A H, Niyogi K K & Fleming, G R (2022) Interplay between LHCSR proteins and state transitions governs the NPQ response in *Chlamydomonas* during light fluctuations. Plant, Cell & Environment. 45: 2428–2445

Stepien P, Johnson GN (2018) Plastid terminal oxidase requires translocation to the grana stacks to act as a sink for electron transport. Proc Natl Acad Sci U S A 115: 9634–9639

Sueoka N (1960) Mitotic Replication of Deoxyribonucleic Acid in Chlamydomonas Reinhardi. Proc Natl Acad Sci 46: 83–91

Syeda AH, Wollman AJM, Hargreaves AL, Howard JAL, Brüning J-G, McGlynn P, Leake MC (2019) Single-molecule live cell imaging of Rep reveals the dynamic interplay between an accessory replicative helicase and the replisome. Nucleic Acids Res 47: 6287–6298

Tardif M, Atteia A, Specht M, Cogne G, Rolland N, Brugière S, Hippler M, Ferro M, Bruley C, Peltier G, et al (2012) PredAlgo: a new subcellular localization prediction tool dedicated to green algae. Mol Biol Evol 29: 3625–3639

Tian L, Nawrocki W J, Liu X, Polukhina I, Van Stokkum I H, Croce R (2019) pH dependence, kinetics and light-harvesting regulation of nonphotochemical quenching in *Chlamydomonas*. Proc. Natl. Acad. Sci. U. S. A. 116: 8320– 8325

Ueki N, Ide T, Mochiji S, Kobayashi Y, Tokutsu R, Ohnishi N, Yamaguchi K, Shigenobu S, Tanaka K, Minagawa J, et al (2016) Eyespot-dependent determination of the phototactic sign in *Chlamydomonas reinhardtii*. Proc Natl Acad Sci U S A 113: 5299–5304

Van Dijk M, Morley T, Rau ML, Saghai Y. (2021) A meta-analysis of projected global food demand and population at risk of hunger for the period 2010–2050. Nature Food 7:494-501

Wollman AJM, Fournier C, Llorente-Garcia I, Harriman O, Payne-Dwyer AL, Shashkova S, Zhou P, Liu T-C, Ouaret D, Wilding J, et al (2022) Critical roles for EGFR and EGFR–HER2 clusters in EGF binding of SW620 human carcinoma cells. J R Soc Interface 19: 20220088

Woo DH, Han K-S, Shim JW, Yoon B-E, Kim E, Bae JY, Oh S-J, Hwang EM, Marmorstein AD, Bae YC, et al (2012) TREK-1 and Best1 Channels Mediate Fast and Slow Glutamate Release in Astrocytes upon GPCR Activation. Cell

151: 25–40
Wu A, Brider J, Busch FA, Chen M, Chenu K, Clarke VC, Collins B, Ermakova M, Evans JR, Farquhar GD, et al (2023) A cross-scale analysis to understand and quantify the effects of photosynthetic enhancement on crop growth and yield across environments. Plant Cell Environ 46: 23–44
Yang T, Liu Q, Kloss B, Bruni R, Kalathur RC, Guo Y, Kloppmann E, Rost B, Colecraft HM, Hendrickson WA (2014) Structure and selectivity in bestrophin ion channels. Science 346: 355–359
Zhang R, Patena W, Armbruster U, Gang SS, Blum SR, Jonikas MC (2014) High-throughput genotyping of green algal mutants reveals random distribution of mutagenic insertion sites and endonucleolytic cleavage of transforming DNA. Plant Cell 26: 1398–1409

Supplemental Figures

0.04% CO_2							
		Days 0-3			**Days 0 to 5**		
	Strain	Mean	SE	*P(T<=t)* two-tail	Mean	SE	*P(T<=t)* two-tail
SGR (μ h^{-1})	WT	0.0389	0.0007		0.0241	0.0010	
	bst4	0.0402	0.0003	0.1652	0.0257	0.0001	0.2036
Doubling time (h)	WT	17.8462	0.3380		28.8436	1.2467	
	bst4	17.2379	0.1255	0.1669	26.9798	0.1491	0.2119
3% CO_2							
		Days 0-2			**Days 0-3**		
	Strain	Mean	SE	*P(T<=t)* two-tail	Mean	SE	*P(T<=t)* two-tail
SGR (μ h^{-1})	WT	0.0679	0.0013		0.0456	0.0011	
	bst4	0.0682	0.0010	0.8626	0.0455	0.0003	0.9436
Doubling time (h)	WT	10.2145	0.1930		15.2239	0.3725	
	bst4	10.1669	0.1510	0.8555	15.2353	0.0878	0.9777

Supplemental Table 1 compares specific growth rates (μ h^{-1}) and cell doubling times of WT and *bst4* strains (n=3) during liquid growth assays at 0.04 and 3 % CO_2 (+/- 2 ppm).

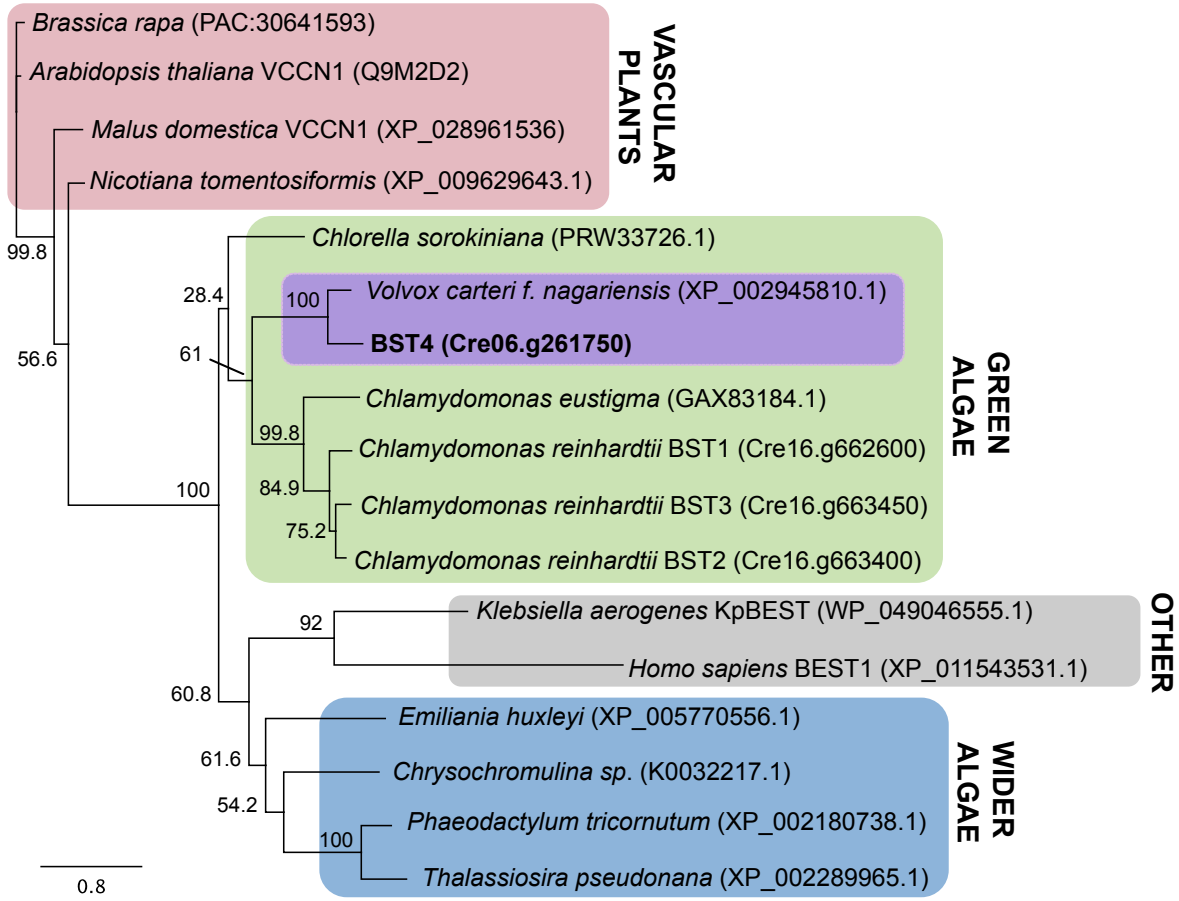

Supplemental Figure 1. BST4 structure and sequence compared to other bestrophins. Phylogenetic analysis of the full length Chlamydomonas BST4 amino acid sequence (bold). The evolutionary history of BST4 was inferred by using the maximum likelihood method based on the Le and Gascuel substitution model with discrete Gamma distribution (5 categories) and 500 bootstrap replicates. The tree is drawn to scale, with branch lengths measured in the number of substitutions per site.

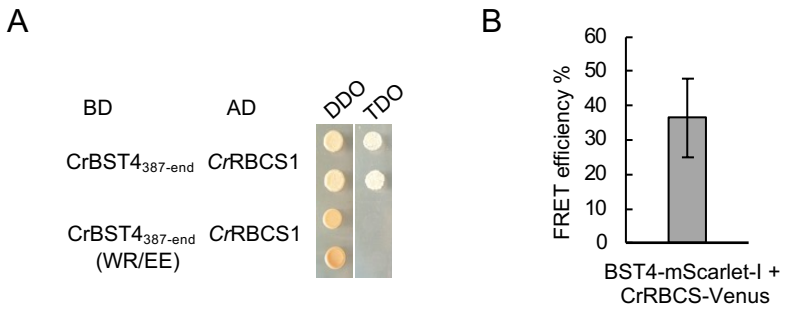

Supplemental Figure 2. Interaction between BST4 and RBCS. A. Yeast-2-hybrid experiment. The disordered region of BST4 C-terminus (amino acid 387-end) and with residues WR from RBMs are changed to EE. Abbreviations: AD, activation domain; BD, binding domain; DDO, double drop out media; TDO, triple drop out media. Growth on TDO indicates an interaction. **B**. FRET efficiency between BST4-mScarlet-I and CrRBCS-Venus. Sensitized-FRET measurement on dual-tagged cells (BST4-Venus and RBCS1-mCherry) showed a moderate FRET efficiency of 35% (n=10).

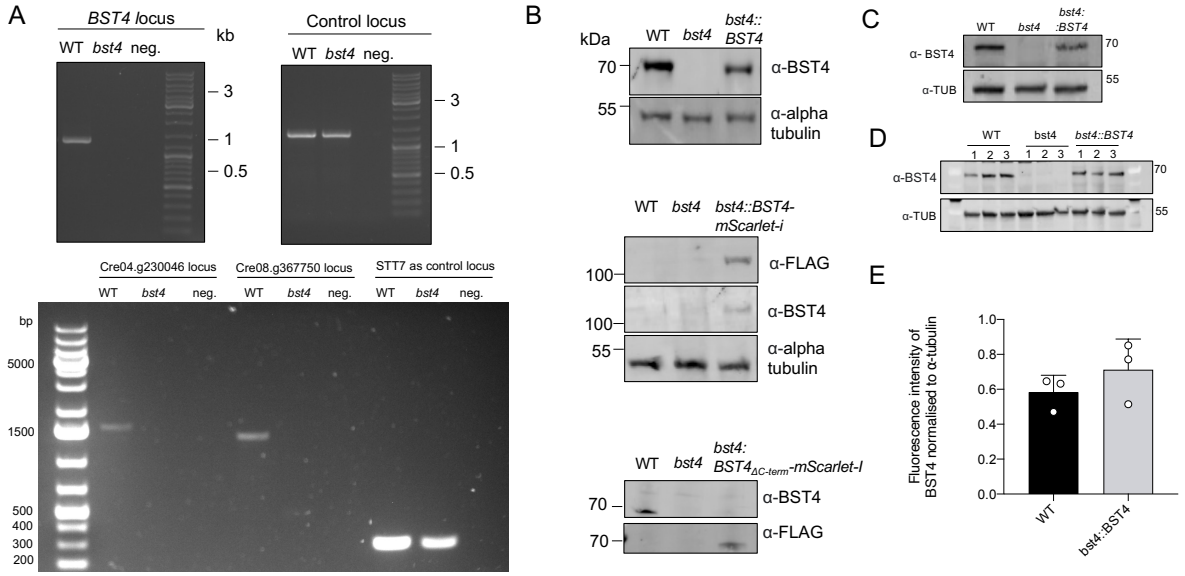

Supplemental Figure 3. Validation of Chlamydomonas BST4 lines. **A.** PCR amplification of the mapped CIB1 insertion sites and control loci of *bst4* (LMJ.RY0402.159478) and WT control strain (CMJ030 (CC-4533; cw15, mt -) gDNA to confirm the insertion of the CIB1 cassette in *bst4.* **B.** Immunoblots confirming the production of BST4 in WT, *bst4, bst4::BST4* and *bst4::BST-truncated* Chlamydomonas lines. **C.** Immunoblot showing the absence of BST4 in the *bst4* knock-out line and presence in the WT and *bst4::BST4* complemented lines. **D.** Western blot used to quantify the amount of BST4 protein detected in WT and *bst4::BST4.* **E.** Immunoblot was used for the quantification of fluorescent intensity as a measure of BST4 protein abundance. All fluorescent intensity measurements were normalized to respective alpha-tubulin loading controls and conducted in triplicate. No statistical difference was observed between WT and *bst4::BST4* BST4 protein abundance (Paired two-tail t-test $p = 0.22$, n=3)

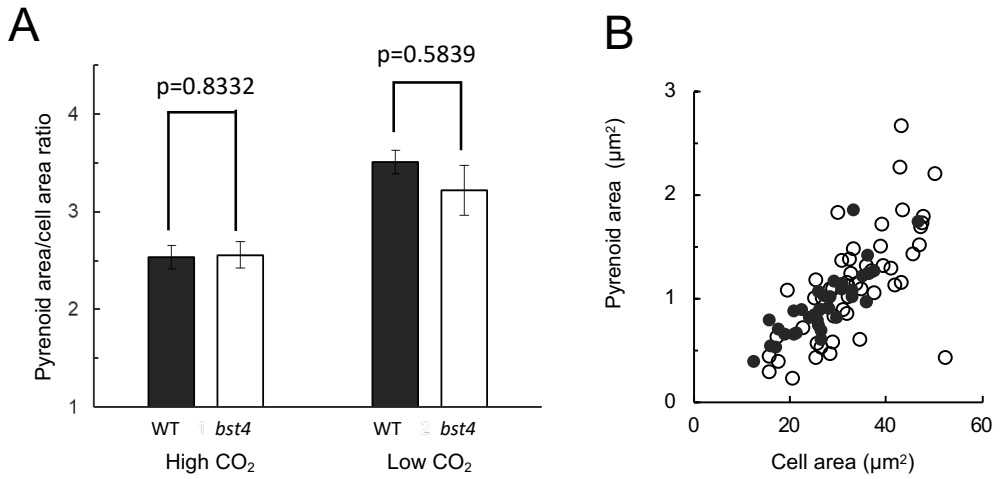

Supplemental Figure 4. Pyrenoid morphology in bst4 vs WT. A. The pyrenoid area to cell area ratio of WT control strain (black) and *bst4* (white) strains at high (3%) and low (0.04%) CO_2 concentrations. Each bar represents the mean value ± SEM (n=40–50). The data for wild type and *bst4* strains were compared using a two sample T-test. The p-values (showing no significant difference) are displayed above the bars**. B.** Pyrenoid area vs cell area of WT and *bst4* at 0.04% [CO_2].

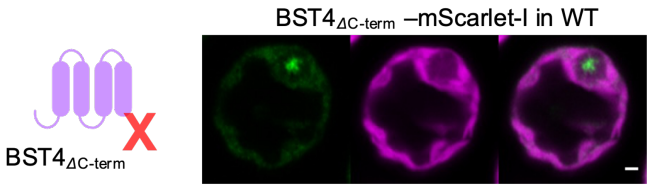

Supplemental Figure 5. Localization of C-terminally truncated BST4 in WT background. BST4$_{\Delta Cterm}$-mScarlet-I fluorescence shown in green and chlorophyll autofluorescence in magenta. Scale is bar 1 µm.

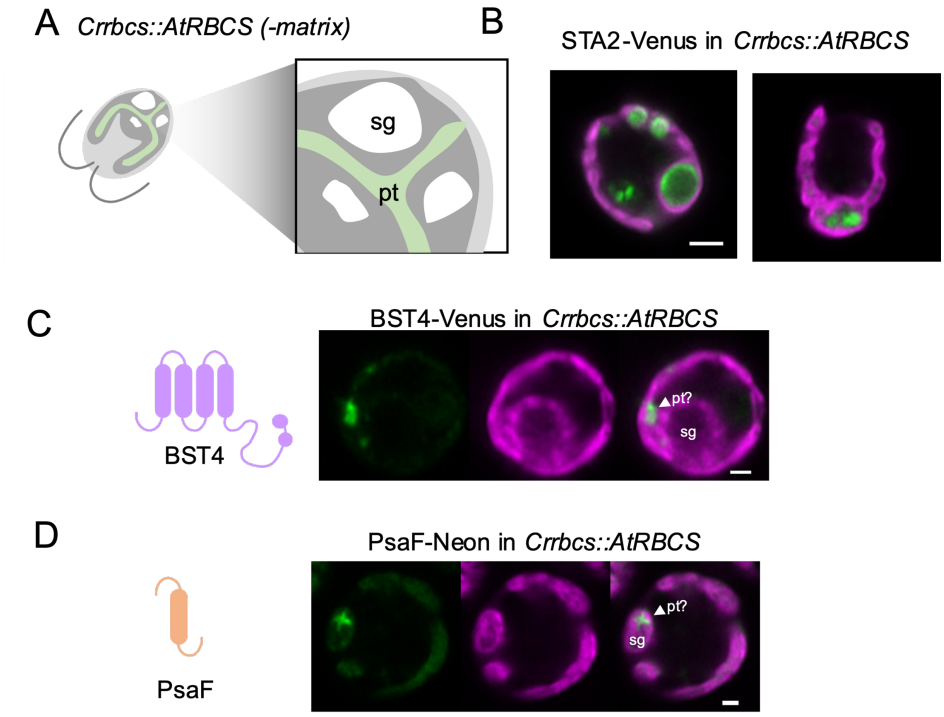

Supplemental Figure 6. Localization of proteins in a pyrenoid matrix-less background. A. Diagram showing a section of the *Crrbcs::AtRBCS* matrix-less mutant (*-matrix*). The nascent pyrenoid tubules (pt) are shown in dark green, starch granules (sg) in white. **B.** Confocal image of starch binding protein STA2 fused to Venus in *Crrbcs::AtRBCS.* Scale bar is 2 µm. **C.** BST4-Venus in a WT Chlamydomonas cell. Scale bar is 1 µm. **D.** PsaF-mNeon in *Crrbcs::AtRBCS*. Venus and mNeonGreen fluorescence are shown in green and chlorophyll autofluorescence in magenta. Scale bar is 1 µm.

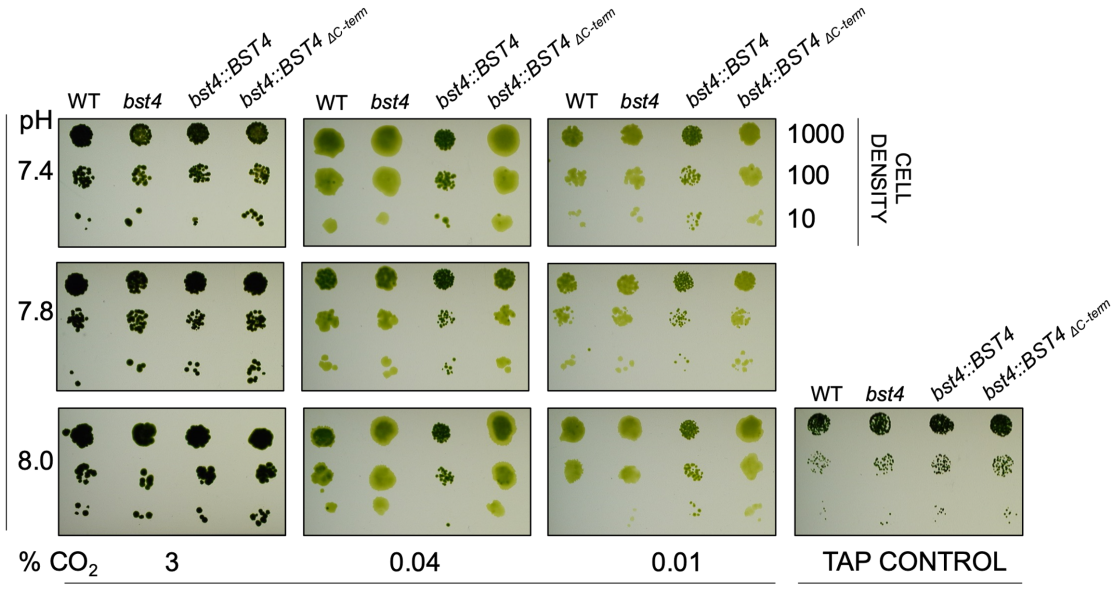

Supplemental Figure 7. Spot test of WT, *bst4* and BST4 complemented lines under CCM induced conditions. *Chlamydomonas* strains were grown in serial dilution on agar plates in saturating light (400 µmol m^{-2} s^{-1}) under a range of CO_2 (+/- 2 ppm) and pH conditions (specified) to induce the CCM. All lines grew comparably to WT across the conditions used and on the low light TAP control plate.

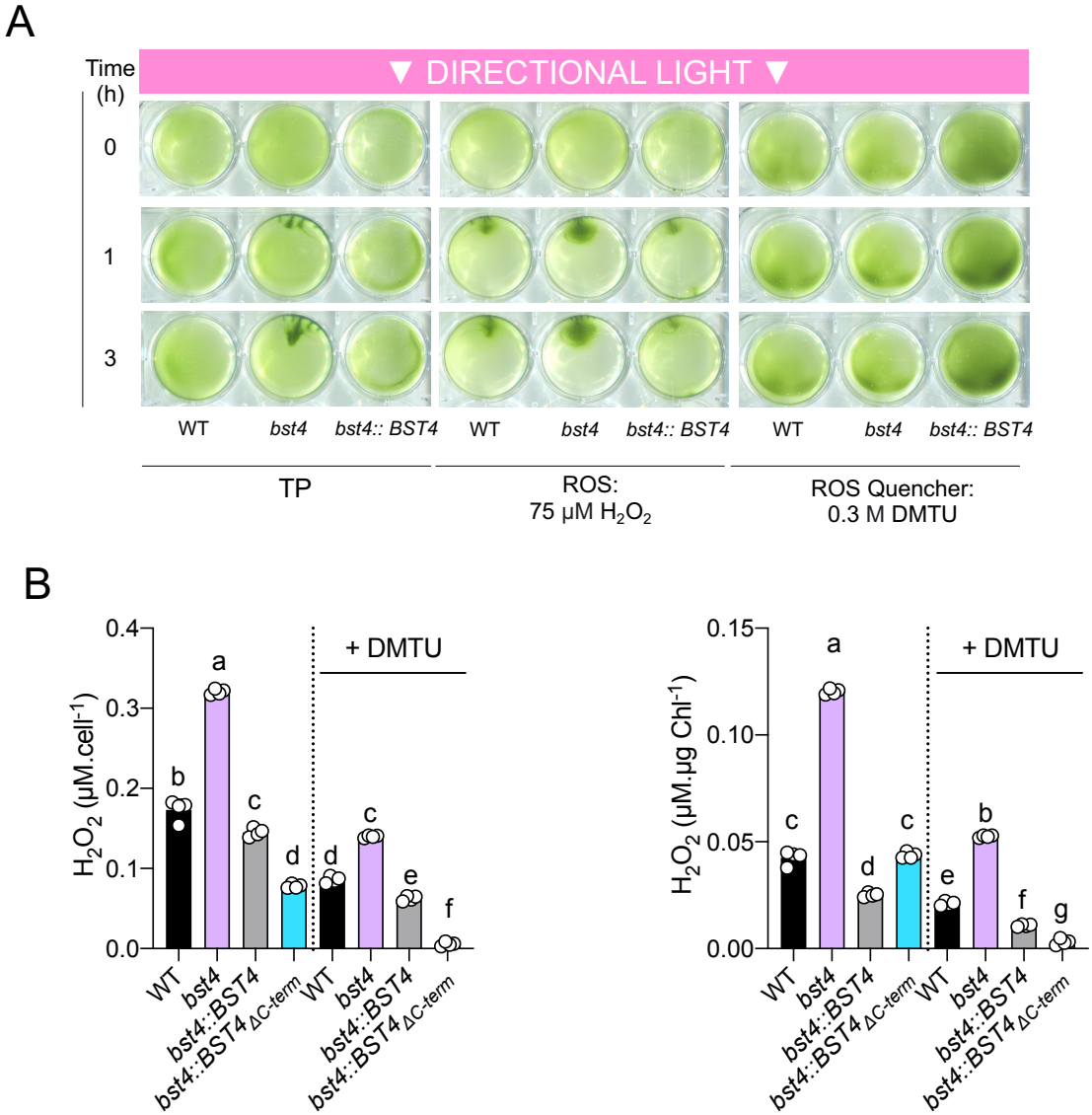

Supplemental Figure 8. Phototaxis and ROS assay. A. TP liquid cultures of Chlamydomonas cells were uniformly distributed on 0.8% (w/v) agar and subjected to directional light (150 µmol m^{-2} s^{-1}). Cell phototaxis was monitored at 0, 1, and 3 h. The assay was performed in the presence of 75 µM ROS hydrogen peroxide (H_2O_2) or 0.3 M ROS quencher N,N'-dimethylthiourea (DMTU). **B.** H_2O_2 assay. Chlamydomonas cells were grown in minimal TP liquid media and exposed to 150 µmol photons $m^{-2}s^{-1}$. A subset of cells were treated with the quencher DMTU. The concentration of H_2O_2 was subsequently quantified using Amplex Red (n=4), and is presented both proportionately to cell density and chlorophyll content. Different letters indicate significance ($p<0.05$) as determined by a one-way ANOVA and Tukey's post-hoc test.

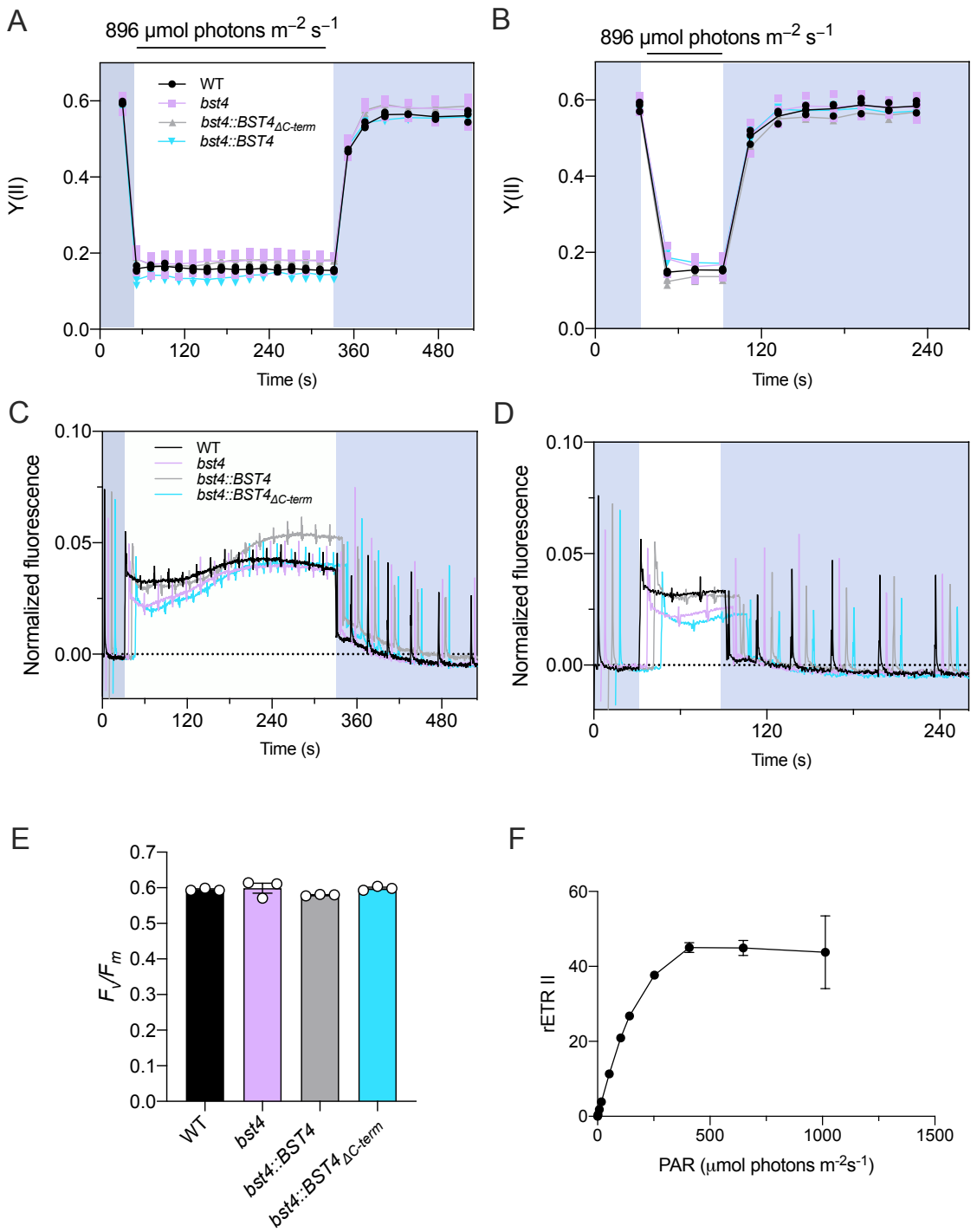

Supplemental Figure 9. Chlorophyll fluorescence measurements. A. Y(II) during 5 min illumination and **B.** One minute illumination. **C.** and **D.** Raw fluorescence curves for A. and B., respectively. Curves are normalized to F_o. Genotypes are artificially spaced by 5 s for clarity. **E.** F_v/F_m measurements **F.** Light curve for WT in the presence of bicarbonate. Points represent the mean of three technical replicates ±SEM.

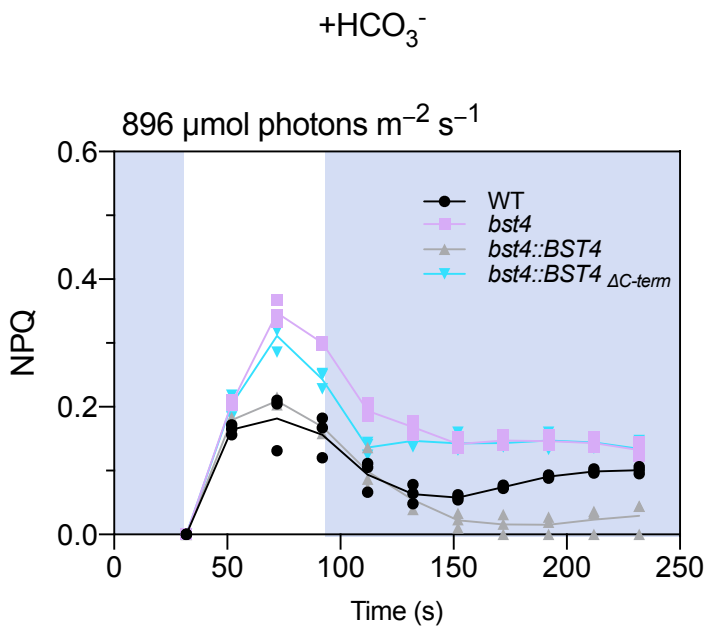

Supplemental Figure 10. NPQ with supplemented bicarbonate. Wild type (WT) and mutants were grown in HS medium at 80 µmol photons m^{-2} s^{-1} and measured at 10 µg Chl ml^{-1}. Cells were supplemented with 500 µM HCO_3^- and then dark adapted for 5 min before the measurements. Dynamics of Non-photochemical photochemical quenching (NPQ) on transition from dark to high light. Kinetics for induction of chlorophyll fluorescence were recorded during 1 min of illumination at 896 µmol photons m^{-2} s^{-1} followed by 5 min in darkness.

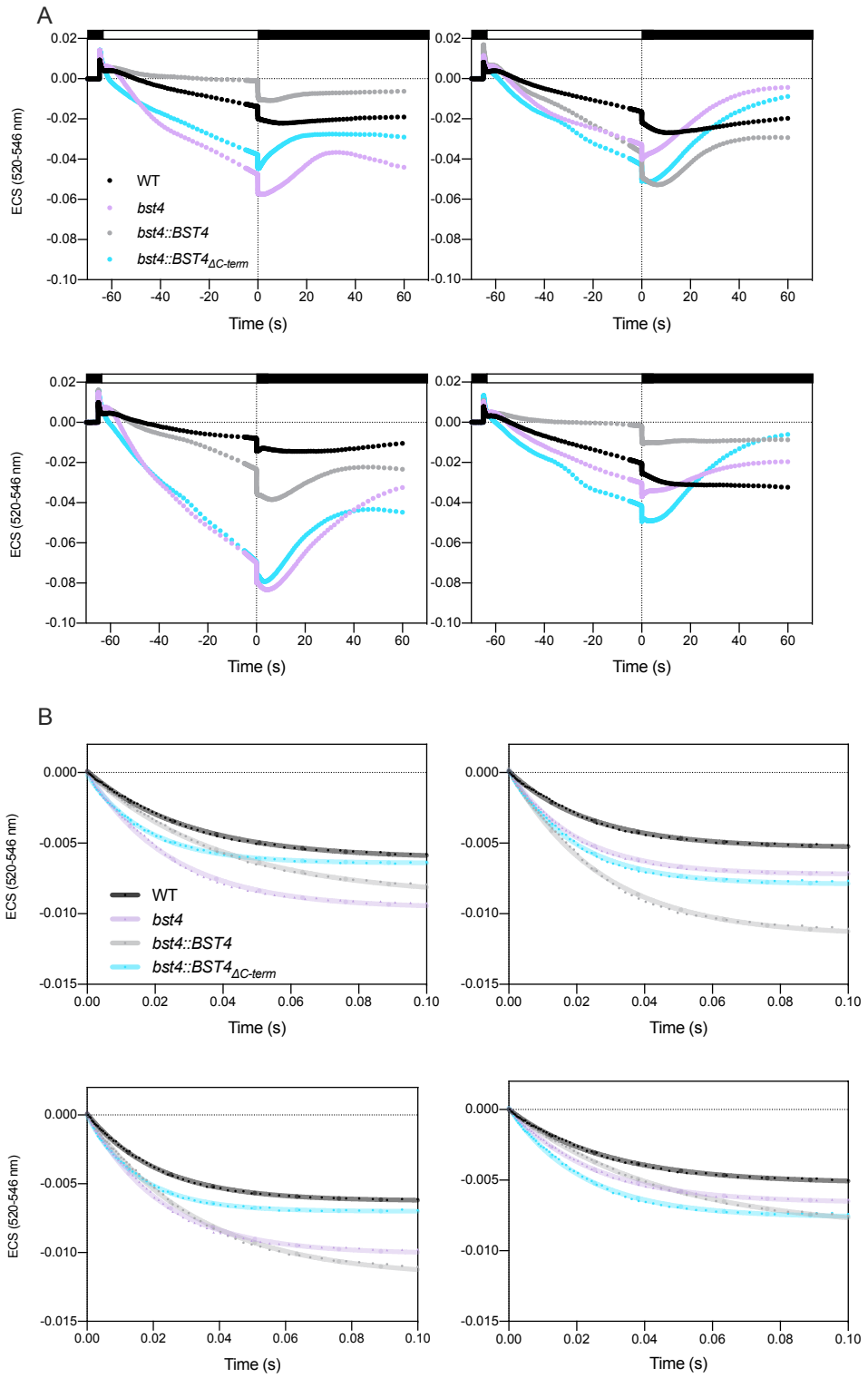

Supplemental Figure 11. Electrochromic shift (**ECS) traces across four biological repeats. A.** Cells resuspended in HS at 150 µg Chl ml^{-1} were dark-adapted for 1 min and then illuminated for 1 min with 890 µmol photons m^{-2} s^{-1} after which the light was switched off to record ECS in darkness. We were unable to calculate the partitioning of the PMF due to non-canonical ECS slow kinetics. **B.** Normalized ECS decay curves. ECS decay of the first 100 ms was fitted to calculate g_{H^+} (s^{-1}) =1/time constant for decay. Data are the means of n=3 technical replicates.

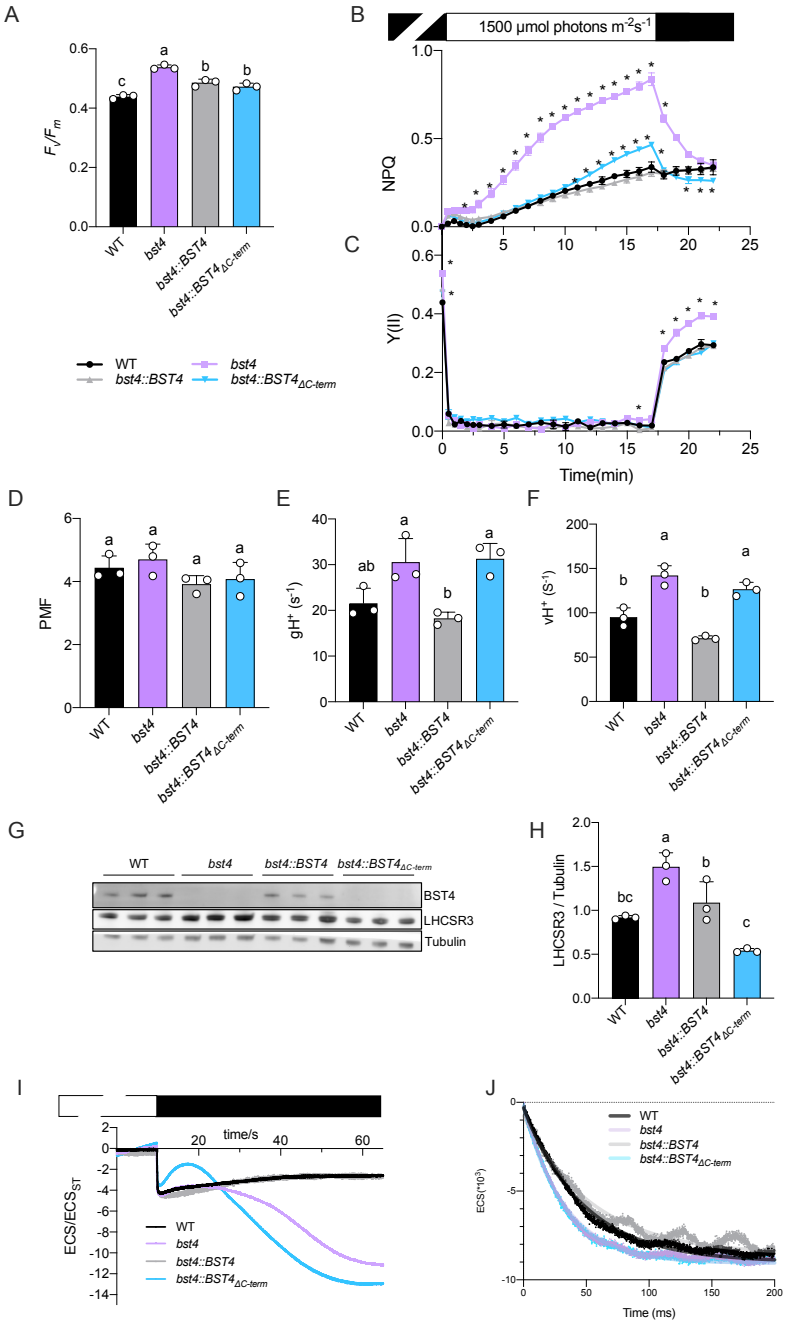

Supplemental Figure 12. Chlamydomonas bst4 mutant has an enhanced NPQ and proton conductance under high light and limiting Ci conditions. Wild type (WT) and mutants were grown on TAP medium at 20 µmol photons m^{-2} s^{-1}, resuspended in TP at 30 µg Chl ml^{-1} and exposed for 3 h to light at 150 µmol photons m^{-2} s^{-1}. The cells were dark adapted for 1 h before the measurements. **A.** Maximum quantum yield of photosystem II. **B.** Dynamics of photosynthesis on transition from dark to high light. Kinetics for induction of chlorophyll fluorescence were recorded during 17 min of illumination at 1500 µmol photons m^{-2} s^{-1} followed by 5 min in darkness. Non-photochemical quenching (NPQ) and **C.** Photosystem II quantum yield (Y(II)). **D to F.** ECS decay kinetics were performed on cells pre-exposed for 10 min to high light and the **D.** total PMF, **E.** g_{H^+}, and **F.** total H^+ flux (v_{H^+}) were determined as described in Methods. Data are the means ± SEM (n=3 replicates). **G.** Immunoblot of NPQ protein LHCSR3 in each genotype compared to tubulin after exposure of cells to 3 h 150 µmol photons m^{-2} s^{-1} in TP. **H.** Fluorescence of LHCSR3 protein band normalized to α-tubulin. Data are the means ± SEM (n=3 replicates). Different letters indicate statistically significant difference among the genotypes (one-way ANOVA test, followed by Tukey's post hoc test, $P < 0.05$). **I.** Representative Electrochromic shift (ECS) curves used to determine PMF values in D. **J.** Representative ECS decay curves. To determine the gH+ parameter in E., ECS kinetics were recorded during 600 ms dark intervals. The ECS decay of the first 100 ms was fitted to calculate gH+ (s^{-1}) =1/time

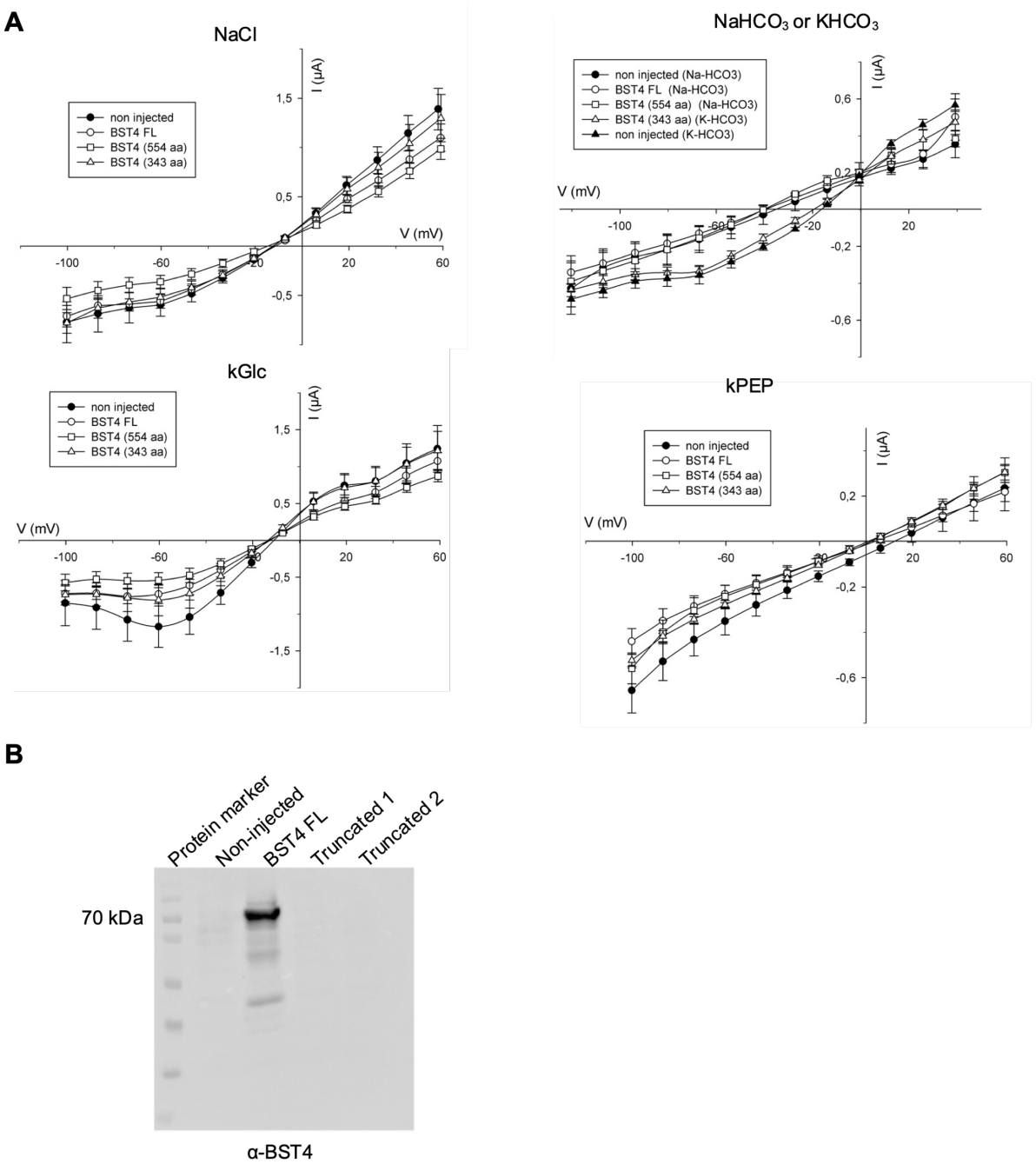

Supplemental Figure 13. No currents were detected for BST4 with any anions tested in Xenopus oocytes A. Steady state currents analysis of oocytes injected with BST4, full length or truncated, compared to non-injected oocytes. The voltage steps start from 60 mV to -100 mV (Cl^-, PEP^-, and Gluconate conditions) 40 mV to -120 mV ($HCO3^-$ conditions, right panel), holding voltage is -20 mV. Recordings were performed on n>4 oocytes. There is no differences between the currents recorded in non-injected oocytes and expressing the protein. **B.** Western Blot analysis of oocytes. Lane 1 is the marker, lane 2 are non-injected oocytes, lane 3 is the full-length protein (about 66 kDa), lanes 3 and 4 are the truncated proteins. We can only detect full length BST4 as the antibody is directed against the C-terminal part of the protein that is removed in the two truncated versions of the channel.

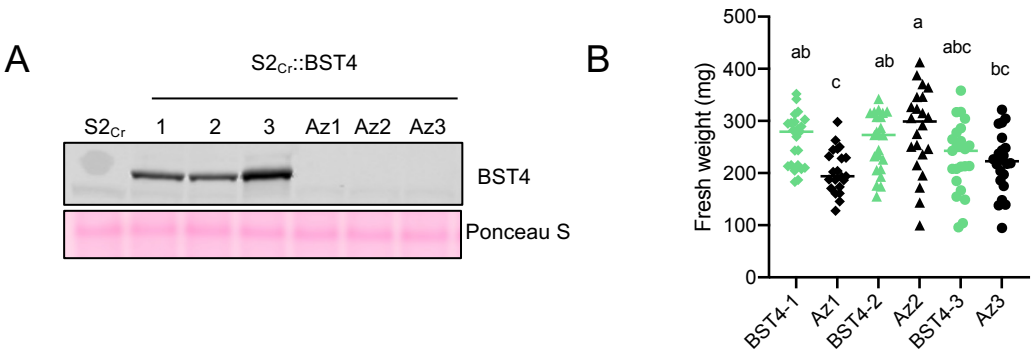

Supplemental Figure 14. Phenotype of BST4 transgenic Arabidopsis line. A. Immunoblot against BST4 of proteins extracted from BST4 no tag lines and Azygous segregants (Az). $S2_{Cr}$ is the parent line. **B.** Fresh weight of 28-day old rosettes, bars represent mean weight for each genotype n=18-21. Different letters indicate statistically significant difference among the genotypes (one-way ANOVA test, followed by Turkey's post hoc test, $P < 0.05$).

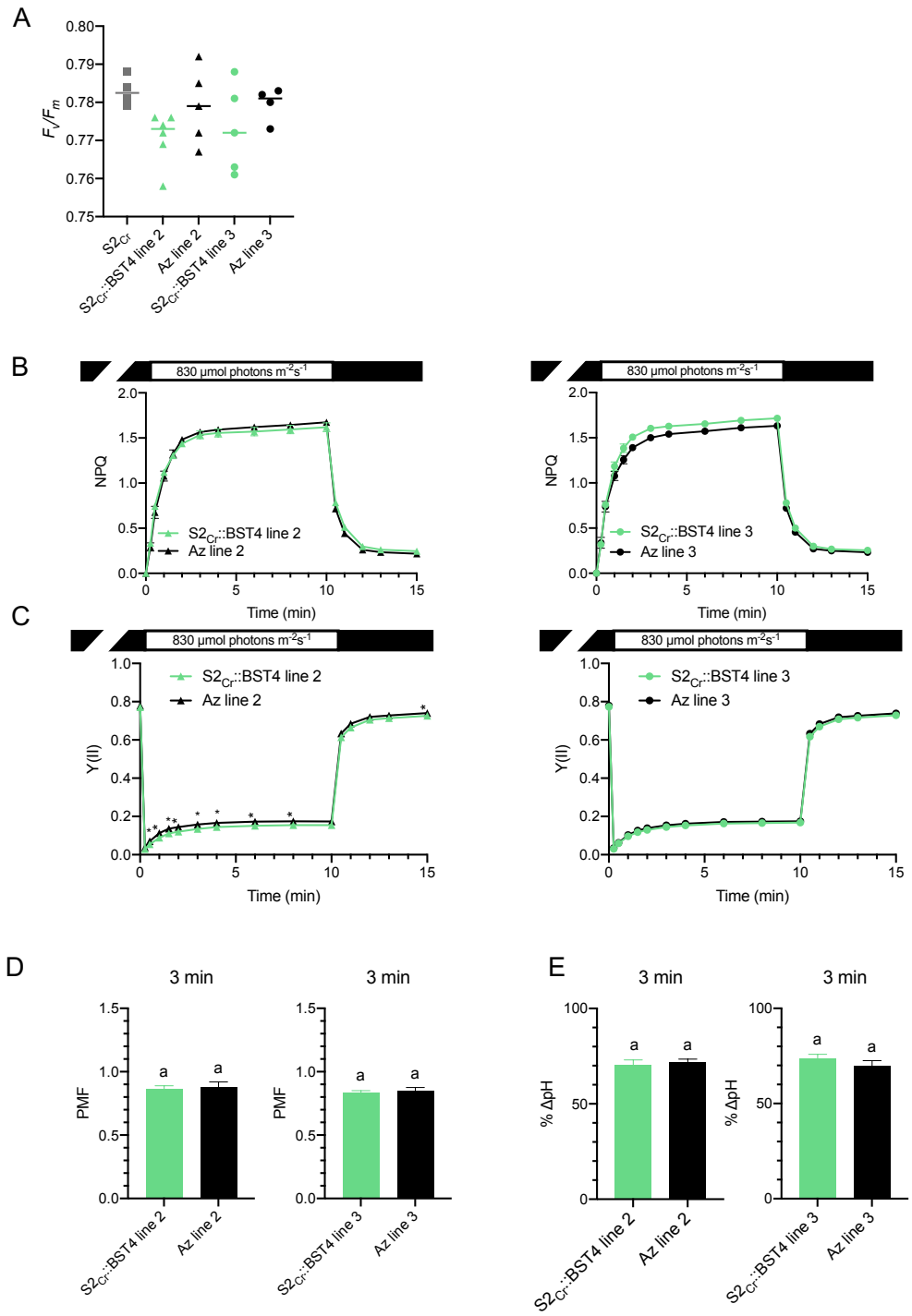

Supplemental Figure 15. Photosynthetic measurements of BST4 transgenic Arabidopsis lines 2 and 3. A. F_v/F_m values measured on attached, 30 min dark adapted leaves of 8-week-old plants (n=15-21). The letters in indicate nonsignificant differences between plants expressing BST4 and their azygous segregants using Tukey post hoc test (P > 0.05). **B.** Non-photochemical quenching (NPQ) as a measure of photoprotection and **C.** photosystem II quantum yield (Y(II)) were recorded during 10 min of illumination at 830 µmol photons m^{-2} s^{-1} followed by a 5-minute dark period. Data are presented as means ± SEM (n=4-6). Asterisks indicate statistical difference between plants expressing BST4 and their Azygous (Az) segregants according to unpaired t-test (P ≤ 0.05). **D.** Proton motive force (PMF) size and **E.** partitioning to pH gradient (ΔpH) after 3 min illumination at 830 µmol photons m^{-2} s^{-1}. Data are means ± SEM (n=5-6). The letters in E and F indicate non-significant differences between plants expressing BST4 and their azygous segregants according to unpaired t-test (P > 0.05).

A. Full length BST4 and homologous sequences

```
>Brassica_rapa_(PAC:30641593)
------------------------------------------------------------------------
------------------------------------------------------------------------
RTLYTHEKWVEHRSSLRHVHHLFSSFSSRVILSLIPPVFFFTSVAIFIASYNSAVAL-------------
DWLPSVFPILR---SSSLPYQLTAPALALLLVFRTEASYSRYEEGRKAWVGIIAGT--DDLARQVICSVDGSG--
---------------DELVIK-----DLLLRYV----AAFPVALKCHVTYGSD-----VARDLRN-----
LIEGDDLSLI--IESKHR-------------PRCVIEFISQSLQL----LKLDDT--------------
KRDLLESKMLHLHEGIGVCEQLMGIPIPLAYTRL-TSRFLVFWHLTL-------PIILWDEC-----
HWIVVPATFISAASLFCIEEVGVLIEEPFPM----LALDELCDL-VHSNIQEAVKSES-----------------
------------------------------------------------------------------------
------------------------------------------------------------------------
------------------------------------------------------------------------
------------------------------------------------------------------------
------------------------------------------------------------------------
------------------------------------
>Q9M2D2_-_VCCN1_Athaliana
MY------------------QSMNLSVSSNFTHRSLLES------------RFPI-----FSTGFR-----
KSVNLKPPRVSSGPE---SNDSGH---------------ETLTDKLIHLLRAVP--------
DWADEIKERGMQQKRSLYTHEKWVEHRSSLRHVRHLLSSFSSRVILSLIPPVFFFTSVAVVIASYNSAVAL----
---------DWLPGIFPILR---SSSLPYQLTAPALALLLVFRTEASYSRYEEGRKAWVGIIAGT--
NDLARQVICSVDSSG-----------------DELIIK-----DLLLRYI----AAFPVALKCHVIYGSD-----
IARDLRN-----LIEADDLSLI--LQAKHR-------------PRCVIEFISQSIQL----LKLDDA--------
------KRDLLESKMLHLHEGIGVCEQLMGIPIPLSYTRL-TSRFLVFWHLTL-------PIILWDEC-----
HWIVVPATFISAASLFCIEEVGVLIEEPFPM----LALDELCDL-VHSNIQEAVKSEKVIRNRIIAKIKLHEFK-
-----HSS--------------------------NGRHRS-----------------------------------
------------------------------------------------------------------------
------------------------------------------------------------------------
------------------------------------------------------------------------
------------------------------------------------------------------------
------------------------------------
>Nicotiana_tomentosiformis_(XP_009629643.1)
M--------------------------TNSRTLFSIQSPTNASFSSHF-TLKTPSK--LQQQSFPSKL-
NFKKLRFSTFKVRCCPQ----QTPQN---------------QNPTSALISILRIIP--------
DWADRIQEEGMKKKRSLYTHESWMQHRSSLRHVRHLFSSLNSRVILSLVPPVIAFTSVAVVIASYNSAVSM----
---------HWLPELFPVLR---ASPLPYQLTAPALALLLVFRTEASYSRFETGKKAWTKVIAGT--
NDFARQVIACVDKS-------------------DAVLK-----AALLQYI----MAFPVALKCHITYGSD-----
IASDLKN-----LLEADDLAVV--LSSKHR-------------PRCIIGFISQCLQS----LHLEGT--------
------KLTQLESKISCFHEGIGVCEQLAGIPIPLSYTRL-TSRFLVLWHLTL-------PIILWDDC-----
HWIVVPATFISAASLFCIEEVGVLIEEPFPM----LALDELCQL-VHDNIQESMANEKKIQERLSAKRKRRFSE-
-----HSQ--------------------------NGWPTS---------------------------------
------------------------------------------------------------------------
------------------------------------------------------------------------
------------------------------------------------------------------------
------------------------------------------------------------------------
------------------------------------
>XP_028961536_Malus_domestica
MLLPSSLSLQTLAPPNADTIQKPHQTLPQNLTLFQLVHP------QHFPTLQFPN-----LPSGPKTL-
KFKLLCSQSPNPNPSP-------PSS---------------SSPVQTLISILRIIP--------
DWSDRTQERGMRQHRTLYDHEKWMHHRSSYRHLRHLLSSLSSRVILSLIPPVIAFTLVAVVIASYNTAVAL----
---------DLLPGIFPLLR---SSSLPYQLTAPALALLLVFRTEASYSRFEEGRKAWTEVIAGA--
NDFARQIISSVETSG-------------------DAQLK-----KALLQYI----VAFPVALKCHVIYGSD-----
IARDLQN-----LLEVDDLLVV--LNSKHR-------------PGCIIQFISRSLQL----LKLEES--------
------RRIMLQSKISCFHEGIGICEQLIGTPIPLSYTRL-TSRFLVLWHLTL-------PIILWDDC-----
HWIVVPATFISAASLFCIEQVGVLIEEPFPM----LALDDLCNS-VRNNVQEALASEKLIRARLAAKGRIQSEQ-
-----QFQ--------------------------NGQPRP---------------------------------
------------------------------------------------------------------------
------------------------------------------------------------------------
------------------------------------------------------------------------
------------------------------------------------------------------------
------------------------------------
>Chlamydomonas_eustigma_(GAX83184.1)
```

```
M-------------------------------------------------------------------
LVHRVHTRSLGNRNQCGRK----------------------LHRVSTFVVKTPTEKPVVA----
DYVLPRSEEARRYFRTVYDFPQWQKHRSPTRLIDRLLQIPRSHVLQNILPSIAWCSSVAGLLTLYMQAYDA----
---------HILPDGFPSFATNNACTSFVNTTTVALSLLLVFRTNVSYGRWDEARKMKGLLVNRS--
RDLMRQVCAMVPEE-------------------DVATK-----AMMAKWT----AAFCRVLRIHFQPEVS-----
LEDEMKG-----LLSPEELEWL--IESKHR-------------PCSVIHMLSQIIYD----SQISAI--------
------CQAQMCNNLTAFEDVLGGCERLLRAPIPVSYTRH-TARFLFTWLTLL-------PFALYNSC-----
GVWTLPVVAGVSAVLCGIEEIGVQIEEPFGI----LPLEAICGR-IQADVMATLKEDAKTRNLRNKVLLIRGPE-
-----HWAMV------------------------NGHSNK-----------------------------------
---------------------------------------------------------------------------
---------------------------------------------------------------------------
---------------------------------------------------------------------------
---------------------------------------------------------------------------
-----------------------------------
>Cre16.g662600.t1.2_(BST1)
M---------------------------------QMQA-----------
NRSSLRASPVRGLGARPLLRALPAGRVARLNVSAQA--KDPNAPIQ---------------
SNPLGTLSSQSGQVA----------
TLPRSEEARKYFRTVYDFPQWQKHRSSYRFAERLFQLSQSHILQNALPAISWVTLVATLVASYGYSYDQ------
-------HMLPDVFPSISPNASCTAFISNTSVALSLLLVFRTNSSYGRWDEARKMWGGLLNRS--
RDIMRQGATCFPDD-------------------QVEAK-----KALARWT----VAFSRALRIHFQPEVT-----
IESELQN-----ILTPAELQML--AKSQHR-------------PVRAIHAISQIIQS----VPMSSI--------
------HQQQMSNNLTFFHDVLGGCERLLRAPIPVSYTRH-TARFLFAWLTLL-------PFALYPTT-----
GWGVVPVCTGIAAVLCGIEEIGVQCEEPFGI----LPLDVICNR-
IQADVMATLKDDADTKTILAEAGLISLIPS----ATSATPVASA----EPVLVSARPSAAPAPNNGLQVRVAM--
-----------------------------------------------------------------------GG-
--------------------ERK*-------------------------------------------------
---------------------------------------------------------------------------
---------------------------------------------------------------------------
-----------------------------------------------------------------
>Cre16.g663400.t2.1_(BST2)
M----------------------------------QC-------------LSSRPVAMGRAGSSALPRL-
PLRAGRVCHLGVRCQAANKDPNAPIQ---------------SNPLGSFSSQLQNQP----------
TLPRSEEARKYFRTVYDFPQWQTHRNQYRLMKRLFSIPQSHVIQNALPSIMWVAFTSTCVAAYMYGYDQ------
-------HMLPEGFPTLAPNAACSAFISNTSVALSLLLVFRTNSSYGRWDEARKMWGGLLNRS--
RDIMRQGATCFPDD-------------------QVEAK-----KALARWV----VAFSRALRIHFQPEVT-----
IESELKN-----ILTPAELQML--AKSQHR-------------PVRAIHAISQIIQS----VPMSSI--------
------HQQQMSNNLTFFHDVLGGCERLLRAPIPVSYTRH-TARFLFAWLTLL-------PFALYGSC-----
GVSVIPVCSGIAAVLCGIEEIGVQCEEPFGI----LPLDVICNR-IQADVMATLKDDADTKTILAEAGLISLRA-
-----NSAMAVENALPDLDSINAAAPNGNGSHNGNGAAV-----------------------------------
-----------------------------------------------------------------PVS-----
----------------------VSAGA-----------------------------------------------
---------------------------------------------------------------------------
-----------------------------------------------------------------SGNGMNV---
------------------------RISPR*-----
>Cre16.g663450.t1.2_(BST3)
M---------------------------------QVSK-----------VPSS------ASARCLPRL-
PVRTSRVCQLSVRCQAANKDPNAPIQ---------------SNPLGSFSSQNSSGAVV--------
TAPRNEDARKYFRTVYDFPQWQKHRSQSRLVRRLFTIPQSHVIQNALPSIMWVTFTSTCVAAYMYGYDL------
-------HILPEGFPTLAPNAACSAFISNTSVALSLLLVFRTNSSYGRWDEARKMWGGLLNRS--
RDIMRQGATCFPDD-------------------QVEAK-----KALARWT----VAFARALRIHFQPEVT-----
IESELQN-----ILTPAELQML--AKSQHR-------------PVRAIHAISQIIQS----VRMSSI--------
------HQQQMSNNLTFFHDVLGGCERLLRAPIPVSYTRH-TARFLFAWLTLL-------PFALYGSC-----
GVSVIPVCTGIAAVLCGIEEIGVQCEEPFGI----LPLDVICNR-IQADVMATLKDDADTKTVLAEAGLISLIP-
-----SMSLPPTEHASPSDPVTAAAAAALAAANGNGAASHSNG-------------------------------
-----------------------------------------NG---------------------
SKPVSTQVPP-----------------PVLAPVTVTS-------------------------------------
---------------------------------------------------------------------------
---------------------------------------------------------------------------
SSGSMNV--------------------------RISPR*-----
>Chlorella_sorokiniana_(PRW33726.1)
M----------------------STAMLAGSRIQLQQPAG--------LGGSRLQ--RAAAPVAAAA-
RLGSVRPAGLQARSTAARRADRSALR---------------VSATASPEAAPVKLS----------
```

GDDLKEANRKHMRSVFDFDLWKKHRSSSRYLRHIVGLGESRIVSGLMAPLTYVMTLSLAVACYNAAAEA------
-------GYLP-VFPELKL--ATNAPFGLTSFALSLLLVFRTNSSYGRWDEARKMWGLIVNRS--
RDFIRQGLGYIPPE-------------------QEELQ-----KMLVRWT----VAYSRSLMCHLRPGED-----
LRVELKD-----TLKPEELEAL--LASTHR-------------PNYVVQVLTAIIKT----
AQLPAAVTNNRDSTGCVPAGAAYRMDENLTVFADVTGGCERILRTPIPLSYTRH-TSRFMMIWLTLL-------
PFTLWDSC-----HWAMLPIAGIVSFLLLGIEEIGVQIEEPFTI----LPLEVISRT-IEGNVWELYRMHSGEA-
--LEKEQAELAN------GQDVQVLNA----QDLVALMAPSAVGNTANGTSRKSLV------------------
VNYGL---

>Cre06.g261750.t1.2_(BST4)
M-----------------------QC--------QLKH----------------------------GA-
RPQSQRPNWLPARAATLRPAVQHGVR---------------RGLTLGVKAAAAPLE--------
DKKMPADMTTRQYRRVVYDFALWAKHRDVNRYLYNLRTIPGSRIIRQLSQPMGVVLAWAALFGFYETCLEA----
---------GVLPSYLPKMTL--MSAEPQGLTSFALSLLLVFRTNSSYGRFDEARKIWGGILNRA--
RNIANQAVTFIPAE-------------------DQAGR-----EAVGKWT----VGFTRALQAHLQEDID-----
LRKELEKA--TPRWSKEEIDML--VNAQHR-------------PIKAISVLSELTRQ----LSITQF--------
------QALQMQENCTFFYDALGGCERLLRTPIPVSYTRH-TARFLTIWLAML-------PLGLWERY-----
HWSMLPVIALIGFLLLGIDEIGISIEEPFGI----LPLDAICGR-AQTDVNSLLKEDPAVMKYVDDVRSGRVKS-
-----PPPLPPAPA----APAAA-------AAAAAAAARSVSP----
QPDVAKTLGSLFTNVRAGVGAVAPGAPLMPQAPVRSPSPTRSVSP--------SFPRASAGTGMPPPVGMNG---
-------ATPRVAAAPPTPPPVSRPAA------------------
PAAAPAAGSGFTMPNFSASLSGLTGGAAAAAKSAADAASSKLTKMADSMSSGAAAPAPPAAPAR-----------
----------PSTSPRPSASSPISSSADADRSDSSRR---PVNWRDELQSLKATRE----------------
PNGNGNGSGVAPAA--GRADADEEALRRFGNLAGRSR--------------SGNG---------------
GGGSSDTELSEANRPRTRPDWRNQL*
>XP_002945810.1_Volvox_carteri_f._nagariensis
M-----------------------QS--------QLQP----------------------------RL-
QLQGTRLNWLPQRSCVQRRSLRVDAT---------------SG------AAPPPPA--------
GKELSNDMVTRQYRRTVYDFSLWAKHRDVNRYLYNLKTIPGSRIIRTLGQPMGIVLAWAAMFGFYETCLES----
---------GVLPSYFPKLTL--MSAEPQGLTSFALSLLLVFRTNSSYGRFDEARKIWGGILNRA--
RNIANQAVTFIPAE-------------------DVAGR-----EAVGKWA----VGFCRALQAHLQEDAN-----
LREELQKA--QPRWSREEIDML--CSAQHSWQQLQSCVNAFW-PIKAISMLSELTRQ----LPISQF--------
------QALQMQENVTFFYDALGGCERLLRTPIPVSYTRI-----------------------------------
---------------------------------LPLDAICTR-AQTDVVSLLKDDPAVVKYISDVRQGRIAP---
---PTEPPVAGA----
APVAAAPPPPPPASAGGGISRSGSPTAQQQPDVMKTVTSMLHNVKAGIGAVAPAPPRPPSPQPRARSP-
RAASPGGPS----PFPRASAGTG--------G----------
AAAAVPSPPPIKPLTSSSSSSSGAVSKDSNNSTATAKKPASAPAASSA----GFSMGFSGLADGAAAAAKSAS-
AAAAKFSKIADSVVAG--TPAAPASEAKRETAA--AAAMQAQPRN---
TPSSSSSTPSAAPANGSSDDDRSSSGRRTAAAVNWREELAALRAGREDAEEPASASASYDREFPSSSWSFSSASS
AAVVQSGDAEDEARRRFGGLAGRGARSDTTTSAAAVMRGNGNGLSENGYGNGYGNDN-
GNGNGNTVEARGARPRTRPDWRNQL-
>Chrysochromulina_sp._(KOO32217.1)
M-----------------------REHPLSYEEYMRQRS----------AGRDPLA--EAVQGQSASM-
ERGVVPPPPVKATPERTEAAFTPPAEFDFFQDVFKPTVESVVKAVVSPGAQQDSDESYMRVPWWEQGSTYSEDQR
KDRRTVFMHDDWKRHRSSERFFRNIKTWPSSGINQALRKELTFVTSVSVFVVLANMLLYQYQDFGGVVHPGPLSF
LDGPIKSLS---LPALPFSMASPVLSLLLVFRTNTAYFRWNEARTLWGGLINNC--RNIVRQTTTMFPNDA----
-------------YHNALK-----KRLATET----ATFIKSLRNFLRGPEDDAT--
LRKELYAYVNQGLMTSAQAEAT--LAAKNR-------------PMFALAAMSATLRK----ANIDEM--------
------YISRMDSTISVLVDLTGANERIFKSPIPLVYTRL-TARFLSVFLTLL-------
PLAMWAALGESWNHWATIPATFILSVFLFGVEEVGIQIEEPFSI----LPLEAMCNGAIEAVQLEMLAAE-----
------------------QSQVFEAAG----DAVAVA-------------------------------------
---

>Emiliania_huxleyi_(XP_005770556.1)


```
EFKEAGREFRQDVYSYNDWRWHRESGHIASAISSVFTSGVGKAMWRETFFVIATAAAVYLYNIGVPVLAAKTAAS
L----PIVAALLGRLPLLHLSLLPLTLSSPALFLLLVFRTNNSYDRWWEARKVWGGVINAS--
RDLARQALALVR---------------------DAELK-----KLMVSQI----
ASYARVLKYHLGPPTPEARDLLRNELVD----NRLPADQVRVI--MEAKHK-------------
PMALLGLVSASLHDSGR-TGLDTV--------------QASKLDQTLSLLTDYLGKCERIVKTPLPLVYTRH-
TARFLSWWLLFL-------PVCLYNQLRA---NWMIVPVSGLIGFFLVGIEDLGNQIEEPFSI----
LPLTAMGTG-IQQSIFEAL-----------------------------------------------------
---------------------------------------------------------------------------
---------------------------------------------------------------------------
---------------------------------------------------------------------------
---------------------------------------------------------------------------
---------------------------------------------------------------------------
>Phaeodactylum_tricornutum_(XP_002180738.1)
MM-------------------------------------------------------RNFASVLLLL-
SSGAAAFAPVQHNGVRTIATPSTPLY---------------GNTKQPPALP--PIK----------
DISYGEESRKYRRTVYSHDDWVKHRSSDRFLRNLLAIGSSGVYKSLAKEVLATTGVATFIVLYNCLVGGYTDLEG
IKHS---ALIESVWAPLMA--LPLAPFTLSSPSLGLLLVFRTNTSYQRWDEARKNWGMNINHT--
RDLVRMGTSFYDNAA-----------------VSSEQRAKDL-KALSLAT----WSFVRAMKRHLSPESEDEQD-
FRRELFE-----RLPAPQAQAI--IDAAHR-------------PNRALFDLSVAIEN----LPMHFL--------
------RKNQVHQAVTIFEDNLGSSERLLTSPVPLFYSRH-TARFLSFWLLLL-------
PFALWDPFAGTWNHVGMIPATAVISIFLFGIEELATQMEEPFTI----LPMQAFCDK-
IGNWCNEIVSWQAGDNGMAVNMPSMISPEGLPELKEPAPVPAMA----VASVAAAMPVMANGDINGDTTGITM--
-DQP-----------------------------------------------HNAIP-----------------
---------------------------------------------------------------------------
---------------------------------------------------------------------------
---------------------------------------------------------------------------
-----------------------------------------------------------------
>Thalassiosira_pseudonana_(XP_002289965.1)
M--------------------------------------------------------------------------
---------------------------------------GPPIDPSVPVT-----------
DQVGEGSRKYRRTVYTHDDWVRHRSPDRFGNNLSTLFNSGIYKQVANEVFATTAVATFVFLWNMIAGGYTDLAGV
QHG---PIIDSPLAQMVG--LPMTAFTILTPSLGLLLVFRTNTSYGRWDEARKMWGLNINHT--
RDLNRMATAWYGNEGNMDSVAFMGGDIPYSQPIDPVQRAYDL-GQVSLFT----WAFVRSMKRHLSPPEEDEED-
FKAELRA-----RLTPEQAENI--INAAHR-------------PNRALFDLSVAIEN----LPMHFL--------
------RKNAINTNLSIFEDTLGGCERLLSSPVPLFYSRH-TARFLSTWLLLL-------
PFGLYEQFKDSWNHIAMIPATAFISVCLFGIEELATQLEEPFTI----LPMQGFCDK-IGGWCDEIVSW-
AGQGQQEYTEENAMSNE------QEMTY-----------------------------------------------
---------------------------------------------------------------------------
---------------------------------------------------------------------------
---------------------------------------------------------------------------
---WR-----------------------------------------------------------------
-----------------------------------------------------
>WP_049046555.1_Kiebsiella_aerogenes
---------------------------------------------------------------------------
---------------------------------------------------------------------------
------MIIRPEQHWFFRLFDWHGSVLSKIVFRLLLNVLMSVIAIISYQWYEQL-------------GI------
-----HLTVAPFSLLGIAIAIFLGFRNSASYSRFVEARNLWGTVLIAE--RTLVRQLKNILPD------------
--------DEETH-----KTLVSYL----VAFSWSLKHQLRK-TD-----PAVDLYR-----LLPKEKVAEI--
LASSMP-------------TNRILLLIGNELGRLREQGKLSDI--------------
TYGLMDNKLDELAHVLGGCERLASTPVPFAYTLI-LQRTVYLFCTLL-------PFALVGDL-----
HYMTPFVSVFISYTFLSWDSLAEELEDPFGTSANDLPLNAMCNT-IERNLMDMTGQHPLPEKMQPDRYYNLT---
---------------------------------------------------------------------------
---------------------------------------------------------------------------
---------------------------------------------------------------------------
---------------------------------------------------------------------------
---------------------------------------------------------------------------
-----------------------------------
>XP_011543531.1_Homo_sapiens
M--------------------------------------------------------------------------
-------------------------------------------------------------------------
TITYTSQVANARLGSFSRLLLCWRGSIYKLLYGEFLIFLLCYYIIRFIYRLALTEEQQL--------------
MFEKLTL--YCDSYIQL--IPISFVLGFYVTLVVTRW------WNQYENLPWPDRLMSLVSGFVEGK--------
-----------DEQGRL--LRRTLIRYANLGNVLILRSVSTAVYKRFP-----SAQHLVQ---
```

```
AGFMTPAEHKQLEKLSLPHNM---------FWVPWVWFANLSMKAWLG---GRIRDPI-------------
LLQSLLNEMNTLRTQCGHLYAYDWISIPLVYTQVVTVAVYSFFLTCLVGRQFLNPAKAYPGHEL---
DLVVPVFTFLQFFFYVGWLKVAEQLINPFGEDDDDFETNWIVDRNLQVSLLAVDEMHQDLPRMEPDMYWNKPEP-
-----QPPYTAASA----QFRRASFMGSTFNISLNKEEMEFQPNQEDEED-----------
AHAGIIGRFLGLQSHDHHPPRANSRTKLLWPKRESLLHEGLPKNHKAAKQ----
NVRGQEDNKAWKLKAVDAFKSAPLYQRPGYYSAPQ-----------TPLSPTPMFFPLEPSA---
PSKLHSVTGI-DTKDKSLKTVSSGAKKSFELLSES--
DGALMEHPEVSQVRRKTVEFNLTDMPEIPENHLKEPLEQSPTNIHTTLKDHMDPYWALENR----------
SVLHLNQGHCIALCPTPASLALSLPFLHNFLGFHHCQSTLDLRPALAWGIYLATFTGILGKC-------------
--SGPFLTSPWY---HPEDFLGPGEGR--------------------
```

B. BST4 and homologous sequences trimmed after the bestrophin domain

```
>Brassica_rapa_(PAC:30641593)
------------------------------------------------------------------------
-------------------------------------------------------------------------
RTLYTHEKWVEHRSSLRHVHHLFSSFSSRVILSLIPPVFFFTSVAIFIASYNSAVAL-------------
DWLPSVFPILR---SSSLPYQLTAPALALLLVFRTEASYSRYEEGRKAWVGIIAGT--DDLARQVICSVDGSG--
---------------DELVIK-----DLLLRYV----AAFPVALKCHVTYGSD-----VARDLRN-----
LIEGDDLSLI--IESKHR-------------PRCVIEFISQSLQL----LKLDDT--------------
KRDLLESKMLHLHEGIGVCEQLMGIPIPLAYTRL-TSRFLVFWHLTL-------PIILWDEC-----
HWIVVPATFISAASLFCIEEVGVLIEEPFPM----LALDELCDL-VHSNIQEAVKSE
>Q9M2D2_-_VCCN1_Athaliana
MY------------------QSMNLSVSSNFTHRSLLES------------RFPI-----FSTGFR-----
KSVNLKPPRVSSGPE---SNDSGH---------------ETLTDKLIHLLRAVP--------
DWADEIKERGMQQKRSLYTHEKWVEHRSSLRHVRHLLSSFSSRVILSLIPPVFFFTSVAVVIASYNSAVAL----
---------DWLPGIFPILR---SSSLPYQLTAPALALLLVFRTEASYSRYEEGRKAWVGIIAGT--
NDLARQVICSVDSSG-----------------DELIIK-----DLLLRYI----AAFPVALKCHVIYGSD-----
IARDLRN-----LIEADDLSLI--LQAKHR-------------PRCVIEFISQSIQL----LKLDDA--------
------KRDLLESKMLHLHEGIGVCEQLMGIPIPLSYTRL-TSRFLVFWHLTL-------PIILWDEC-----
HWIVVPATFISAASLFCIEEVGVLIEEPFPM----LALDELCDL-VHSNIQEAVKSE
>Nicotiana_tomentosiformis_(XP_009629643.1)
M--------------------------TNSRTLFSIQSPTNASFSSHF-TLKTPSK--LQQQSFPSKL-
NFKKLRFSTFKVRCCPQ----QTPQN---------------QNPTSALISILRIIP--------
DWADRIQEEGMKKKRSLYTHESWMQHRSSLRHVRHLFSSLNSRVILSLVPPVIAFTSVAVVIASYNSAVSM----
---------HWLPELFPVLR---ASPLPYQLTAPALALLLVFRTEASYSRFETGKKAWTKVIAGT--
NDFARQVIACVDKS-------------------DAVLK-----AALLQYI----MAFPVALKCHITYGSD-----
IASDLKN-----LLEADDLAVV--LSSKHR-------------PRCIIGFISQCLQS----LHLEGT--------
------KLTQLESKISCFHEGIGVCEQLAGIPIPLSYTRL-TSRFLVLWHLTL-------PIILWDDC-----
HWIVVPATFISAASLFCIEEVGVLIEEPFPM----LALDELCQL-VHDNIQESMANE
>XP_028961536_Malus_domestica
MLLPSSLSLQTLAPPNADTIQKPHQTLPQNLTLFQLVHP------QHFPTLQFPN-----LPSGPKTL-
KFKLLCSQSPNPNPSP-------PSS---------------SSPVQTLISILRIIP--------
DWSDRTQERGMRQHRTLYDHEKWMHHRSSYRHLRHLLSSLSSRVILSLIPPVIAFTLVAVVIASYNTAVAL----
---------DLLPGIFPLLR---SSSLPYQLTAPALALLLVFRTEASYSRFEEGRKAWTEVIAGA--
NDFARQIISSVETSG------------------DAQLK-----KALLQYI----VAFPVALKCHVIYGSD-----
IARDLQN-----LLEVDDLLVV--LNSKHR-------------PGCIIQFISRSLQL----LKLEES--------
------RRIMLQSKISCFHEGIGICEQLIGTPIPLSYTRL-TSRFLVLWHLTL-------PIILWDDC-----
HWIVVPATFISAASLFCIEQVGVLIEEPFPM----LALDDLCNS-VRNNVQEALASE
>Chlamydomonas_eustigma_(GAX83184.1)
M-------------------------------------------------------------------
LVHRVHTRSLGNRNQCGRK----------------------LHRVSTFVVKTPTEKPVVA----
DYVLPRSEEARRYFRTVYDFPQWQKHRSPTRLIDRLLQIPRSHVLQNILPSIAWCSSVAGLLTLYMQAYDA----
---------HILPDGFPSFATNNACTSFVNTTTVALSLLLVFRTNVSYGRWDEARKMKGLLVNRS--
RDLMRQVCAMVPEE-------------------DVATK-----AMMAKWT----AAFCRVLRIHFQPEVS-----
LEDEMKG-----LLSPEELEWL--IESKHR-------------PCSVIHMLSQIIYD----SQISAI--------
------CQAQMCNNLTAFEDVLGGCERLLRAPIPVSYTRH-TARFLFTWLTLL-------PFALYNSC-----
GVWTLPVVAGVSAVLCGIEEIGVQIEEPFGI----LPLEAICGR-IQADVMATLKED
>Cre16.g662600.t1.2_(BST1)
M---------------------------------QMQA-----------
NRSSLRASPVRGLGARPLLRALPAGRVARLNVSAQA--KDPNAPIQ---------------
```

```
SNPLGTLSSQSGQVA----------
TLPRSEEARKYFRTVYDFPQWQKHRSSYRFAERLFQLSQSHILQNALPAISWVTLVATLVASYGYSYDQ------
-------HMLPDVFPSISPNASCTAFISNTSVALSLLLVFRTNSSYGRWDEARKMWGGLLNRS--
RDIMRQGATCFPDD-------------------QVEAK-----KALARWT----VAFSRALRIHFQPEVT-----
IESELQN-----ILTPAELQML--AKSQHR-------------PVRAIHAISQIIQS----VPMSSI--------
------HQQQMSNNLTFFHDVLGGCERLLRAPIPVSYTRH-TARFLFAWLTLL-------PFALYPTT-----
GWGVVPVCTGIAAVLCGIEEIGVQCEEPFGI----LPLDVICNR-IQADVMATLKDD
>Cre16.g663400.t2.1_(BST2)
M--------------------------------QC-------------LSSRPVAMGRAGSSALPRL-
PLRAGRVCHLGVRCQAANKDPNAPIQ---------------SNPLGSFSSQLQNQP----------
TLPRSEEARKYFRTVYDFPQWQTHRNQYRLMKRLFSIPQSHVIQNALPSIMWVAFTSTCVAAYMYGYDQ------
-------HMLPEGFPTLAPNAACSAFISNTSVALSLLLVFRTNSSYGRWDEARKMWGGLLNRS--
RDIMRQGATCFPDD-------------------QVEAK-----KALARWV----VAFSRALRIHFQPEVT-----
IESELKN-----ILTPAELQML--AKSQHR-------------PVRAIHAISQIIQS----VPMSSI--------
------HQQQMSNNLTFFHDVLGGCERLLRAPIPVSYTRH-TARFLFAWLTLL-------PFALYGSC-----
GVSVIPVCSGIAAVLCGIEEIGVQCEEPFGI----LPLDVICNR-IQADVMATLKDD
>Cre16.g663450.t1.2_(BST3)
M---------------------------------QVSK-----------VPSS------ASARCLPRL-
PVRTSRVCQLSVRCQAANKDPNAPIQ---------------SNPLGSFSSQNSSGAVV--------
TAPRNEDARKYFRTVYDFPQWQKHRSQSRLVRRLFTIPQSHVIQNALPSIMWVTFTSTCVAAYMYGYDL------
-------HILPEGFPTLAPNAACSAFISNTSVALSLLLVFRTNSSYGRWDEARKMWGGLLNRS--
RDIMRQGATCFPDD-------------------QVEAK-----KALARWT----VAFARALRIHFQPEVT-----
IESELQN-----ILTPAELQML--AKSQHR-------------PVRAIHAISQIIQS----VRMSSI--------
------HQQQMSNNLTFFHDVLGGCERLLRAPIPVSYTRH-TARFLFAWLTLL-------PFALYGSC-----
GVSVIPVCTGIAAVLCGIEEIGVQCEEPFGI----LPLDVICNR-IQADVMATLKDD
>Chlorella_sorokiniana_(PRW33726.1)
M-----------------------STAMLAGSRIQLQQPAG--------LGGSRLQ--RAAAPVAAAA-
RLGSVRPAGLQARSTAARRADRSALR---------------VSATASPEAAPVKLS----------
GDDLKEANRKHMRSVFDFDLWKKHRSSSRYLRHIVGLGESRIVSGLMAPLTYVMTLSLAVACYNAAAEA------
-------GYLP-VFPELKL--ATNAPFGLTSFALSLLLVFRTNSSYGRWDEARKMWGLIVNRS--
RDFIRQGLGYIPPE-------------------QEELQ-----KMLVRWT----VAYSRSLMCHLRPGED-----
LRVELKD-----TLKPEELEAL--LASTHR-------------PNYVVQVLTAIIKT----
AQLPAAVTNNRDSTGCVPAGAAYRMDENLTVFADVTGGCERILRTPIPLSYTRH-TSRFMMIWLTLL-------
PFTLWDSC-----HWAMLPIAGIVSFLLLGIEEIGVQIEEPFTI----LPLEVISRT-IEGNVWELYRMH
>Cre06.g261750.t1.2_(BST4)
M-----------------------QC--------QLKH----------------------------GA-
RPQSQRPNWLPARAATLRPAVQHGVR---------------RGLTLGVKAAAAPLE--------
DKKMPADMTTRQYRRVVYDFALWAKHRDVNRYLYNLRTIPGSRIIRQLSQPMGVVLAWAALFGFYETCLEA----
---------GVLPSYLPKMTL--MSAEPQGLTSFALSLLLVFRTNSSYGRFDEARKIWGGILNRA--
RNIANQAVTFIPAE-------------------DQAGR-----EAVGKWT----VGFTRALQAHLQEDID-----
LRKELEKA--TPRWSKEEIDML--VNAQHR-------------PIKAISVLSELTRQ----LSITQF--------
------QALQMQENCTFFYDALGGCERLLRTPIPVSYTRH-TARFLTIWLAML-------PLGLWERY-----
HWSMLPVIALIGFLLLGIDEIGISIEEPFGI----LPLDAICGR-AQTDVNSLLKED
>XP_002945810.1_Volvox_carteri_f._nagariensis
M-----------------------QS--------QLQP----------------------------RL-
QLQGTRLNWLPQRSCVQRRSLRVDAT---------------SG------AAPPPPA--------
GKELSNDMVTRQYRRTVYDFSLWAKHRDVNRYLYNLKTIPGSRIIRTLGQPMGIVLAWAAMFGFYETCLES----
---------GVLPSYFPKLTL--MSAEPQGLTSFALSLLLVFRTNSSYGRFDEARKIWGGILNRA--
RNIANQAVTFIPAE-------------------DVAGR-----EAVGKWA----VGFCRALQAHLQEDAN-----
LREELQKA--QPRWSREEIDML--CSAQHSWQQLQSCVNAFW-PIKAISMLSELTRQ----LPISQF--------
------QALQMQENVTFFYDALGGCERLLRTPIPVSYTRI----------------------------------
---------------------------------LPLDAICTR-AQTDVVSLLKDD
>Chrysochromulina_sp._(KOO32217.1)
M-----------------------REHPLSYEEYMRQRS----------AGRDPLA--EAVQGQSASM-
ERGVVPPPPVKATPERTEAAFTPPAEFDFFQDVFKPTVESVVKAVVSPGAQQDSDESYMRVPWWEQGSTYSEDQR
KDRRTVFMHDDWKRHRSSERFFRNIKTWPSSGINQALRKELTFVTSVSVFVVLANMLLYQYQDFGGVVHPGPLSF
LDGPIKSLS---LPALPFSMASPVLSLLLVFRTNTAYFRWNEARTLWGGLINNC--RNIVRQTTTMFPNDA----
-------------YHNALK-----KRLATET----ATFIKSLRNFLRGPEDDAT--
LRKELYAYVNQGLMTSAQAEAT--LAAKNR-------------PMFALAAMSATLRK----ANIDEM--------
------YISRMDSTISVLVDLTGANERIFKSPIPLVYTRL-TARFLSVFLTLL-------
PLAMWAALGESWNHWATIPATFILSVFLFGVEEVGIQIEEPFSI----LPLEAMCNGAIEAVQLEMLAAE
>Emiliania_huxleyi_(XP_005770556.1)
-----------------------------------------------------------------------
```

```
------------------------------------------------------------
EFKEAGREFRQDVYSYNDWRWHRESGHIASAISSVFTSGVGKAMWRETFFVIATAAAVYLYNIGVPVLAAKTAAS
L----PIVAALLGRLPLLHLSLLPLTLSSPALFLLLVFRTNNSYDRWWEARKVWGGVINAS--
RDLARQALALVR---------------------DAELK-----KLMVSQI----
ASYARVLKYHLGPPTPEARDLLRNELVD----NRLPADQVRVI--MEAKHK-------------
PMALLGLVSASLHDSGR-TGLDTV--------------QASKLDQTLSLLTDYLGKCERIVKTPLPLVYTRH-
TARFLSWWLLFL-------PVCLYNQLRA---NWMIVPVSGLIGFFLVGIEDLGNQIEEPFSI----
LPLTAMGTG-IQQSIFEAL---
>Phaeodactylum_tricornutum_(XP_002180738.1)
MM-----------------------------------------------------------RNFASVLLLL-
SSGAAAFAPVQHNGVRTIATPSTPLY---------------GNTKQPPALP--PIK----------
DISYGEESRKYRRTVYSHDDWVKHRSSDRFLRNLLAIGSSGVYKSLAKEVLATTGVATFIVLYNCLVGGYTDLEG
IKHS---ALIESVWAPLMA--LPLAPFTLSSPSLGLLLVFRTNTSYQRWDEARKNWGMNINHT--
RDLVRMGTSFYDNAA-----------------VSSEQRAKDL-KALSLAT----WSFVRAMKRHLSPESEDEQD-
FRRELFE-----RLPAPQAQAI--IDAAHR-------------PNRALFDLSVAIEN----LPMHFL--------
------RKNQVHQAVTIFEDNLGSSERLLTSPVPLFYSRH-TARFLSFWLLLL-------
PFALWDPFAGTWNHVGMIPATAVISIFLFGIEELATQMEEPFTI----LPMQAFCDK-IGNWCNEIVSWQ
>Thalassiosira_pseudonana_(XP_002289965.1)
M-----------------------------------------------------------------------
---------------------------------------GPPIDPSVPVT-----------
DQVGEGSRKYRRTVYTHDDWVRHRSPDRFGNNLSTLFNSGIYKQVANEVFATTAVATFVFLWNMIAGGYTDLAGV
QHG---PIIDSPLAQMVG--LPMTAFTILTPSLGLLLVFRTNTSYGRWDEARKMWGLNINHT--
RDLNRMATAWYGNEGNMDSVAFMGGDIPYSQPIDPVQRAYDL-GQVSLFT----WAFVRSMKRHLSPPEEDEED-
FKAELRA-----RLTPEQAENI--INAAHR-------------PNRALFDLSVAIEN----LPMHFL--------
------RKNAINTNLSIFEDTLGGCERLLSSPVPLFYSRH-TARFLSTWLLLL-------
PFGLYEQFKDSWNHIAMIPATAFISVCLFGIEELATQLEEPFTI----LPMQGFCDK-IGGWCDEIVSW-
>WP_049046555.1_Kiebsiella_aerogenes
-----------------------------------------------------------------------
-----------------------------------------------------------------------
------MIIRPEQHWFFRLFDWHGSVLSKIVFRLLLNVLMSVIAIISYQWYEQL-------------GI------
-----HLTVAPFSLLGIAIAIFLGFRNSASYSRFVEARNLWGTVLIAE--RTLVRQLKNILPD------------
--------DEETH-----KTLVSYL----VAFSWSLKHQLRK-TD-----PAVDLYR-----LLPKEKVAEI--
LASSMP-------------TNRILLLIGNELGRLREQGKLSDI--------------
TYGLMDNKLDELAHVLGGCERLASTPVPFAYTLI-LQRTVYLFCTLL-------PFALVGDL-----
HYMTPFVSVFISYTFLSWDSLAEELEDPFGTSANDLPLNAMCNT-IERNLMDMTGQH
>XP_011543531.1_Homo_sapiens
M-----------------------------------------------------------------------
-----------------------------------------------------------------------
TITYTSQVANARLGSFSRLLLCWRGSIYKLLYGEFLIFLLCYYIIRFIYRLALTEEQQL--------------
MFEKLTL--YCDSYIQL--IPISFVLGFYVTLVVTRW------WNQYENLPWPDRLMSLVSGFVEGK--------
-----------DEQGRL--LRRTLIRYANLGNVLILRSVSTAVYKRFP-----SAQHLVQ---
AGFMTPAEHKQLEKLSLPHNM---------FWVPWVWFANLSMKAWLG---GRIRDPI-------------
LLQSLLNEMNTLRTQCGHLYAYDWISIPLVYTQVVTVAVYSFFLTCLVGRQFLNPAKAYPGHEL---
DLVVPVFTFLQFFFYVGWLKVAEQLINPFGEDDDDFETNWIVDRNLQVSLLAVDEMH
```

Supplemental Figure 16. Sequences used to generate MAFFT alignments used to generate the phylogenetic trees included in this manuscript. FASTA files of MAFFT alignments of **A.** Full length and **B.** trimmed after the bestrophin domain BST4 and homologous amino acid sequences.